Study on Photo-regulation of Duplex Formation and Dissociation by SNA modified with Photo-responsive Nucleobases

(光応答性核酸塩基導入 SNA による二重鎖形成と解離の光制御に関する研究)

Yuuhei Yamano

2021

Contents

Chapter 1. General Introduction

1-1. DNA: deoxyribonucleic acid

Since DNA: deoxyribonucleic acid is the carrier of genetic information in most living things and involved in various intracellular phenomena, it is one of the most important biomolecules that studied actively in the fields of biology and medicine.

DNA is a biopolymer that consisted by nucleotide monomers (Figure. 1-1a). Nucleotides are composed of ribose sugar, phosphate and either of four nucleobases: Adenine (A), Thymine (T), Cytosine (C), Guanine (G). The most important property of nucleic acids is forming a duplex. Base pairing *via* hydrogen bonds between A and T or C and G enables specific duplex formation between DNA strands with complementary sequences (Figure. 1-1b). Phosphate and ribose sugar determine the overall structure of the duplex, which is generally the right-handed double helix structure (Figure. 1-1c). The first report of this interesting DNA property by Watson and Crick in 1953, greatly contributed to reveal the mechanism by which DNA carries and maintains genes.[1]
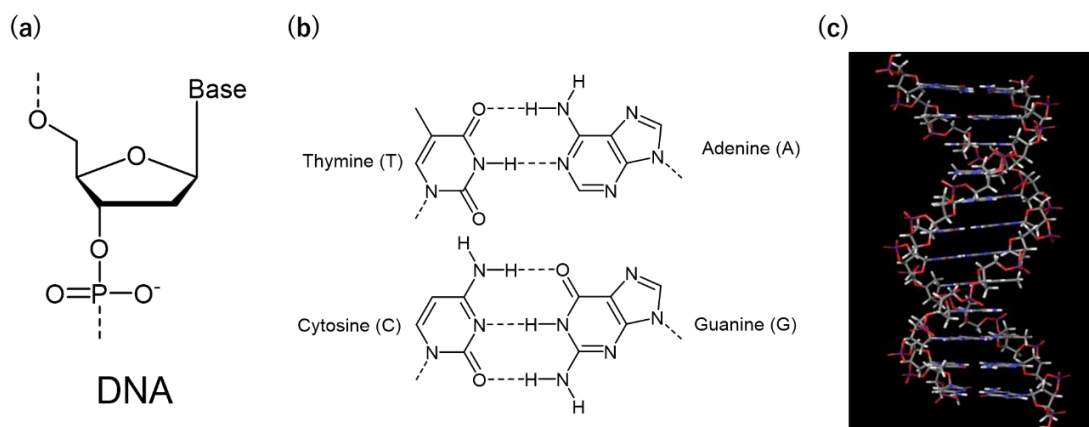
Figure. 1-1 (a) Chemical structures of nucleotide unit of DNA and (b) Watson-Crick base pairs of nucleobases. (c) The structure canonical DNA duplex (B-DNA).

1-2. DNA as a nanomaterial

The discovery of property that form canonical duplex with sequence specific manner also implied that DNA is the programable supermolecule and it can be great bearer of nanotechnology. Development of efficient chemical synthesis of DNA oligomer using phosphoramidite greatly contributed realization and prosperity of this "DNA nanotechnology". [2] Thanks to this method, nowadays, we can obtain DNA with any length and sequence easily.

The concept of DNA nanotechnology was proposed by Seeman *et al*. By utilizing the mutual duplexes formation of multiple single-stranded DNAs, they succeeded in creating DNA nanoarchitectures with various geometric structures including 2D lattice and 3D cube structures (Figure. 1-2). [3]
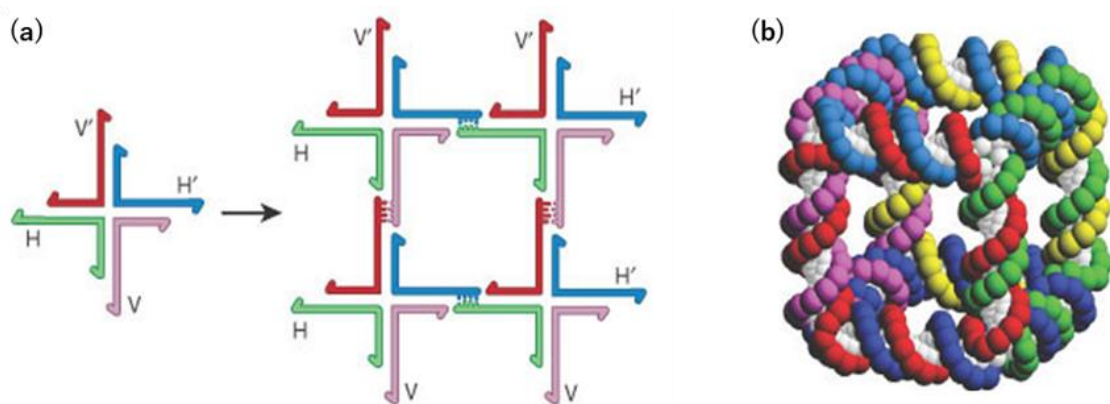
Figure 1-2. (a) Self-assembly of branched DNA molecules and (b) Cube-like structure composed of interconnected DNA. Reprinted from Ref. 3b.

DNA origami: another important methodology that play a central role in DNA nanotechnology was reported by Rothemund in 2006. [4] DNA origami is the method that prepare various nanoarchitectures by folding one long circular DNA strand (scaffold strand) through hybridization with some short DNA strands (staple strands). Due to its versatility that create DNA nano-structures with any shape easily, DNA origami

technology is applied in various fields,[5] for example, single molecule sensing and imaging of biomolecules and fabrication of drag carriers.
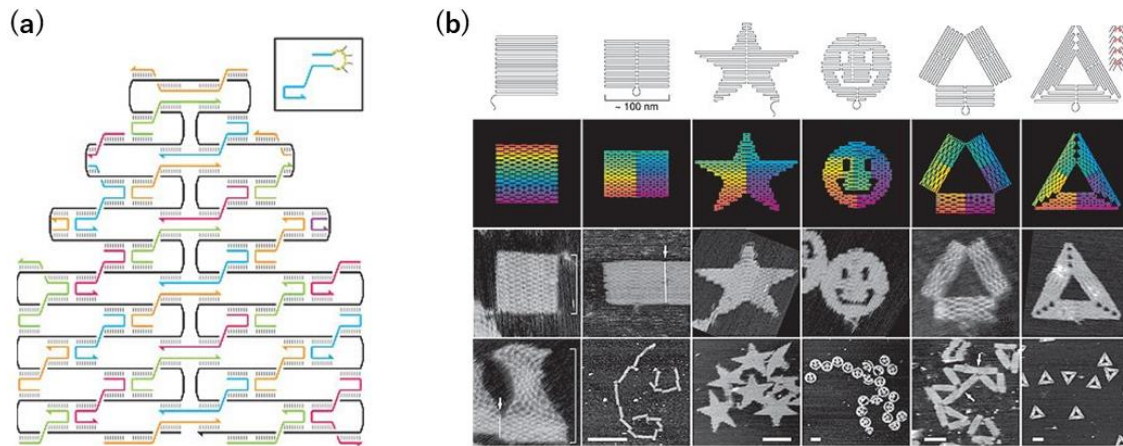
Figure. 1-3 (a) Design of DNA-origami devised by Rothemund, (b) AFM image of DNA-origami structures. Reprinted from Ref. 4

As mentioned above, DNA is a molecule with high utility as a nanomaterial. However, there are some drawbacks to the natural DNA as nanomaterials. First, the "thermal" stability of the duplex is low. While this subtle stability based on non-covalent interactions is advantageous in transcribing genetic information, it makes DNA nanomaterials fragile at high temperatures. Second, DNA duplex is not responded positively to external stimuli. This "chemical" insensitivity is necessary for maintaining the genetic information, however, limit degree of freedom in designing dynamic or functional nanomaterials. So that, few smart designs of nanorobots using only natural DNA have been reported and most of them based on toehold strand exchange using nucleic acid strands or enzymes as stimuli. [6] In addition, third, when we aim to develop the nanomaterial intended for long-term use *in vivo*, low enzyme resistance of natural DNA should also be drawback.

In order to overcome above drawbacks and expand the utility of DNA as nanomaterials, many artificial nucleic acids have been developed by modifying natural DNA so far.

1-3. Functionalization of DNA with modified nucleobases

Modification of the nucleobase moiety has been widely studied because it has little effect on the overall structure of the duplex and it is easy to add new functions (Figure. 1-4).
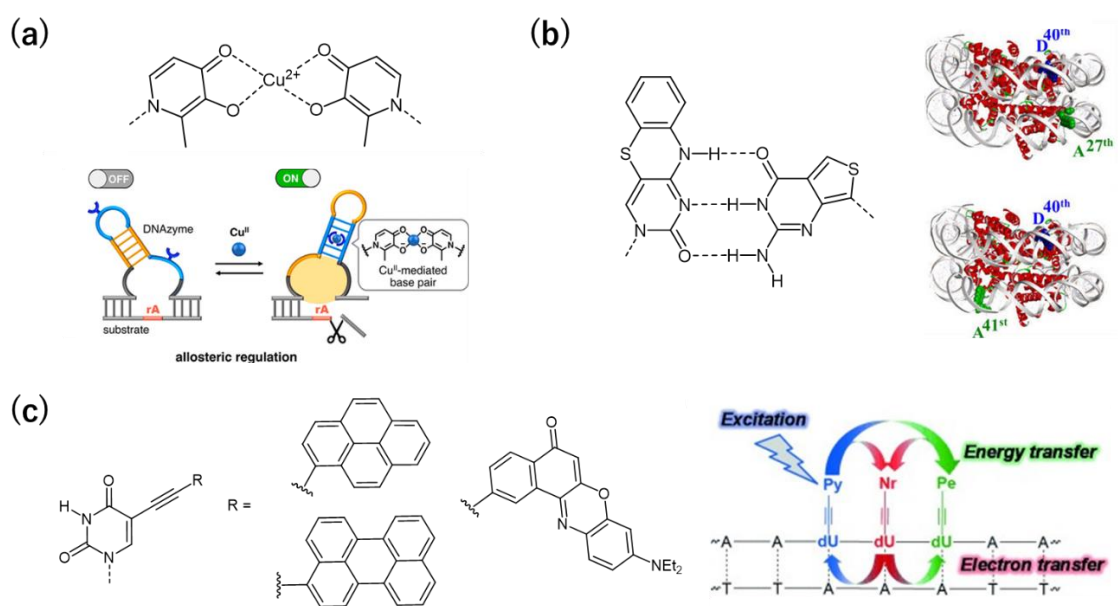
Figure. 1-4 Examples of functional base surrogates. Reprinted from Ref. 8, 10 and 11.

The first pseudo base pairs were reported by Kool *et al*. [7] These base surrogates form pairs based on hydrophobic interactions, overturning the conventional wisdom that hydrogen bonds are essential for duplex formation. Shionoya *et al*. developed artificial bases that form base pairs through metal complex formation (Figure. 1-4a). [8a, b] This technology has been applied to artificial DNAzyme whose activity can be regulated by adding copper ions. [8c] The DNA containing a fluorescent base surrogate for FRET devised by Wilhelmsson *et al*. [9] and Sugiyama *et al*. [10a] These pairs are used in some applications including the analysis of the nucleosome structure (Fig.1-4b). [10b]

Wagenknecht *et al*. have succeeded in incorporating some chromophores into DNA as base surrogates and confirmed that energy transfer or long-distance photo-induced electron transfer occur between these chromophores (Fig.1-4c). [11] These studies have supported the potential of DNA for new applications such as light harvesting systems and nanoelectronics. Artificial nucleobase-introduced DNA that can be replicated, transcribed, and translated was developed by Romesberg *et al*. [12] and Hirao *et al*. [13] These studies have expanded the genetic information of DNA and enabled the production of semi-synthetic organisms (SSOs).
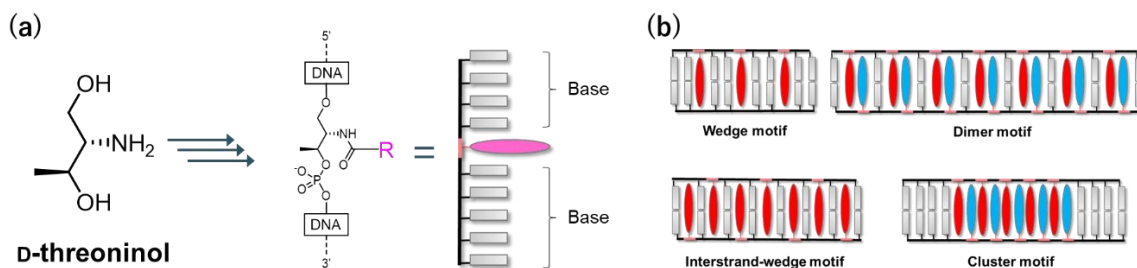
Figure. 1-5 (a) Design of functional motifs by the combination of base surrogates synthesized *via* D-threoninol with natural nucleotides. (b) Four functional motifs designed with functionalized d-threoninol incorporated on one or both strands of a duplex.

On the other hand, our group has succeeded in functionalizing DNA with a novel approach. An acyclic backbone, D-threoninol, was adopted for this purpose. [14a] This simple backbone allows us to introduce various functional molecules into DNA strand as "Pseudo Base-Pairs" and four functional DNA motifs can be prepared easily (Figure.1-5). [14b] Especially, when cationic planar molecules were introduced *via* D-threoninol, duplex was greatly stabilized based on both π-π stacking interaction and electrostatic interaction. [15] One of the successful examples of functional DNA using this design is photo-responsive DNA. In the first system, azobenzene derivatives were tethered to DNA *via* D-threoninol (Fig.1-6). [14a, 16] *Trans*-form azobenzene has a planar structure and

stabilizes the duplex. On the other hand, *cis*-form azobenzene is non-planar and destabilizes the duplex based on steric hindrance. As UV/Vis irradiation convert them reversibly (photo-isomerization), duplex formation/dissociation can be controlled by photo-irradiation.
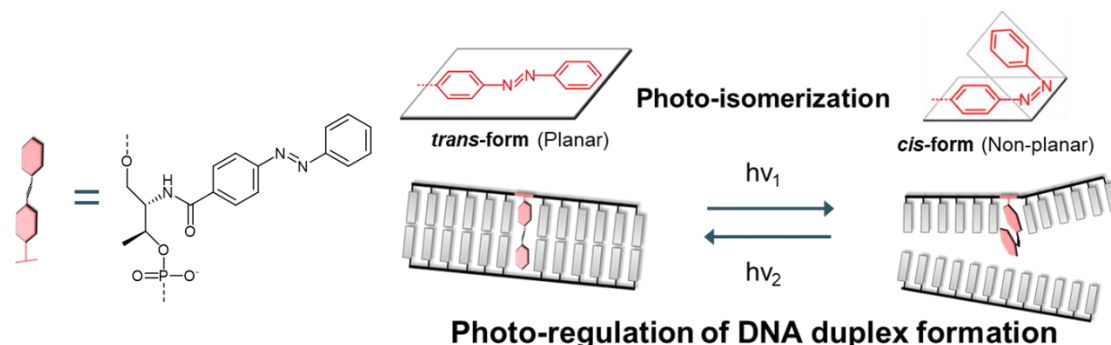
Figure. 1-6 Photo-regulation of DNA duplex using azobenzene derivatives

By utilizing various azobenzene derivatives, the photo-regulatory efficiency improved and photo-control using only visible light was also achieved. Since light is a "clean resource" that does not contaminate the reaction system, these functional DNAs are applied to various dynamic DNA nanomaterials so far.[16e]
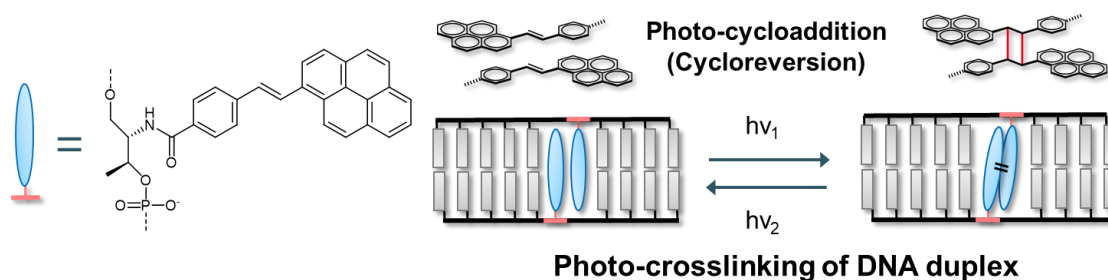
Figure. 1-7 Photo-reactive pseudo base pairs for DNA crosslinking

Inter-strand crosslink type DNA is another important design of photo-responsive DNA devised by our group. Here, two stilbene derivatives [17] or styrylpyrene [18] are introduced at base-pairing positions on complementary DNA strands. These chromophores cause

cycloaddition/cycloreversion upon light irradiation, so the strands are photo-crosslinked reversibly. Note that, virtually no complete dissociation of the duplexes occurs after the cross-linking reaction proceeds: the DNA strands are covalently linked. This "amazing" stabilization of the duplex increases the robustness of DNA as a nanomaterial and contributes to the expansion of its application.[19] In addition, our group also succeeded in verifying the reactivity of cycloaddition reactions between heterologous stilbene derivatives using this design, showing that DNA can be used as an "attractive reaction field".[17b]

1-4. XNA

Xeno nucleic acids (XNAs), synthetic analogues of DNA include backbones different from natural D-ribose, have also attracted attention as new bearers of nanomaterial, since they have many attractive and unique features.
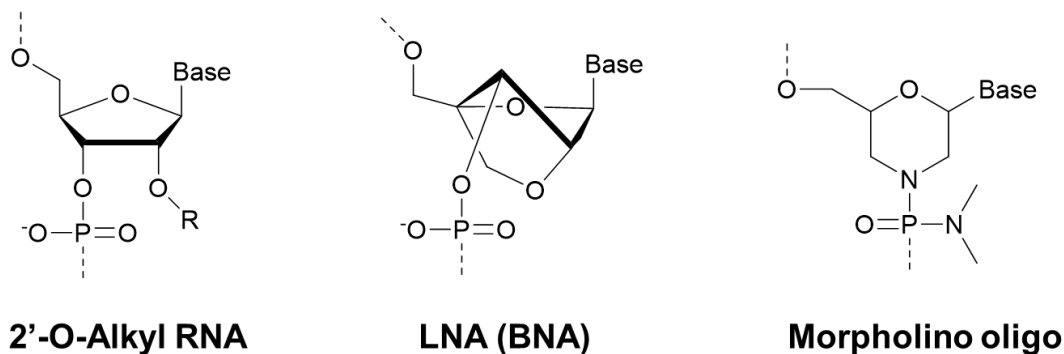
Figure. 1-8 Chemical structures of representative cyclic XNAs.

XNAs are divided into cyclic type and acyclic type. Cyclic XNA generally has backbone that partially modified D-ribose (Figure. 1-8).[20-22] These rigid structures, represented by LNA, contribute to the improvement of enzyme resistance. Furthermore, in most cases, duplex forming ability of cyclic artificial nucleic acids is higher than that of natural

nucleic acids: DNA and RNA because the entropic loss of duplex formation is minimized. On the other hand, cyclic artificial nucleic acids having a significantly modified overall structure, such as Morpholino oligo, have also been developed for application to medicine. Removal of the negative charge of phosphate moiety allow it to bind with complementary RNA strongly. Due to these excellent characteristics, cyclic artificial nucleic acids are the most promising candidates for various nanomaterials or pharmaceuticals like antisense oligomer. However, because of their rigid and complex structure, synthesis of monomer is cumbersome. In addition, the similarity of chemical structure to natural nucleic acids (D-ribose) makes enzyme resistance incomplete. These disadvantages can hinder the prosperity of nanotechnology by cyclic XNAs.
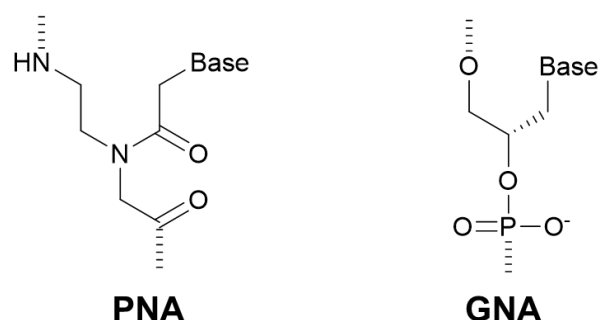
Figure. 1-9 Chemical structures of representative acyclic XNAs.

In contrast, acyclic XNAs are nucleic acid analogs with extremely flexible structures (Figure. 1-9)[23, 24] Bold modifications of the ribose moiety promise them extremely high nuclease resistance. One of the most successful examples of acyclic XNA is PNA：peptide nucleic acid. Since PNA has a neutral backbone that mimics peptides, it can form highly stable duplexes with PNA, DNA or RNA without requiring cation condensation. This property allows PNAs to be candidates for various biological tools. However, actually, the absence of charge also reduces the water solubility of PNA oligomers, making it

difficult to handle as materials. Prior to PNA, another representative acyclic XNA, GNA: glycol nucleic acid, has also been reported. Despite of very simple structure containing phosphodiester bonds, GNA formed a very stable homoduplex. This finding indicates that no cyclic structure is required for stable duplex formation. However, GNA did not form duplex with native nucleic acids except for very limited sequences. Therefore, there was a demand for the development of acyclic artificial nucleic acids that can form stable duplex with natural nucleic acids and that ensure water solubility.
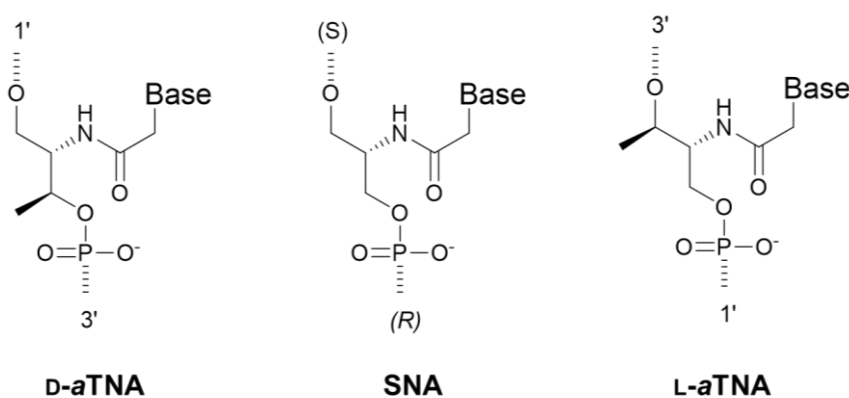
Figure. 1-10 Chemical structures of D-*a*TNA, SNA and L-*a*TNA

Encouraged by these pioneering works, our group has also reported several acyclic XNAs so far. First, D-*a*TNA: acyclic D-threoninol nucleic acid, which is an XNA that uses the D-threoninol as backbone, was developed. [25] D-*a*TNA formed a highly stable duplex with the complementary D-*a*TNA sequence. However, D-*a*TNA was unable to form double strands with DNA and RNA. Next, SNA: Serinol nucleic acid, which has a more flexible backbone D-*a*TNA, was developed. [26] Fortunately, SNA can hybridize not only with SNA but also *a*TNA, RNA and DNA. In other words, SNA is the first example of a phosphodiester bond-containing acyclic artificial nucleic acid that can stably form duplex with natural nucleic acids. Furthermore, interestingly, L-*a*TNA, which is an enantiomer

of D-*a*TNA, also forms duplex with RNA and DNA, and its binding affinity surpass that of SNA. [27] This result suggested that the increased rigidity due to the methyl group introduced at the appropriate position contributes to the stabilization of the duplex. In addition, the CD spectrum showed that the homo-duplex of L-*a*TNA adopt a right-handed helical structure, whereas that of D-*a*TNA is left-handed. So, the stable duplex formation of L-*a*TNA with natural nucleic acids can also be related to this helical preference.

Anyway, our group has succeeded in creating three acyclic XNAs with unique characteristics. Due to its high orthogonality to natural RNA and DNA, D-*a*TNA has the potential to be used as a component of nano-materials that are not interfered with by natural nucleic acids *in vivo*. On the other hand, SNA and L-*a*TNA, which has a high binding affinity with natural nucleic acids, are great candidates for probes and drugs that target natural nucleic acids as well as nanomaterials. In addition, SNA can form duplex with both enantiomer of *a*TNA,[28] so it should also act as an intermediary to convey sequence information of natural nucleic acids to D-aTNA. In other words, there is no doubt that SNA is the most versatile nucleic acid analog among the three XNAs.

1-5. Purpose of this study

As mentioned above, SNA has more attractive features than natural nucleic acids, and is a promising player for next-generation nano-materials and nucleic acid drugs. Incorporation of additional functionalities to SNA would further expand the scope of its application.

In this study, we attempted to develop photo-responsive SNA. In Chapter 2, novel modified nucleobase [PV]A: Pyrenylvinyl adenine was developed and introduced into SNA for this purpose. Based on reversible photo-crosslinking reactions of them, the ability of

SNA that form duplexes was successfully regulated. In Chapter 3, modified nucleobases, whose response wavelength distinct from ^{PV}A, were synthesized. New variation of photo-crosslink type base surrogates and utilizing of heterogeneous photo-crosslinking reactions of them allowed us to orthogonal photo-control of multiple SNAs hybridization.

1-6. References

[1] J. D. Watson, F. H. C. Crick, *Nature* **1953**, *171*, 737-738.

[2] (a) Beaucage, S. L.; Caruthers, M. H. *Tetrahedron Lett.* **1981**, *22*, 1859; (b) Beaucage, S. L; Iyer, R. P. *Tetrahedron Lett.* **1992**, *48*, 2223.

[3] (a) J. H. Chen, N. C. Seeman, *Nature* **1991**, *350*, 631-633; (b) N. C. Seeman *Nature* **2003**, *421*, 427; (c) J. P. Zheng, J. J. Birktoft, Y. Chen, T. Wang, R. J. Sha, P. E. Constantinou, S. L. Ginell, C. D. Mao, N. C. Seeman, *Nature* **2009**, *461*, 74-77.

[4] P. W. K. Rothemund, *Nature* **2006**, *440*, 297-302.

[5] F. Hong, F. Zhang, Y. Liu, H. Yan, *Chem. Rev.* **2017**, *117*, 12584–12640.

[6] (a) B. Yurke, A. J. Turberfield, A. P. Mills, F. C. Simmel, J. L. Neumann, *Nature* **2000**, *406*, 605-608. (b) J. S. Shin, N. A. Pierce, *J. Am. Chem. Soc.* **2004**, *126*, 10834-10835; (c) W. B. Sherman, N. C. Seeman, *Nano Lett.* **2004**, *4*, 1801. (d) J. Valero, N. Pal, S. Dhakal, N. G. Walter, M. Famulok, *Nat. Nanotechnol.* **2018**, *13*, 496–503; (e) J. Valero, F. M. Famulok, *Angew. Chem. Int. Ed.* **2020**, *59*, 16366 –16370.

[7] (a) R. X.-F. Ren, N. C. Chaudhuri, P. L. Paris, S. Rumney IV, E. T. Kool, *J. Am. Chem. Soc.* **1996**, *118*, 7671; (b) E. T. Kool, J. C. Morales, K. M. Guckian, *Angew. Chem. Int. Ed.* **2000**, *39*, 990–1009.

[8] (a) K. Tanaka, A. Tengeiji, T. Kato, N. Toyama, M. Shionoya, *Science* **2003**, *299*, 1212-1213; (b) K. Tanaka, G. H. Clever, Y. Takezawa, Y. Yamada, C. Kaul, M. Shionoya, T. Carell, *Nature Nanotechnol.* **2006**, *1*, 190-194; (c) T. Nakama, Y. Takezawa, D. Sasaki, M. Shionoya, *J. Am. Chem. Soc.* **2020**, *142*, 10153–10162.

[9] K. Börjesson, S. Preus, A. H. El-Sagheer, T. Brown, B. Albinsson, L. M. Wilhelmsson, *J. Am. Chem. Soc.* **2009**, *131*, 4288–4293.

[10] (a) J. H. Han, S. Yamamoto, S. Park, H. Sugiyama, *Chem. Eur. J.* **2017**, *23*, 7607– 7613; (b) J. H. Han, S. Park, F. Hashiya, H. Sugiyama, *Chem. Eur. J.* **2018**, *24*, 17091-17095.

[11] (a) P. Ensslen, H.-A. Wagenknecht, *Acc. Chem. Res.* **2015**, *48*, 2724-2733; (b) P. Ensslen, F. Brandl, S. Sezi, R. Varghese, R.-J. Kutta, B. Dick, H.-A. Wagenknecht, *Chem. Eur. J.* **2015**, 21, 9349-9354; (c) P. Ensslen, S. Gärtner, K. Glaser, A. Colsmann, H.-A. Wagenknecht, *Angew. Chem. Int. Ed.* **2016**, 55, 1904-1908.

[12] (a) D. A. Malyshev, F. E. Romesberg, *Angew. Chem. Int. Ed.* **2015**, *54*, 11930-11944; (b) Y. J. Seo, S. Matsuda, F. E. Romesberg, *J. Am. Chem. Soc.* **2009**, *131*, 5046-5047; (c) D. A. Malyshev, Y. J. Seo, P. Ordoukhanian, F. E. Romesberg, *J. Am. Chem. Soc.* **2009**, *131*, 14620-14621

[13] (a) I. Hirao, T. Mitsui, M. Kimoto, S. Yokoyama, *J. Am. Chem. Soc.* **2007**, *129*, 15549-15555; (b)

T. Mitsui, M. Kimoto, Y. Harada, S. Yokoyama, I. Hirao, *J. Am. Chem. Soc.* **2005**, *127*, 8652-8658; (c) I. Hirao, Y. Harada, M. Kimoto, T. Mitsui, T. Fujiwara, S. Yokoyama, *J. Am. Chem. Soc.* **2004**, *126*, 13298-13305.

[14] (a) H. Asanuma, X. G. Liang, H. Nishioka, D. Matsunaga, M. Z. Liu, M. Komiyama, *Nat. Protoc.* **2007**, *2*, 203–212; (b) H. Asanuma, H. Kashida, Y. Kamiya, *Chem. Rec.* **2014**, *14*, 1055– 1069.

[15] H. Kashida, H. Ito, T. Fujii, T. Hayashi, H. Asanuma, *J. Am. Chem. Soc.* **2009**, *131*, 9928- 9930.

[16] (a) H. Kashida, X. G. Liang, H. Asanuma, *Curr. Org. Chem.,* **2009**, *13*, 1065-1084; (b) H. Asanuma, T. Ito, T. Yoshida, X. G. Liang, M. Komiyama, *Angew. Chem. Int. Ed.,* **1999**, *38*, 2393-2395; (c) H. Asanuma, X. G. Liang, T. Yoshida, M. Komiyama, *Chembiochem,* **2001**, *2*, 39-44. (d) H. Asanuma, T. Takarada, T. Yoshida, X. G. Liang, M. Komiyama, *Angew. Chem. Int. Ed.* **2001**, *40*, 2671–2673. (e) Y. Kamiya, H. Asanuma, *Acc. Chem. Res.* **2014**, *47*, 1663−1672.

[17] (a) H. Kashida, T. Doi, T. Sakakibara, T. Hayashi, H. Asanuma, *J. Am. Chem. Soc.* **2013**, *135*, 7960-7966; (b) T. Doi, H. Kashida, H. Asanuma, *Org. Biomol. Chem.* **2015**, *13*, 4430-4437.

[18] T. Doi, H. Kawai, K. Murayama, H. Kashida, H. Asanuma, *Chem. Eur. J.* **2016**, *22*, 10533-10538.

[19] Y. Kamiya, K. Iishiba, T. Doi, K. Tsuda, H. Kashida, H. Asanuma, *Biomater. Sci.* **2015**, *3*, 1534-1538.

[20] (a) S. K. Singh, P. Nielsen, A. A. Koshkin, J. Wengel, *Chem. Commun.* **1998**, 455-456; (b) S. Obika, D. Nanbu, Y. Hari, J. Andoh, K. Morio, T. Doi, T. Imanishi, *Tetrahedron Lett.* **1998**, *39*, 5401-5404; (c) H. Kaur, B. R. Babu, S. Maiti, *Chem. Rev.* **2007**, *107*, 4672-4697.

[21] (a) H. Inoue, Y. Hayase, A. Imura, S. Iwai, K. Miura, E. Ohtsuka, *Nucleic Acids Res.* **1987**, *15*, 6131-6148; (b) T. P. Prakash, *Chem. Biodivers.* **2011**, *8*, 1616-1641.

[22] J. Summerton, D. Weller, *Antisense Nucleic Acid Drug Dev.* **1997**, *7*, 187-195.

[23] (a) P. E. Nielsen, M. Egholm, R. H. Berg, O. Buchardt, *Science* **1991**, *254*, 1497-1500; (b) P. Wittung, P. E. Nielsen, O. Buchardt, M. Egholm, B. Norden, *Nature* **1994**, *368*, 561-563.

[24] (a) L. L. Zhang, A. Peritz, E. Meggers, *J. Am. Chem. Soc.* **2005**, *127*, 4174-4175; (b) M. K. Schlegel, A. E. Peritz, K. Kittigowittana, L. Zhang, E. Meggers, *ChemBioChem* **2007**, *8*, 927-932.

[25] H. Asanuma, T. Toda, K. Murayama, X. Liang, H. Kashida, *J. Am. Chem. Soc.* **2010**, *132*, 14702-14703.

[26] (a) H. Kashida, K. Murayama, T. Toda, H. Asanuma., *Angew. Chem. Int. Ed.*, **2011,** *50*, 1285-1288; (b) K. Murayama, Y. Tanaka, T. Toda, H. Kashida, H. Asanuma, *Chem. Eur. J.*, **2013,** *19*, 14151-14158.

[27] K. Murayama, H. Kashida, H. Asanuma, *Chem.Commun.* **2015**, *51*, 6500-6503.

[28] K. Murayama, R. Nagao, H. Asanuma, *ChemistrySelect* **2017**, *2*, 5624– 5627.

Chapter 2. Development of photo-crosslinkable nucleobase analogue for photo-controlling hybridization ability of SNA

2-1. Abstract

Our group reported novel acyclic XNA, SNA that totally consisted by serinol backbone. Since SNA has strong hybridization ability for complementary SNA and RNA, and has far higher enzyme-resistance than other XNAs, it is a promising tool for various biological applications, unachievable by natural nucleic acids.

In this study, for further expansion of the scope of SNA's application, we attempted to photo-regulate duplexes of SNA. In order to photo-regulate the hybridization event of SNA, photo-responsive nucleobase 8-pyrenylvinyl adenine (^{PV}A) was newly designed and incorporated into SNA. One ^{PV}A residue in SNA strand caused photo-isomerization reaction mainly upon the visible light irradiation. However, hybridization of SNA duplexes could not regulate though this reaction. On the other hand, when two ^{PV}As were introduced into SNA strand, they caused photo-cycloaddition/cycloreversion by Vis/UV-A light irradiation, which induced intra-strand photo-crosslinking of SNA. Analyses of UV-Vis, fluorescence, CD, and HPLC data demonstrated high conversion ratio, rapid response, selectivity, and reversibility of these reactions. The distortion caused by photo-crosslinking allowed SNA strand to dissociate almost completely from the complementary strand and the reverse reaction: photo-cycloreversion allowed re-formation of the duplex.

It should be note that effective photo-control of SNA duplex formation was achieved at

constant temperature. This is first example of reversible photo-switching of XNA duplexes formation, and this is also first example of reversible photo-control of the duplex using only photo-cycloaddition reaction and photo-cycloreversion reaction. Moreover, this novel strategy would be applicable to other acyclic XNAs for their photo-regulation. This approach using [PV]A should make SNAs candidates for use as photo-regulated biological tools.

2-2. Introduction

XNAs, synthetic analogues of DNA and RNA carrying scaffolds different from natural D-ribose, impart new functions and high nuclease resistance in biological applications of nucleic acids.[1] Recently, pure XNAs that do not include any natural nucleotides have attracted attention as a new nanomaterial for nanomachines and nanoarchitectures.[2] Our group has also developed the novel acyclic XNA: SNA which can hybridize with DNA and particularly with RNA.[3] Notably, SNA could be applied to various biological tools such as antisense-mediated exon skipping,[4a] anti-miRNA oligonucleotides,[4b] and detection of mRNA in cells.[4c] Incorporation of additional functionalities to SNA would further expand the scope of its application. One of the useful functions is stimulus-responsivity in which a function is activated in response to an external stimulus such as pH, heat, or metal ion binding.[5] Among potential external stimuli, light is an ideal trigger because spatiotemporal control is possible without contaminating the solution.[6] For reversible photo-regulation, photochromic molecules that cause various reactions upon irradiation have been developed and introduced into DNA.[7] Our group has also developed photo-responsive DNA and RNA by introducing azobenzene *via* D-threoninol or other acyclic diols into oligonucleotides. Thus, photo-controllable DNA has been

developed actively.[8] However, photo-regulation of acyclic XNAs has not yet been achieved, despite the great applicability of them.
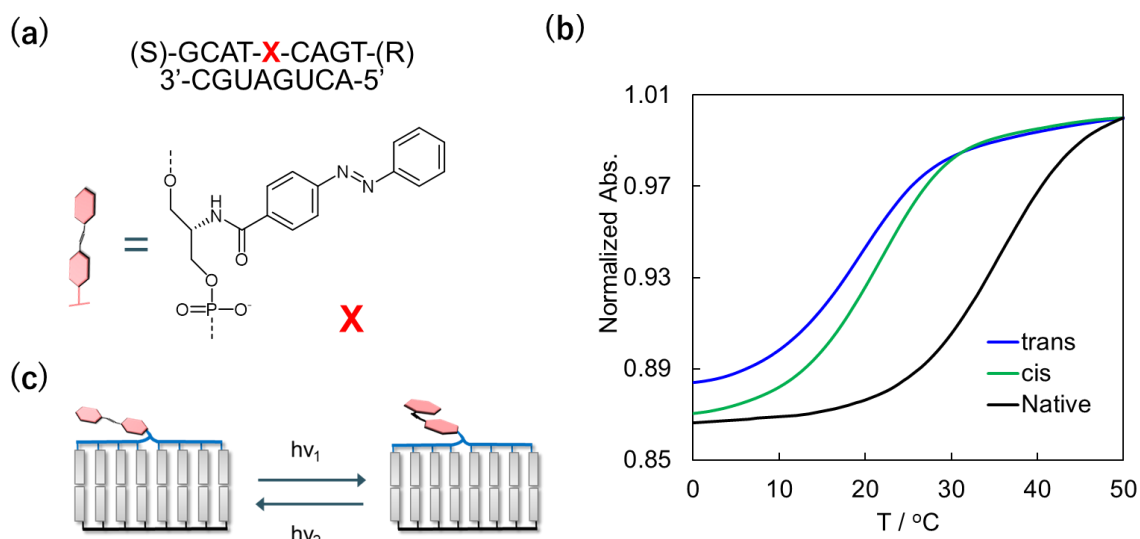

Figure. 2-1 Photo-regulation of SNA/RNA duplex using azobenzene (a) Sequences used in this study and chemical structure of Serinol-Azobenzene (X) (b) Melting profile of duplex between RNA and SNA containing X in *trans* (blue line, T_m = 19.8 °C) and in *cis* (green line, T_m = 21.5 °C). The *cis*-isomerization of azobenzene did not induce any destabilization. The T_m of the duplex with an unmodified SNA (GCATCAGT) was 35.0 °C (black line). Conditions: 100 mM NaCl, 10 mM phosphate buffer (pH 7.0). The concentration of oligonucleotides was 2.0 μM. (c) SNA does not allow intercalation of azobenzene derivative.

Recently, we tried to photo-regulate SNA through photo-isomerization of azobenzene derivative (Figure. 2-1a). As a result, unfortunately, SNA/RNA duplex did not show any difference of T_ms between *trans*-form and *cis*-forms. Moreover, duplex was significantly destabilized by incorporation of azobenzene derivative (Figure. 2-1b). Detailed analysis of absorption spectra suggested that azobenzene did not intercalate into duplexes even in *trans*-form (Figure. 2-1c). In addition, even when the complementary strand was changed to SNA, duplex formation was not controlled as well. In other words, the photo-control method for DNA that based on additional introduction of azobenzene cannot be applied to SNA: new methodologies for controlling acyclic XNAs were required.

2-3. Method

2-3-1. Modification of the nucleobases

In this study, establishment of new method for photo-controlling duplex forming ability of SNA is aimed. To achieve this goal, SNA should be modified properly so that it does not interfere with the duplex formation prior to photo-irradiation. Modification of the nucleobase can meet this demand. In particular, 5-position of pyrimidine or the 8-position of purine base is adopted generally since modification at these positions doesn't disrupt canonical base pairing of DNA or RNA, and the modification moiety is located in the major groove of duplex. (Figure.2-2).[9] Similar strategy that does not require intercalation of functional molecules should also be applied to photo-control of acyclic XNAs.
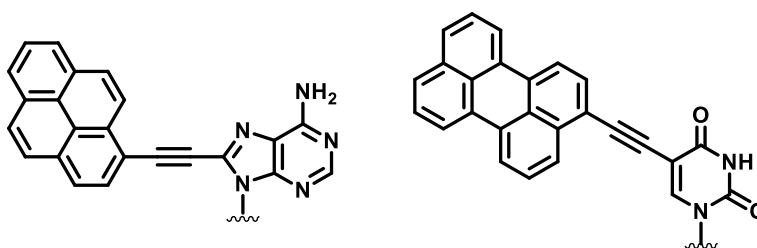

Figure. 2-2 Typical examples of modified nucleobases that do not destabilize a canonical DNA (or RNA) duplex.

2-3-2. Utilizing of photo-cycloaddition reaction

Photo-isomerization reactions have generally been used for controlling the duplex formation. Also, there are examples of control duplex stability by incorporating photo-isomerizing type nucleobase analogs into DNA (Figure. 2-3).[10] However, the effect of photo-isomerization of these analogs on duplex stability is limited, and there are only few examples that controlled duplex formation and dissociation completely using this method. In addition, diazo group-bearing nucleobase analogs that mimic azobenzene suffer also from the low thermal stability of the *Cis*-form: isomerization by heat. In other words, for

controlling duplex formation more efficiently, another reaction that causes a large structural change in response only by light stimulus should be utilized.
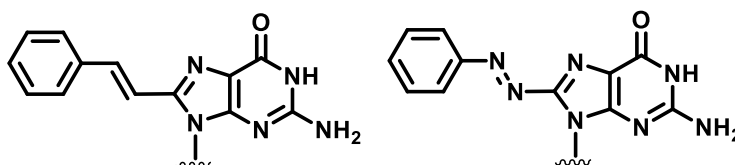

Figure. 2-3 Photochromic nucleobase analogs that reversibly photo-isomerize have also been reported.

We thought that the [2+2] photo-cycloaddition reaction is another great candidate of photo-reaction for controlling duplex because covalent bonds are formed reversibly by using two kinds wavelengths of light and do not respond to other stimuli such as heat.[11] In particular, styrylpyrene, whose reaction can be easily controlled by visible light and UV-A, is used in various fields such as photo-crosslinking and photo-ligation of various polymers including DNA.[12] However, to the best of our knowledge, these reversible [2+2] photo-cycloaddition reactions have not yet been applied to regulate canonical duplex formation and dissociation. Based on these findings, in this study, we aimed to develop a novel photo-responsive modified nucleobase that mimicked the reactivity of styrylpyrene.

2-3-3. [PV]A : 8-pyrenylvinyl adenine

We designed 8-pyrenylvinyl adenine ([PV]A) as a novel photo-responsive nucleobase analog (Figure. 2-3a) and introduced it into SNA instead of canonical adenine. This analog should not interfere with canonical base pairing with thymine or uracil (Figure. 2-4b).

Note that this adenine analog has a structure very similar to styrylpyrene. This structural similarity implied that ^{PV}A residues can also cause photo-crosslinking, and allowed novel strategy for photo-regulation that utilizes SNA containing two ^{PV}As (Figure. 2-3c). In this strategy, irradiation with visible light is expected to induce intrastrand crosslinking through the [2+2] photocycloaddition between the neighboring ^{PV}As, distorting the SNA strand and resulting in duplex dissociation: severe destabilization. Irradiation with UV-A light should regenerate ^{PV}A *via* cycloreversion reaction and allow duplex formation. Unlike azobenzene-based photo-regulation, which can be induced thermally, the cycloaddition and cycloreversion reactions of ^{PV}A should proceed only photochemically.
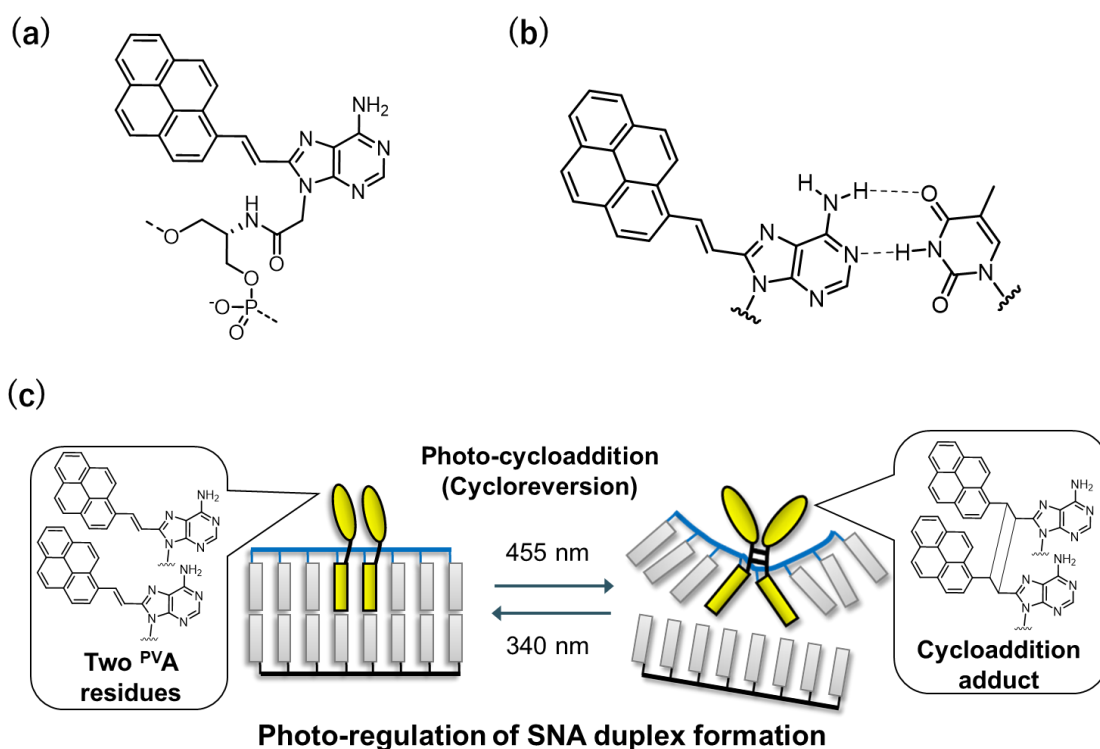

Figure. 2-4 (a) Chemical structures of 8-pyrenylvinyl adenine (^{PV}A) introduced SNA. (b) ^{PV}A can form Watson-Click type base pairs with thymine or uracil in complementary strand. (c) Scheme and illustration of reversible photo-regulation of SNA by utilizing intrastrand photo-cross-linking of ^{PV}As in the SNA strand.

2-4. Results and Discussion

2-4-1. Synthesis of ^{PV}A-SNA oligomer
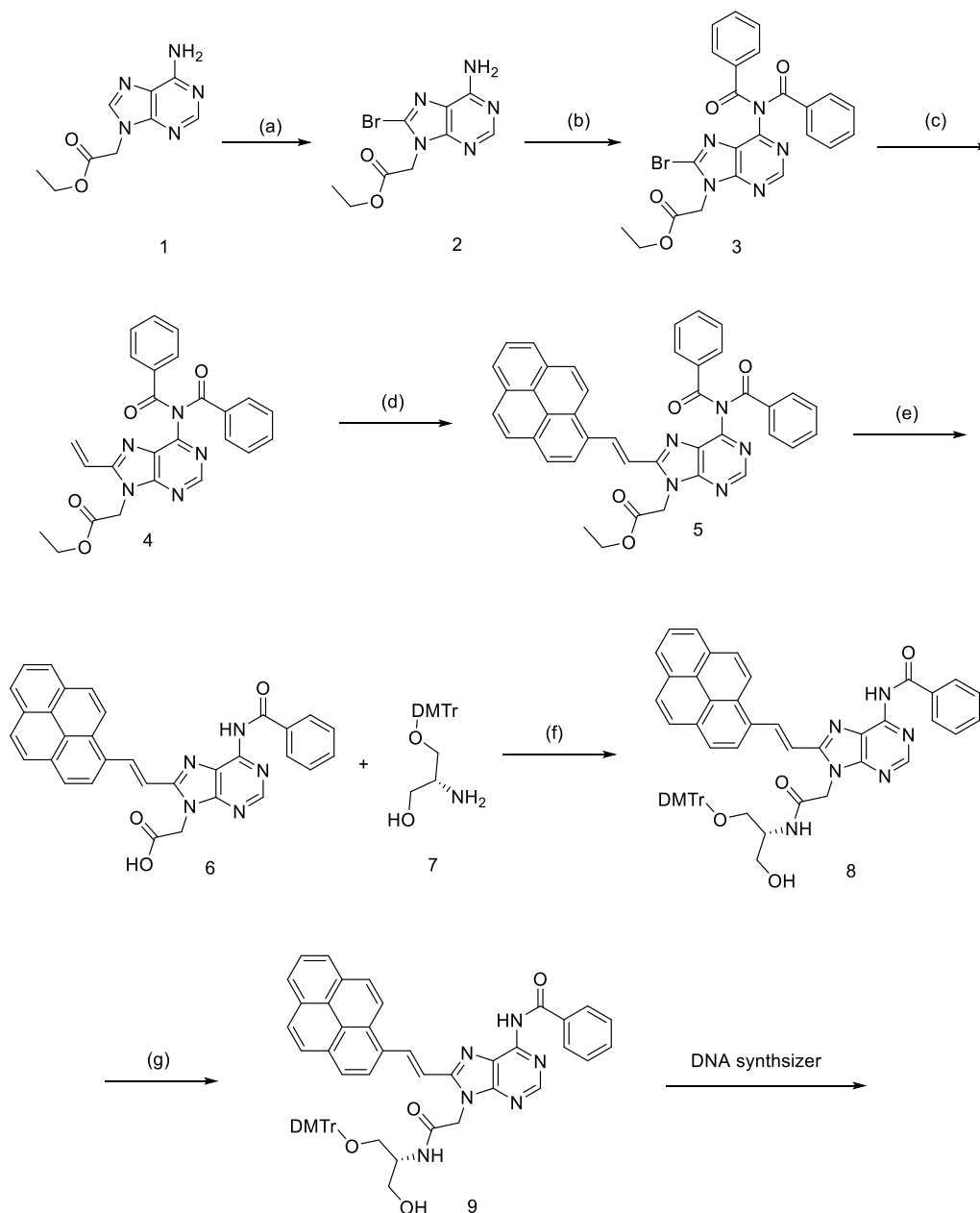
Scheme. 2-1 Synthesis of the phosphoramidite monomer of SNA-^{PV}A. Reagents and conditions: a) Br$_2$, 10% Na$_2$HPO$_4$ aq, 1,4-dioxane, room temperature, 10 min.; b) benzoyl chloride, dry pyridine, room temperature, 30 min.; c) Pd(PPh$_3$)$_4$, tributylvinyltin, dry NMP, 110 °C, 10 min.; d) 1-bromopyrene, Pd(Ac)$_2$, triphenylphosphine, triethylamine, dry DMF, 110 °C, 30 min.; e) NaOH, MeOH, H$_2$O, room temperature, 20 min.; f) DMT-MM, triethylamine, DMF, room temperature, 1 h.; g) 2-cyanoethyl diisopropylchlorophosphoramidite, Et$_3$N, dry CH$_2$Cl$_2$, 0 °C, 30 min

We synthesized phosphoramidite monomer of SNA-^{PV}A using compounds 1 as starting material (Scheme. 2-1). Then, we prepared three SNA sequences with two ^{PV}A residues at different positions (SNA-P2P, SNA-P1P, and SNA-P0P) using this ^{PV}A-monomer and A, T, C, G SNA monomer (Table. 2-1). For the analysis of photo-reactivity in monomeric ^{PV}A, we also prepared an SNA tethering a single ^{PV}A (SNA-P).

Table. 2-1 SNA Sequences containing ^{PV}A residues.

	Sequence
SNA-P2P	(*S*)-GC^{PV}**A**TT^{PV}**A**GC-(*R*)
SNA-P1P	(*S*)-TCG^{PV}**A**T^{PV}**A**GA-(*R*)
SNA-P0P	(*S*)-GCT^{PV}**A**^{PV}**A**TGC-(*R*)
SNA-P	(*S*)-GCT^{PV}**A**ATGC-(*R*)

2-4-2. Interaction of ^{PV}A residues introduced into SNA strand

Insight into the interactions between ^{PV}As in SNA-PnP series was provided by comparing whose absorption and fluorescence spectras with SNA-P. Absorption spectra of the SNA-P2P strand showed a band at λ = 350–500 nm (λ_{max} = 400 nm) (Figure. 2-5a). This hypsochromic shift with respect to SNA-P strand suggested the H-aggregate formation of ^{PV}As in SNA-P2P strand. Emission of ^{PV}As in SNA-P2P strand bathochromically shifted compared with that of SNA-P (Figure. 2-5b). This results clearly indicated the excimer formation of ^{PV}As at ground state. Similar wavelength shifts were also observed at SNA-P1P and SNA-P0P (Figure. S2-3), suggesting that these chromophores were located in close enough to undergo photo-cycloaddition in the SNA-PnP series.
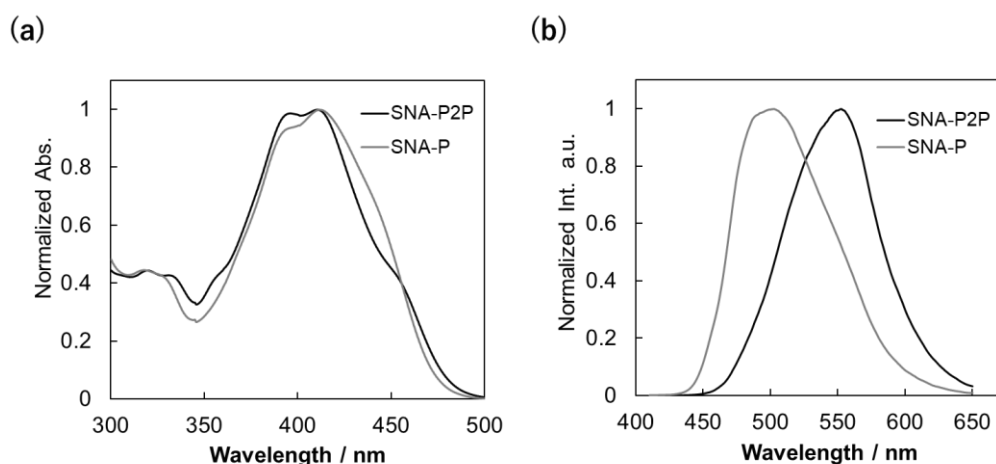
Figure. 2-5 (a) Normalized absorption spectra of SNA-P2P and SNA-P sequences. (b) Fluorescence spectra of SNN/RNA and SN/RNA duplexes. λ_{ex} = 400 nm. Conditions: 100 mM NaCl, 10 mM phosphate buffer (pH 7.0), 20 °C. Concentration of SNA was 5.0 M.

2-4-3. Reactivity of [PV]As in single stranded SNA

First, in order to verify the photo-reaction of SNA containing two [PV]As, we irradiated single stranded SNA-P2P with 455 nm light. The absorption band at around 400 nm present before irradiation immediately decreased and almost disappeared after 2 min (Figure. 2-6a). Simultaneously, new bands appeared at 270 and 354 nm, which correspond to absorption bands of alkylpyrene. A similar behavior was observed upon photo-crosslinking of styrylpyrene,[13] suggesting that an intra-strand photo-adduct of two [PV]As was formed. Upon irradiation of the cross-linked product with 340 nm light, the initial absorption bands were restored, indicating the recovery of [PV]A monomers (Figure. 2-6b). Furthermore, isosbestic points at 330 and 361 nm are indicative of selective photo-cycloaddition and cycloreversion reaction between the two [PV]A residues.

The fluorescence spectra before and after the light irradiation reaction were also measured (Figure. 2-7 and S2-1). After irradiation at 455 nm, the emission corresponding to [PV]A disappeared almost completely. Further irradiation at 340 nm restored the initial peak. On the other hand, interestingly, when the sample after 455 nm irradiation was

excited at λ = 340 nm, alkylpyrene-like fluorescence was observed: suggesting the formation of crosslink adduct. The series of results suggests the progression of reversible photo-cycloaddition reaction.
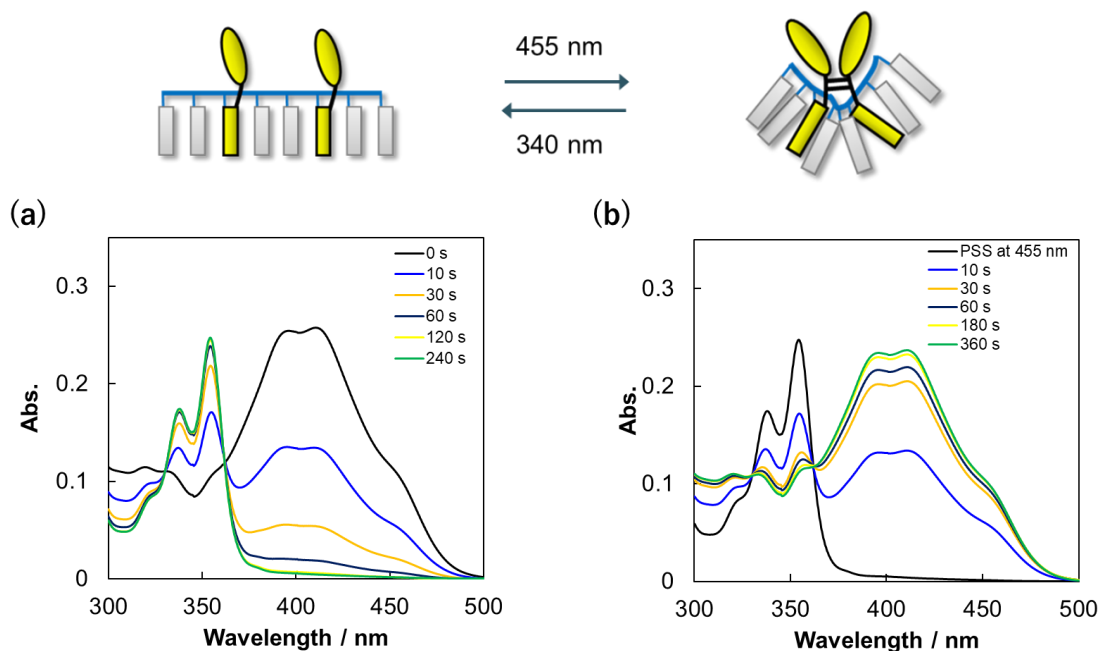

Figure. 2-6 (a) Absorption spectra of SNA-P2P after indicated times of irradiation with 455 nm light. (b) Absorption spectra of at photo-stationary state (PSS) at 455 nm and after irradiation for the indicated times with 340 nm light. Irradiation was performed at 20 °C. Conditions: 100 mM NaCl, 10 mM phosphate buffer (pH 7.0), 20 °C. Concentration of SNA was 5.0 M.
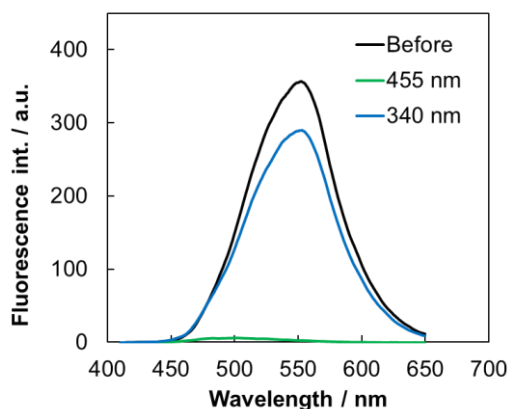

Figure. 2-7 Fluorescence spectra and of SNA-P2P before irradiation (black lines), PSS at 455 nm light (green lines), and PSS at 340 nm light (blue lines). λ_{ex} = 400 nm. Solution conditions were 5.0 μM duplex, 100 mM NaCl, 10 mM phosphate buffer (pH 7.0) at 20 °C. PSS was attained by irradiation with 455 nm for 4 min or 300 nm for 6 min.

HPLC analysis of SNA-P2P was also performed to analyze the photo-reaction (Figure. 2-8 and S2-2). The peak with retention time of 25 min present before light irradiation almost completely disappeared upon irradiation with 455 nm light, and a new single peak appeared at shorter retention time (18 min), corresponding to the intra-strand photo-crosslinked product of SNA-P2P. Eventually, irradiation with 340 nm light restored the initial peak accompanied with decreasing peak of adduct.
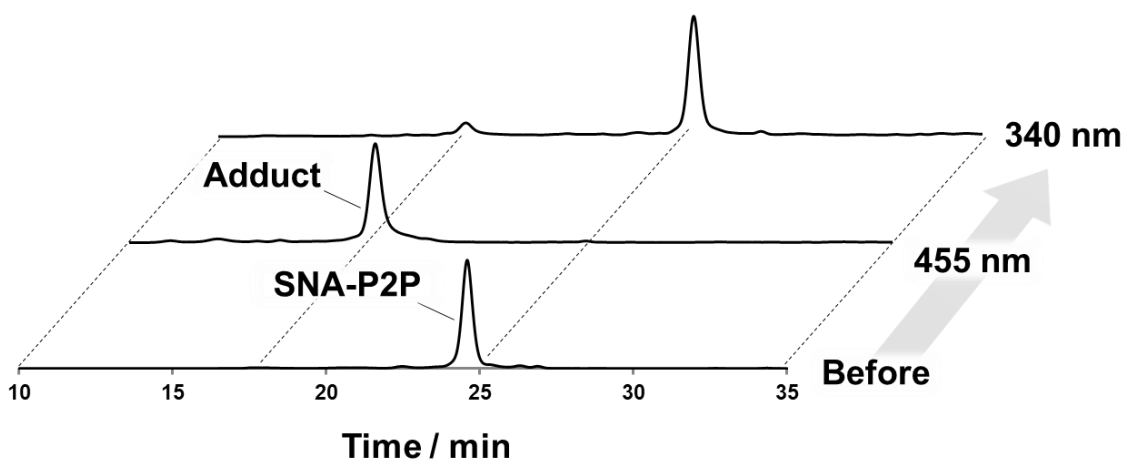

Figure. 2-8 Reversed-phase HPLC profiles of single-stranded SNA-P2P before and after irradiation at 455 nm for 360 s and 340 nm for 360 s. Absorbance was monitored at 260 nm.

Next, in order to verify whether [PV]As in SNA also respond to thermal-stimulus, we kept SNA-P2P and their cycloaddition adduct at 80 °C. (Figure. 2-9). As a result, the absorption spectra of them did not change at all even after 3 hours had passed, and it was indicated that both of them had extremely high thermal stability. In other words, [PV]A in SNA did not cause an unintended reaction by heat unlike azobenzene: only responds to photo-stimulus.
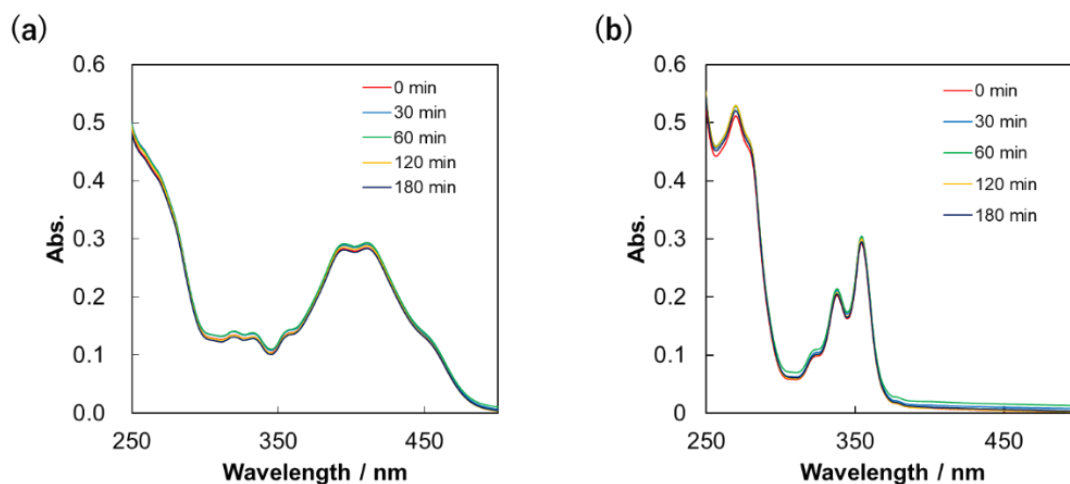
Figure. 2-9 Thermal stability of SNA-P2P (a) before irradiation and (b) at PSS with 455 nm light. Absorption spectra were measured after incubation at 80 °C for an hour (orange line) and three hours (red line). No spectral change was observed even after heating for three hours, indicating sufficient thermal stability of both photo stationary states. Conditions: 100 mM NaCl, 10 mM phosphate buffer (pH 7.0). The concentration of oligomer or duplex was 5.0 μM.
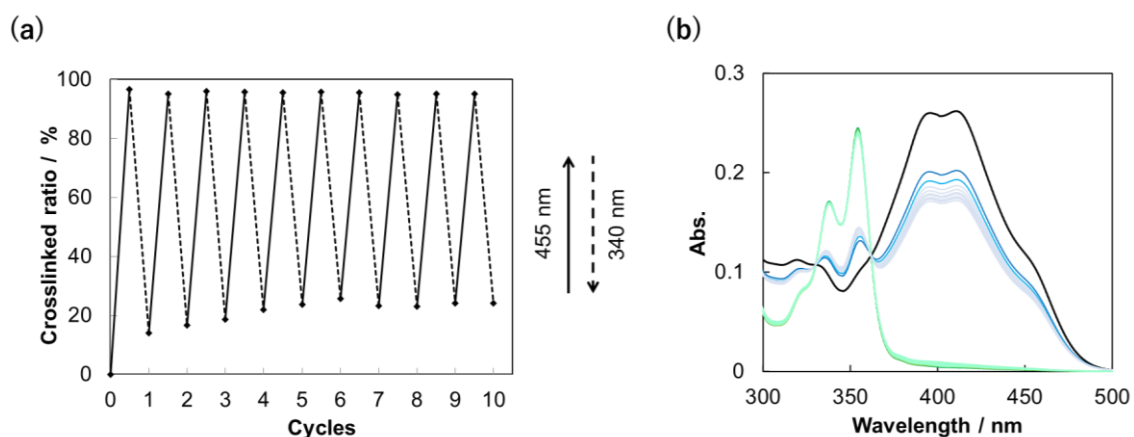
Figure. 2-10 (a) Percent crosslink after the indicated number of photo-switching cycles. Irradiation times were 120 s at 455 nm and 60 s at 340 nm. The percent crosslink was calculated from absorbance at 400 nm recorded after each irradiation. (b) Absorption spectra of single-stranded SNA-P2P after repeated irradiation cycles. Conditions: 100 mM NaCl, 10 mM phosphate buffer (pH 7.0), 20 °C. The concentration of SNA was 5.0 μM. Irradiation with 455 nm for 2 min, 340 nm for 1 min.

The reversibility of the ^{PV}As cross-linking reaction in SNA-P2P was investigated by repeated irradiation with 455 nm and 340 nm light. As a result, it was found that 10 cycles of repetitive photo-switching of the ^{PV}A was possible with only a little photo-bleaching (Figure. 2-10).

These experiments confirmed that the intra-strand crosslinking of ^{PV}As in a single-stranded SNA occurred rapidly, reversibly, and efficiently by only light stimulus.

2-4-4. Effect of the position of the substitution with ^{PV}A

2-4-4-1. Effect on photo-reactivity

Next, we evaluated the effect of an interval between two ^{PV}As on the photo-crosslinking reaction by analysis of single stranded SNA-P2P, SNA-P1P, and SNA-P0P. As a result, all of three modified SNAs caused similar reactions: efficient photo-crosslinking reaction by 455 nm irradiation (Figure. S2-3, S2-4a and S2-5a). The reaction rate of photo-crosslinking reaction did not change significantly depending on interval between ^{PV}As. The reverse reaction: photo-cycloreversion by 340 nm irradiation was also observed in each modified SNA sequence, however, it was slightly suppressed when ^{PV}A in SNA-P0P (Figure. S6b). The reaction in SNA-P0P was slightly slower than in the other oligomers and eventually 67% of ^{PV}A was restored by irradiation with 340 nm for 720 s; same irradiation can restore more than 90% of ^{PV}A in other SNA-PnP series. A blue shift of the absorption band and a red shift of fluorescent emission of ^{PV}As in SNA-P0P with respect to SNA-P2P and SNA-P1P suggested that the ^{PV}As in SNA-P0P are interacting more strongly than those in other SNA-PnP series. This stronger stacking-interaction of ^{PV}As is one possible reason for the slight suppression of the cycloreversion reaction in SNA-

P0P. Anyway, intra-strand photo-cycloaddition/cycloreversion of ^{PV}As in single stranded SNA-PnP series were efficiently caused regardless of interval between two ^{PV}As.

On the other hand, when single stranded SNA-P was exposed to 455 nm light, ^{PV}A in SNA-P mainly caused *cis*-isomerization reaction: same as reported photochromic arylvinyl guanines. In addition, a small amount of inter-strand photo-crosslinking reaction was also induced by irradiation (Figure. S2-7). These reactions were not observed at all in the SNA-PnP series. Presumably, stacking interaction of the two ^{PV}As suppressed these reactions and allowed the selective progression of the intra-strand photo-crosslinking reaction.
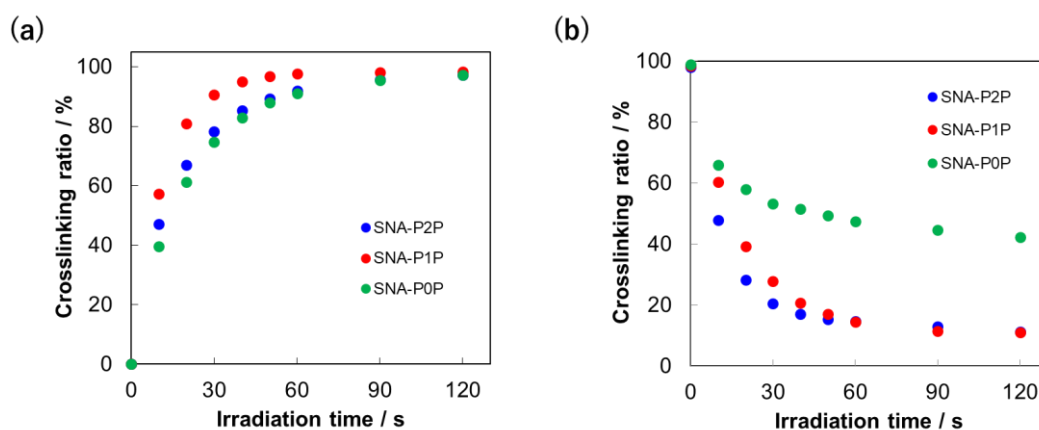

Figure. 2-11 Dependence of percent crosslink on the time of irradiation with (a) 455 nm and (b) 340 nm light in the single strand. The percentages of crosslinked products were calculated from absorbance at 400 nm.

2-4-4-2. Effect on duplex stability

In order to determine the effect of ^{PV}As substitution on the duplex stability, we measured melting temperatures (T_m) of all modified SNA/RNA duplexes at before irradiation (Table. 2-2, Figure. 2-12). As a result, SNA-P/RNA duplex was slightly destabilized compared to the control SNA-N/RNA duplex, suggesting that ^{PV}A can pair with uracil as canonical

adenine does. However, SNA-P2P and SNA-P1P did not form duplexes with complementary RNA. The strong stacking interaction between the two ^{PV}A residues presumably distorted the SNA strand seriously and suppressed duplex formation even before irradiation. On the other hand, the T_m of SNA-P0P/RNA duplex was closed to that of SNA-N/RNA duplex. This result suggested that the adjacent ^{PV}A residues in SNA-P0P adopt a stacked structure in the single strand that is similar to that in the duplex (Figure S9). In addition, this non-covalent interaction of adjacent ^{PV}As can increase the rigidity of the single-strand SNA and reduce the entropy loss associated with duplex formation.

The circular dichroism (CD) spectra of the SNA-P/RNA duplex and SNA-P0P/RNA duplex at before light irradiation were also measured (Figure. S2-10 and S2-14). As a result, CDs of both duplexes has a positive band at $\lambda = 260$ nm, which is in good agreement with the unmodified SNA/RNA duplex, suggesting that ^{PV}A substitution does not significantly affect the overall structure of the A-form duplex. In addition, in the SNA-P0P / RNA duplex, CD derived from the exciton coupling of ^{PV}A was also confirmed around 400 nm, suggesting that ^{PV}A was arranged along the spiral of the SNA/RNA duplex. Interestingly, the shape of the absorption and fluorescence spectra of the SNA-P0P/RNA duplex was more similar to the other SNA-PnP series than the single-stranded SNA-P0P (Figure. S2-10a). This implies that the interaction between ^{PV}As was slightly weakened by forming a duplex. Therefore, the reversibility of the cross-linking reaction of SNA-P0P / RNA should be better than that of single strand.

All the above results showed that the best design for controlling the formation and dissociation of SNA duplexes is SNA-P0P: SNA containing adjacent ^{PV}As.
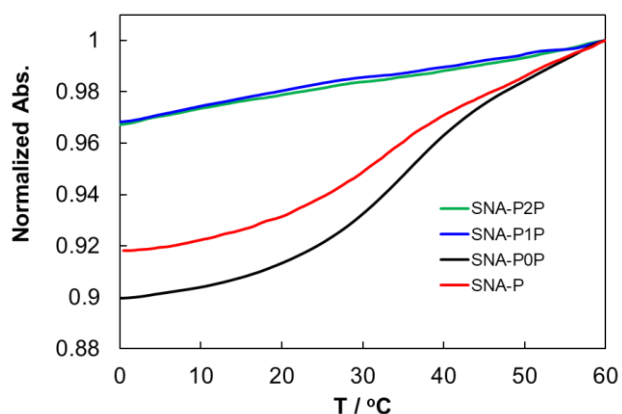
Figure. 2-12 Melting profiles of SNAs with complementary RNA. Conditions: 5.0 μM oligonucleotide, 100 mM NaCl, 10 mM phosphate buffer (pH 7.0).

Table. 2-2 Melting temperature (T_m) of SNA-PnP/RNA duplexes and SNA-P/RNA duplex

T_m with complementary RNA	
SNA-P2P/RNA	N.A.
SNA-P1P/RNA	N.A.
SNA-P0P/RNA	35.1 °C
SNA-P/RNA	30.0 °C
SNA-N/RNA	35.0 °C

2-4-5. Photo-regulation of SNA/RNA duplex formation

Next, we examined the photo-regulation of SNA-P0P/RNA duplex formation. Upon irradiation with 455 nm light at 20 °C, a temperature at which all strands are involved in duplex structures, the absorption band at around 400 nm decreased with irradiation time (Figures. 2-13 and S2-9). Irradiation for 1 h resulted in almost complete photo-crosslinking (Figure 2-13b green plots). The photo-crosslinking reaction was slower than that observed when SNA-P0P was single stranded. Upon irradiation with 340 nm light, 90% of the cross-linking was reversed within 15 min (Figure 2-13b, blue plots), clearly demonstrating efficient photo-cycloreversion. It should be noted that photo-

28

cycloreversion in the presence of complementary RNA was more effective than in its absence as we expected. The progress of this reversible photo-crosslinking reaction was also confirmed from changing of the fluorescence intensity of ^{PV}A (Figures. S2-12).
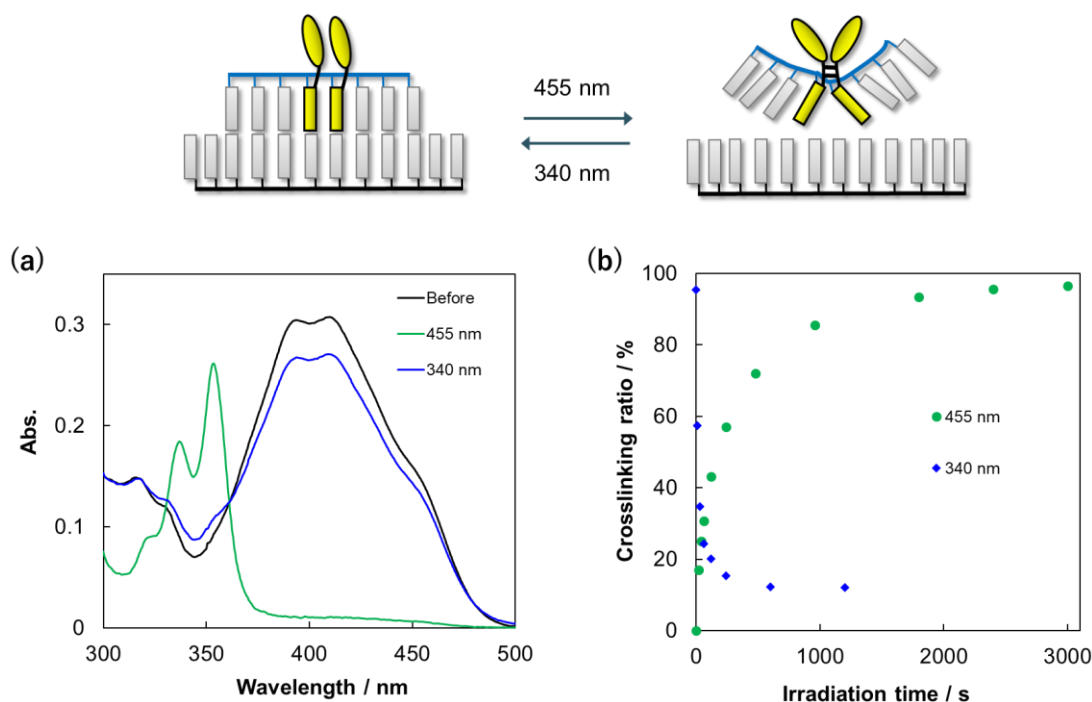

Figure. 2-13 (a) Absorption spectra of SNA-P0P/RNA duplex before (black lines) and after irradiation with 455 nm light (green lines) and 340 nm light (blue lines). Solution conditions were 5.0 μM duplex, 100 mM NaCl, 10 mM phosphate buffer (pH 7.0) at 20 °C. (b) Crosslinking ratio of ^{PV}As in SNA-P0P/RNA duplex at each irradiation time. Crosslinking ratio was calculated from absorbance at 400 nm, assuming crosslinked product has no absorbance at 400 nm.

Irradiation with 455 nm light also eliminated the induced CD at around 400 nm, which also indicated progress of cycloaddition reaction of ^{PV}A residues (Figure. 2-14b). In addition, after visible light irradiation the CD of SNA-P0P/RNA around 260 nm was in good agreement with that of single-stranded RNA (Figure. S2-11, complementary strand of SNA-P0P), suggesting that crosslinked SNA-P0P did not interact with RNA: duplex dissociation. Irradiation with 340 nm light restored the initial CD signals.
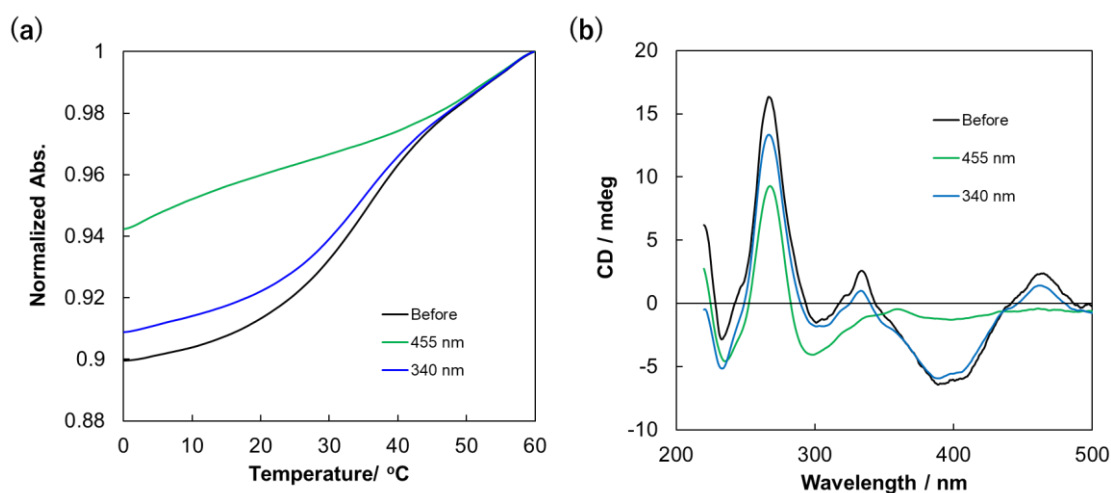
29

Figure. 2-14 (a) Melting temperature and (b) CD spectra of SNA-P0P/RNA duplex before (black lines) and after irradiation with 455 nm light (green lines) and 340 nm light (blue lines). Solution conditions were 5.0 μM duplex, 100 mM NaCl, 10 mM phosphate buffer (pH 7.0) at 20 °C.

Table. 2-3 Melting temperature (T_m) of SNA-P0P/RNA after 455 nm and 340 nm irradiation.

T_m with complementary RNA	
455 nm	N.A.
340 nm	36.2 °C

Melting temperatures were measured after irradiation at 455 nm and 340 nm to confirm whether duplex formation was regulated by the reversible photo-crosslinking reaction. As a result, expectedly, no melting transition was observed after irradiation at 455 nm, proving that the duplex was dissociated (Figure. 2-14a). By virtue of the high reactivity of the cycloreversion, irradiation with UV light restored sigmoidal melting, and duplex stability (T_m) was almost the same as before irradiation. (Table. 2-3).

In the presence of the complementary RNA, repetitive photo-regulation by alternating irradiation with 455 and 340 nm light was also possible without significant photobleaching (Figure. 2-15).
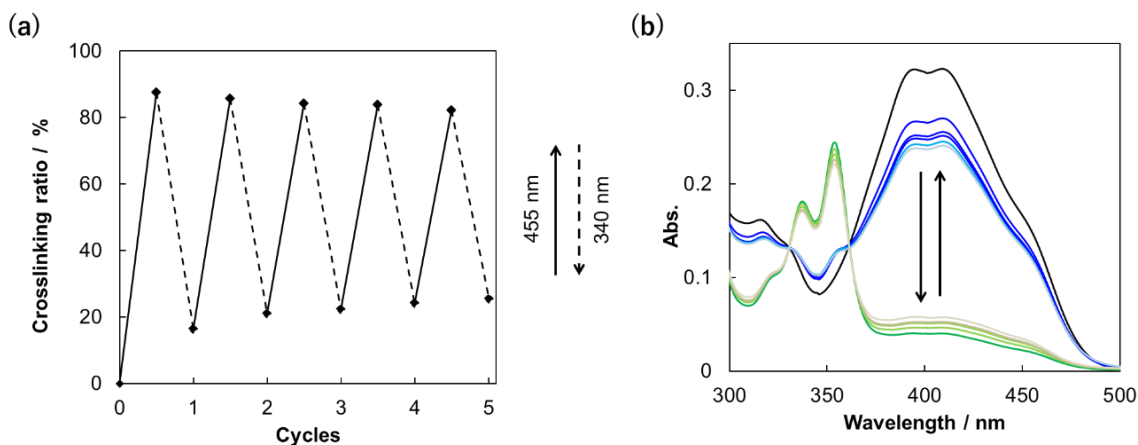
Figure. 2-15 Percent crosslink of SNA-P0P/RNA after multiple photo-switching cycles. Samples were irradiated at 455 nm for 30 min and at 340 nm for 10 min. The reaction ratios were calculated by using absorption spectra recorded after each irradiation. (f) Absorption spectra of SNA-P0P/RNA after repeated irradiation cycles. Conditions: 100 mM NaCl, 10 mM phosphate buffer (pH 7.0), 20 °C. The concentration of duplex was 5.0 μM.

We also irradiated with 455 nm and 340 nm light for SNA-P/RNA duplex at 20 °C. Change in absorption spectra suggested that photo-irradiation at 455 nm caused only *cis*-isomerization of ^{PV}A in SNA-P: suppression of inter-strand crosslinking (Figure S2-15a). Subsequently irradiation at 340 nm restored the initial absorption of SNA-P/RNA (Figure. S2-15b). Melting temperature of SNA-P/RNA duplex decreased after 455 nm irradiation and recovered by 340 nm irradiation (Figure. S2-15 and Table. S2-2, $\Delta T_m = 5.4$ °C). These results indicate that duplex stability of SNA/RNA can be photo-regulated also by steric hindrance of the *cis*-^{PV}A, however, the effect was limited. Moreover, as described above, introduction of multiple ^{PV}As at separated position in SNA cannot be guaranteed duplex stability at before irradiation. That is why, the method based on photo-isomerization cannot lead to complete dissociation of SNA. In other words, efficient control of duplex formation/dissociation is possible only by utilizing the cross-linking reaction of ^{PV}As.

2-4-6. Evaluation of photo-control of SNA/RNA duplex formation by fluorescence

Next, we aimed to evaluate photo-control of dissociation and re-formation of the duplex by fluorescence (Figure. 2-16). For this purpose, a quencher was attached to the end of the SNA strand, and a fluorophore was attached to the end of the complementary RNA strand. Prior to light irradiation, SNA form duplex with RNA, fluorescence should be quenched by adjacent quencher. On the other hand, if the duplex dissociates based on photo-crosslinking, the fluorophore separates from the quencher and fluorescence intensity is enhanced. That is why, using this system, dissociation ratio of duplex can be calculated from change of fluorescence intensity directly.
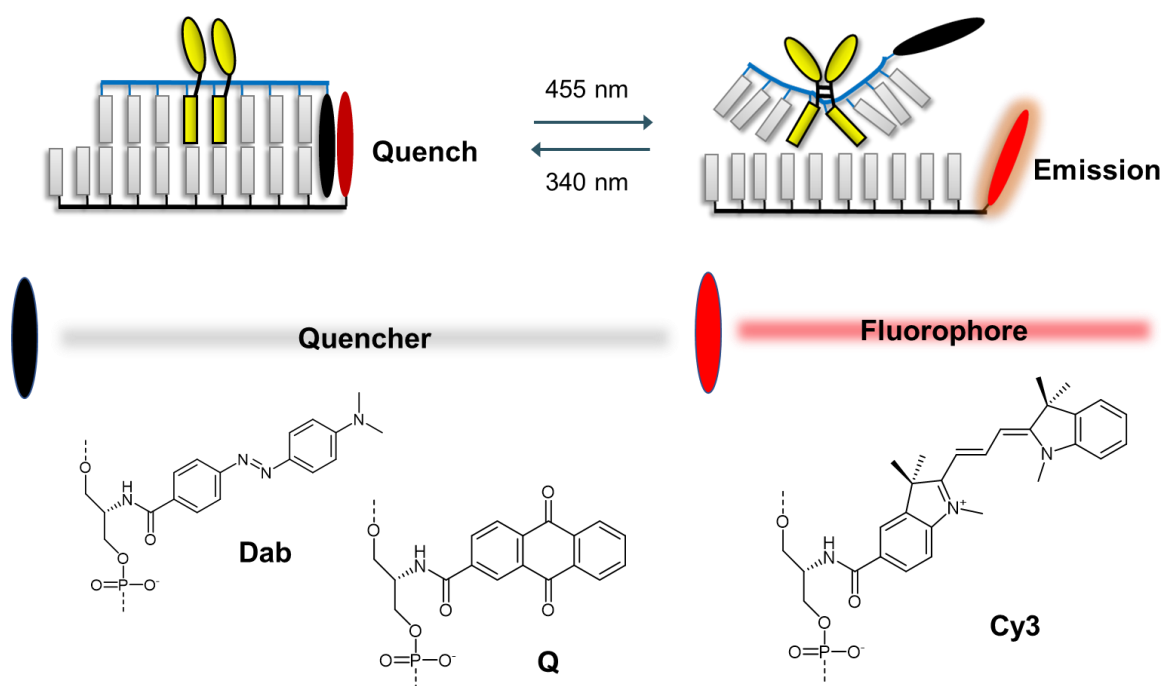

Figure. 2-16 Analysis of hybridization of SNA/RNA based on the change in fluorescence change induced by light irradiation at 20 °C. Illustration of the design of this experiment. Fluorescence from Cy3 tethered to the RNA is quenched by duplex formation with SNA containing dabcyl or anthraquinone.

2-4-6-1. Effect of the fluorophore and quencher on photo-reactivity and duplex stability

In this design, quencher in SNA and fluorophore in RNA should not inhibit duplex formation at before irradiation and must not quench the reversible cycloaddition of ^{PV}As. In this study, we prepared SNA containing DABCYL: Dab or anthraquinone: Q as a quencher, and RNA containing Cy3 as a fluorophore, and investigated a pair suitable for fluorescence observation of duplex formation.

Prior to light irradiation, the melting temperature of the SNA-P0P/Cy3-RNA duplex was first measured (Table. 2-4). As a result, it was shown that the introduction of Cy3 does not significantly destabilize the duplex (T_m = 27.7 °C). Furthermore, the introduction of each quencher increased the T_m of the SNA/RNA duplex. In particular, the strong interaction between Cy3 and Dab in SNA-P0P-Dab/Cy3-RNA greatly contributed to the stabilization of the duplex.

Table. 2-4 Sequence of quencher introduced ^{PV}A-SNA for fluorescence observation of duplex formation and melting temperatures of duplexes with complementary Cy3-RNA

	Sequence	T_m with complementary Cy3-RNA
SNA-P0P	(S)-GCT^{PV}**A**^{PV}**A**TGC-(R)	27.7 °C
SNA-P0P-Dab	(S)-**Dab**-GCT^{PV}**A**^{PV}**A**TGC-(R)	40.2 °C
SNA-P0P-Q	(S)-**Q**-GCT^{PV}**A**^{PV}**A**TGC-(R)	28.0 °C

Next, Single stranded SNA-P0P-Dab and SNA-P0P-Q were exposed to 455 nm light and 340 nm light to investigate the effect of each quencher on reactivity of ^{PV}A. The ^{PV}A in SNA-P0P-Dab has much lower reactivity than that in SNA-P0P, and the ^{PV}As were not

sufficiently crosslinked in this system even after 3 hours irradiation of visible light (Figure. 2-17a). The large overlap between the absorption spectrum of Dab and the fluorescence spectrum of ^{PV}A suggests that efficient energy transfer (FRET) from ^{PV}A to Dab occurs, and this is presumably the main cause of the extremely low reactivity in SNA-P0P-Dab.
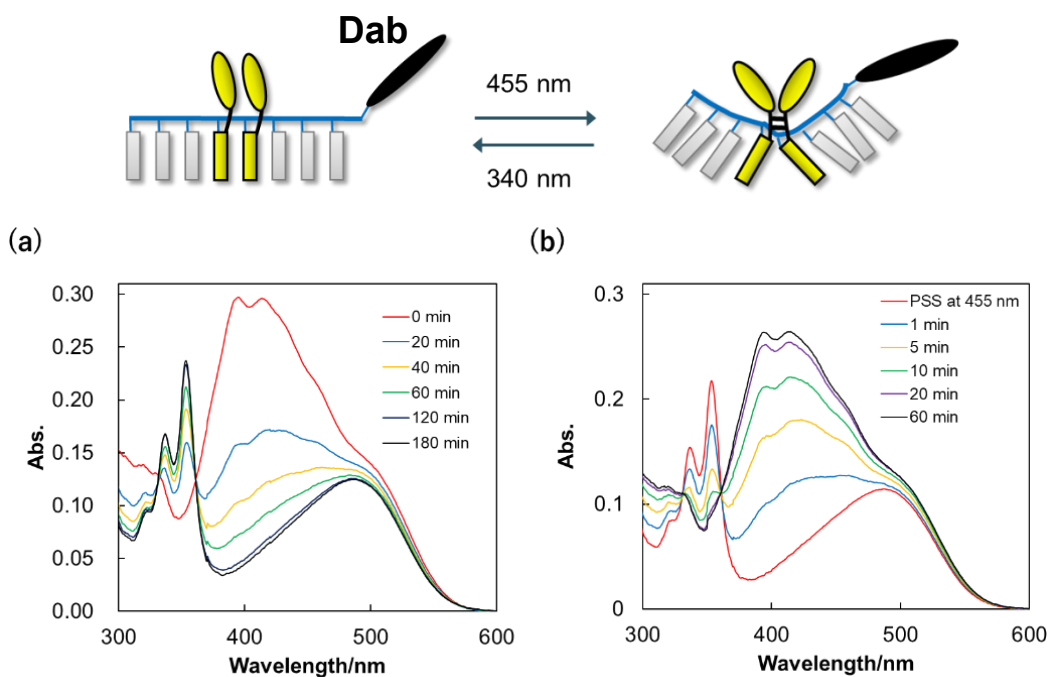

Figure. 2-17 Absorption spectra of SNA-P0P-Dab upon irradiation with (a) 455 nm light followed by (b) 340 nm light. Reactions were significantly slower than that of SNA. Conditions: 100 mM NaCl, 10 mM phosphate buffer (pH 7.0), 20 ºC. The concentration of oligomer or duplex was 5.0 μM.

On the other hand, over 80% of SNA-P0P-Q was crosslinked after 1 hour irradiation of visible light, and the decrease in reactivity to SNA-P0P was not as remarkable as that of SNA-P0P-Dab (Figure. 2-18a). Trapping of excited electron of ^{PV}A by anthraquinone which is a strong electron acceptor should also inhibit the photo-crosslinking reaction, but whose effect seems to be much smaller than the energy transfer between ^{PV}A and Dab.

  In addition, when crosslink adducts of either quencher introduced ^{PV}A-SNA were exposed to UV-A light, they caused cycloreversion (Figure. 2-17b and 2-18b). Eventually, in these systems, over 70% of ^{PV}A was restored, which is more efficient than SNA-P0P.

This result indicated that each quencher did not interfere with the reverse reaction and decreased reactivity of photo-crosslinking worked in favor of cycloreversion by UV-A.
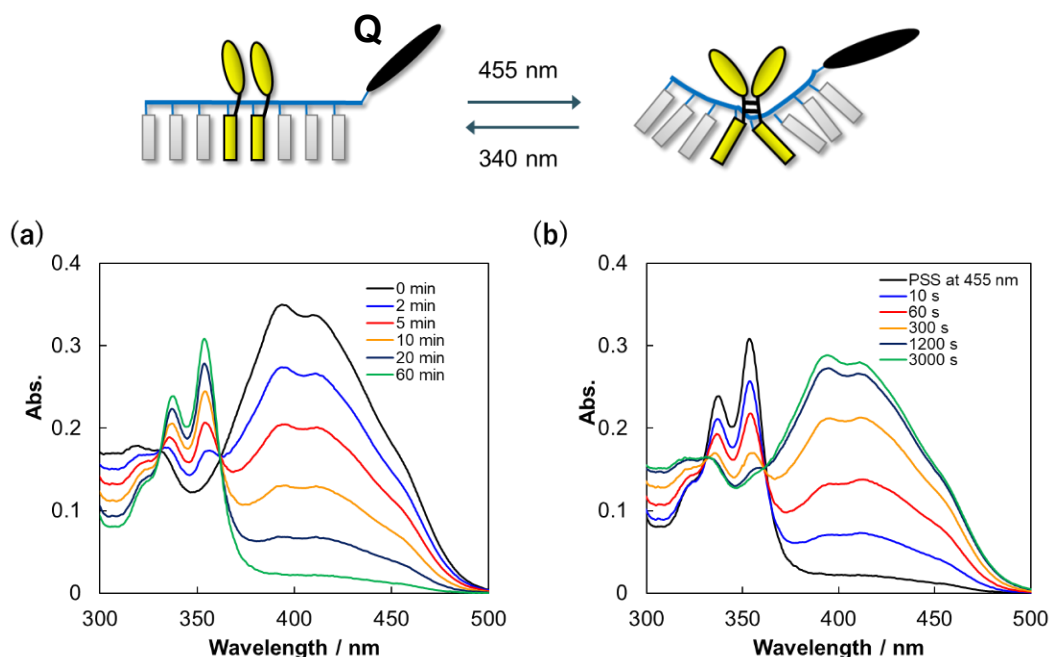

Figure. 2-18 Absorption spectra of SNA-P0P-Q upon irradiation with (a) 455 nm light followed by (b) 340 nm light. Reactions were significantly slower than that of SNA. Conditions: 100 mM NaCl, 10 mM phosphate buffer (pH 7.0), 20 °C. The concentration of oligomer or duplex was 5.0 μM.

The SNA-P0P/Cy3-RNA duplex was also irradiated with Vis/UV-A light to investigate the effect of Cy3 tethered to RNA on reactivity. Change in absorption spectra suggest that cycloaddition and cycloreversion of SNA-P0P/Cy3-RNA occurred on approximately the same time scale as the SNA-P0P/RNA system, suggesting that Cy3 has little effect on photo-reactivity (Figure. 2-19).

Based on the above results, we selected SNA-P0P-Q/Cy3-RNA for fluorescence observation of duplex formation.
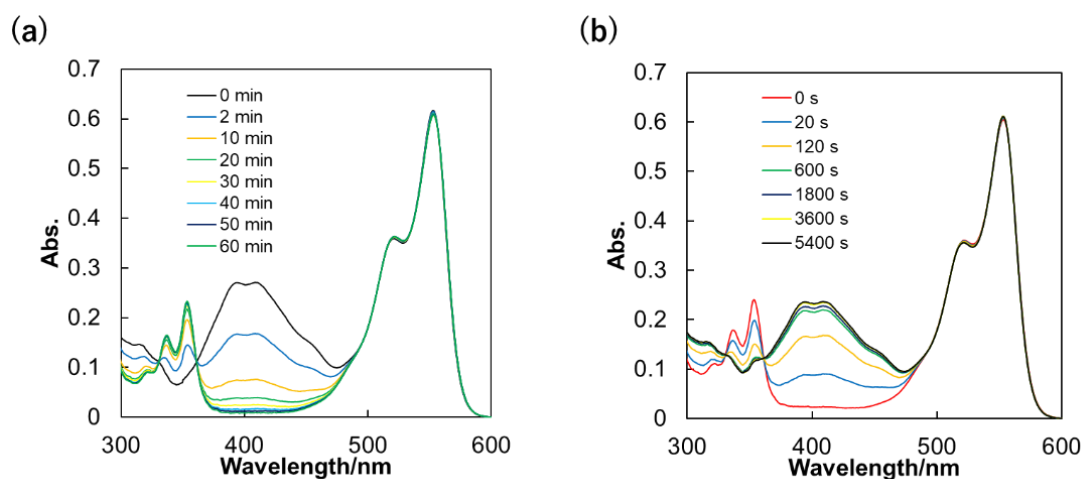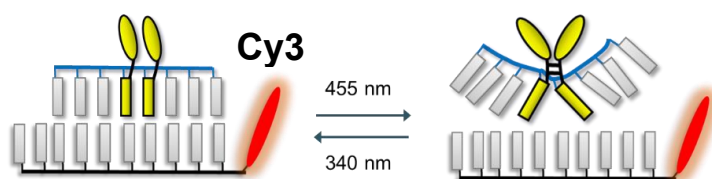
Figure. 2-19 Absorption spectra of SNA-P0P/RNA-Cy3 after irradiation with (a) 455 nm light followed by (b) 340 nm light. Conditions: 100 mM NaCl, 10 mM phosphate buffer (pH 7.0), 20 °C. The concentration of oligomer or duplex was 5.0 μM. Introduction of Cy3 into complementary RNA strand does not significantly affect to reactivity of photo-cycloaddition/cycloreversion.

2-4-6-2. Fluorescence analysis of duplex formation/dissociation

First, we obtained dissociation ratio of SNA-P0P-Q/Cy3-RNA duplex from melting profiles by fluorescent change of both single stranded Cy3-RNA and the duplex. As a result, it was confirmed that nearly 80% of the SNA-P0P-Q/Cy3-RNA formed duplex at temperature below 20 °C (Figure. S2-17a). In other words, irradiating light at this temperature range should allow us to observe the duplex formation/dissociation.

455 nm light was irradiated for the SNA-P0P-Q/Cy3-RNA duplex at 5 °C, 10 °C, 15 °C, and 20 °C (Figure. 2-20a and S2-17b, c). As a result, the photo-crosslinking reaction proceeded at all temperature, however, there was a large difference in reactivity. In particular, the reactivity remarkably decreased at the low temperatures. On the other hand, at 20 ° C, the photo-crosslinking reaction proceeded over 70% by irradiation with visible

light for 3 hours, indicated that 20 °C is optimal for fluorescence observation of duplex dissociation based on crosslinking. When 340 nm light was subsequently irradiated at 20 °C for 50 min, cycloreversion also progressed more than 80% (Figure. 2-20b).
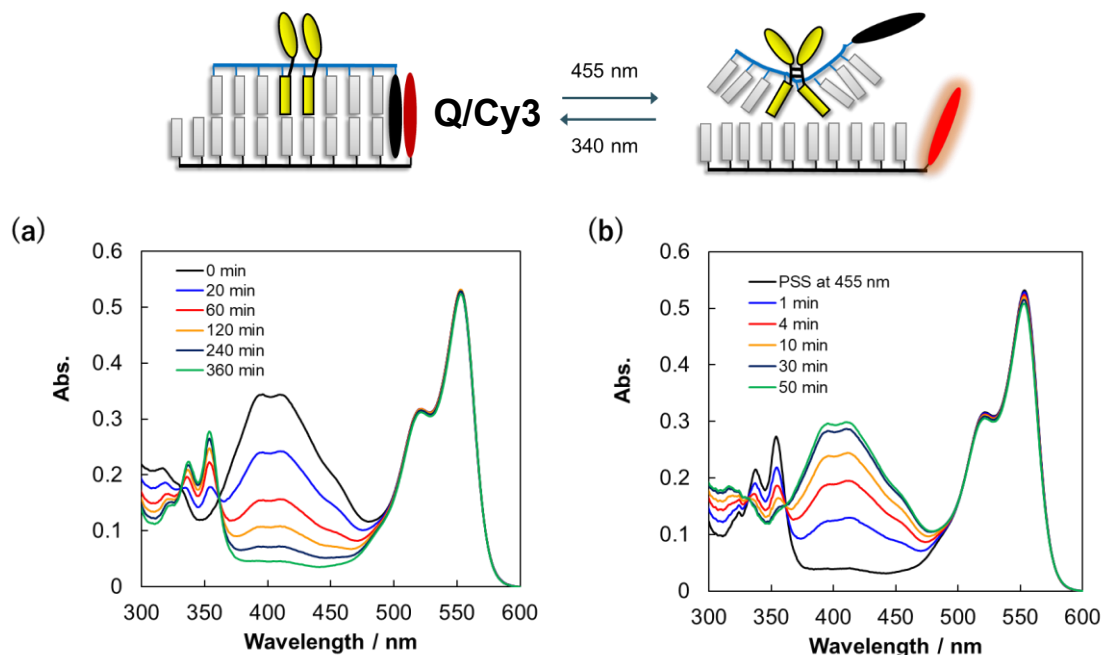

Figure. 2-20 Absorption spectra of SNA-P0P-Q/RNA-Cy3 upon irradiation with (a) 455 nm light followed by (b) 340 nm light. Conditions: 100 mM NaCl, 10 mM phosphate buffer (pH 7.0), 20 °C. The concentration of oligomer or duplex was 5.0 μM.

Irradiation at 455 nm also increased the emission intensity of Cy3 in SNA-P0P-Q/Cy3-RNA, which means dissociation of the duplex. We calculated dissociation ratio of duplex by using the fluorescence intensity of 5 °C SNA-P0P-Q/Cy3-RNA that completely forms a duplex and of single stranded Cy3-RNA, and plotted it against irradiation time of visible light (Figure. 2-21a and S2-19). As a result, and nearly 80% of the duplexes were dissociated after 3 hours irradiation. Furthermore, there was a correlation between the dissociation ratio of the duplex and percent crosslinking of [PV]A, demonstrated that the dissociation of the duplex is based on the cross-linking reaction.

Upon subsequent irradiation with 340 nm for 50 min, emission intensity decreased with about 70% of the duplexes re-formed (Figure. 2-21a and S2-18a).

Three cycles of photo-crosslinking were performed without serious deterioration of duplex formation (Figure. 2-21b and S2-20). Thus, the fluorescence analysis directly confirmed reversible photo-regulation of SNA/RNA duplex formation and dissociation at constant temperature.
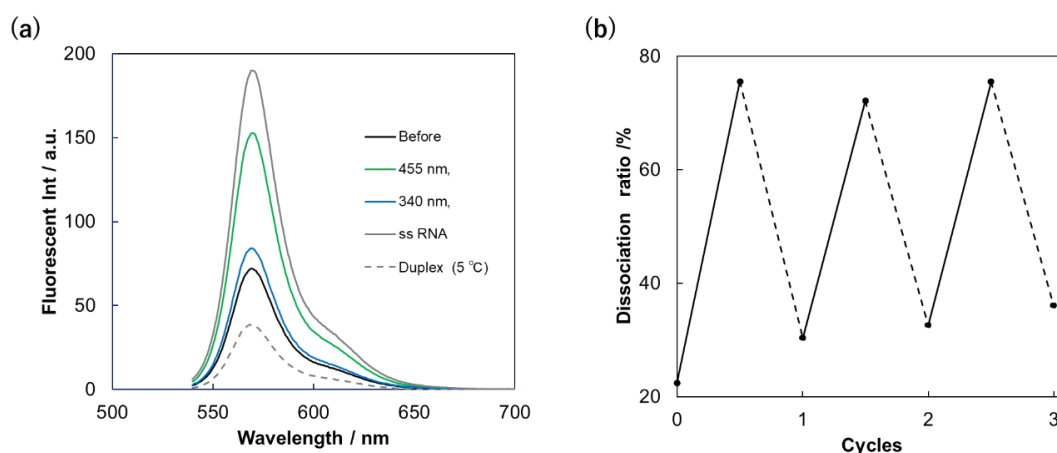
Figure. 2-21 (a) Fluorescence spectra of SNA-P0P-Q/RNA-Cy3 before irradiation (black line) and after irradiation with 455 nm for 3 h (green line), followed by 340 nm for 50 min (blue line). Analysis of single-stranded RNA-Cy3 (gray line) is shown as a reference of complete dissociation, and SNA-P0P-Q/RNA-Cy3 at 5 °C (broken line) is shown as a reference for 100% duplex. (b) dissociation ratio of duplex after multiple photo-switching cycles calculated from fluorescence intensity.

2-4-7. Photo-regulation of SNA/XNA duplex formation

As mentioned above, it was clarified that the formation of SNA/RNA duplex can be reversibly photo-controlled by utilizing the photo-crosslinking of ^{PV}A in SNA.

Following this success, finally, we examined whether the same methodology could be applied to the photo- control of hybridization between SNA and XNA. SNA or L-aTNA was prepared as a complementary XNA strand, and Vis/UV-A light was irradiated for each ^{PV}A-SNA/XNA duplex.

2-4-7-1. Photo-regulation of SNA/SNA duplex formation

Prior to light irradiation for [PV]A-SNA/SNA duplex, we investigated whether the SNA-PnP series forms stable duplex with complementary SNAs. As a result, only SNA-P0P was allowed to form a stable duplex, which was similar result with the SNA/RNA duplex system (Figure. S2-21 and Table 2-4).
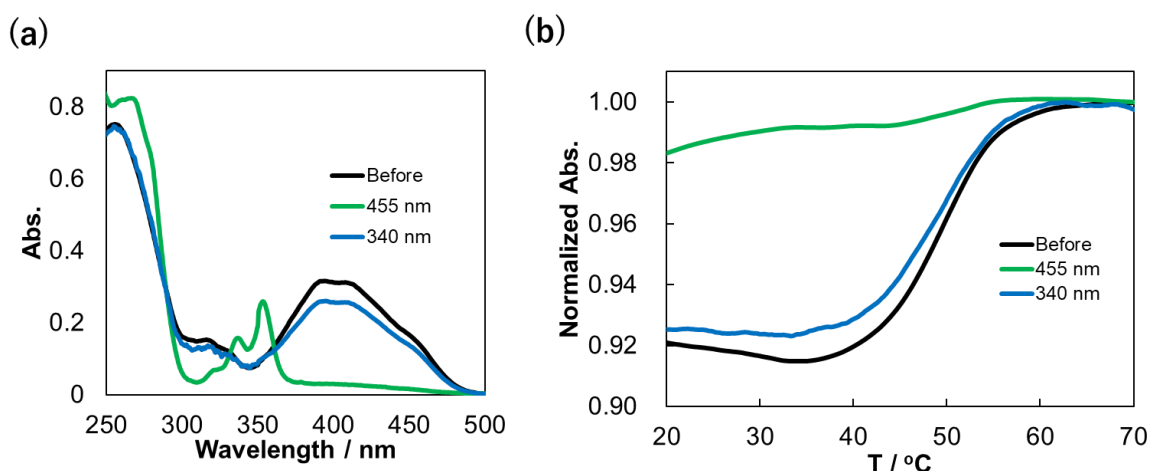

Figure. 2-22 (a) Absorption spectra and (b) Melting temperature of SNA-P0P/SNA duplex before (black lines) and after irradiation with 455 nm light (green lines) and 340 nm light (blue lines). Solution conditions were 5.0 μM duplex, 100 mM NaCl, 10 mM phosphate buffer (pH 7.0) at 40 ℃.

Table. 2-5 Melting temperature (T_m) of SNA-P0P/SNA after 455 nm and 340 nm irradiation.

	T_m with complementary SNA
Before irradiation	49.9 ℃
455 nm	N.A.
340 nm	49.5 ℃

When SNA-P0P/SNA duplex was exposed to visible light at 40 ℃ the photo-crosslinking reaction proceeded (Figure. 2-22). visible light irradiation for 240 min converted more than 90% of [PV]A into crosslinked adduct. After 455 nm irradiation, the melting temperature remarkably decreased, confirmed that duplex was completely dissociated at

40 °C (Figure. 2-22b green line and Table. 2-5). Upon irradiation with UV-A light for 30 minutes restored ^{PV}A and restored sigmoidal melting (Figure. 2-22b blue line). In other words, the photo-crosslinking reaction of ^{PV}A could be applied to the control of hybridization between SNAs.

2-4-7-2. Photo-regulation of SNA/L-*a*TNA duplex formation

We also verified the photo-control of SNA duplex forming when L-*a*TNA was used as the complementary strand. Reversible photo-crosslinking reaction proceeded efficiently by irradiation with Vis/UV-A light at 40 °C (Figure. 2-23a). T_m of SNA-P0P/L-*a*TNA duplex significantly reduced after the photo-crosslinking ($\Delta T_m > 50$ °C), whereas the cycloreversion reaction regenerated formation of duplex (Figure. 2-23b and Table. 2-5).

Interestingly, the photo-crosslinking reaction of ^{PV}A in SNA/SNA was faster than in SNA/L-*a*TNA. As there is no significant difference in the melting temperatures of these duplexes, difference in reactivity should be explained not by the dissociation ratio of the duplexes before irradiation but by their duplexes structure mainly. As a result of measuring the CD spectra of both duplexes before irradiation, CD based on the exciton coupling of ^{PV}A was confirmed only in the SNA/L-*a*TNA duplex (Figure. S2-24). Presumably, ^{PV}As in SNA/L-*a*TNA duplex stacked along the right-handed double helix structure, whereas co-facial stacking of ^{PV}A was allowed in the SNA/SNA duplex. This difference in stacking of ^{PV}A is one of the possible reasons for difference in reactivity. Anyway, hybridization of SNA was also successfully photo-controlled even when acyclic XNAs were used for the complementary strands. In other words, this novel strategy using ^{PV}A is extremely versatile and should be applicable to other various acyclic XNAs for their photo-regulation.
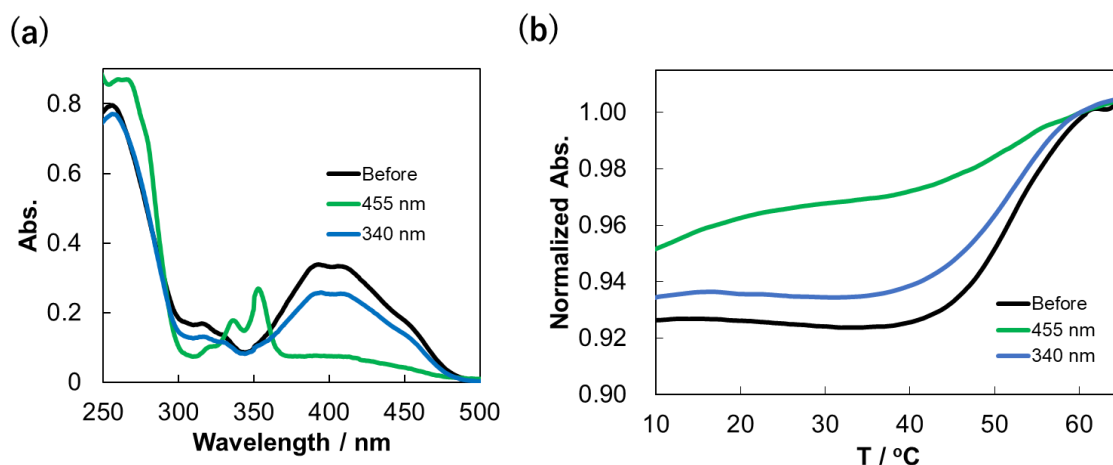
Figure. 2-23 (a) Absorption spectra and (b) Melting temperature of SNA-P0P/L-*a*TNA duplex before (black lines) and after irradiation with 455 nm light (green lines) and 340 nm light (blue lines). Solution conditions were 5.0 µM duplex, 100 mM NaCl, 10 mM phosphate buffer (pH 7.0) at 40 °C.

Table 2-6. Melting temperature (T_m) of SNA-P0P/L-*a*TNA after 455 nm and 340 nm irradiation.

	T_m with complementary L-*a*TNA
Before irradiation	52.1 °C
455 nm	N.A.
340 nm	51.2 °C

2-5. Conclusion

In this chapter, a novel methodology for photo-controlling hybridization between SNA and the complementary strand was developed. For this purpose, new modified nucleobase: 8-pyrenylvinyl adenine (^{PV}A) was designed and introduced into SNA.

^{PV}A residues in SNA can be induced to undergo intra-strand [2 + 2] photo-cycloaddition by 455 nm light. Effective cycloreversion of the ^{PV}A photo-dimer results from irradiation with 340 nm light. These reactions occurred in high yield, rapidly, selectively, and reversibly.

41

Prior to light irradiation, the adjacent [PV]A residues in SNA (SNA-P0P) did not affect the stability and whole structure of SNA/RNA and SNA/SNA duplexes significantly.

After the [PV]A-SNA/RNA duplex was irradiated with 455 nm light, the melting temperature of duplex remarkably decreased, and 340 nm light irradiation restored duplex stability. Fluorescence analysis utilizing Cy3-labeled RNA and anthraquinone-labeled [PV]A-SNA revealed that dissociation and re-formation of SNA/RNA duplex were caused by the reversible photo-crosslinking reaction of [PV]A.

Moreover, even when using acyclic XNAs: SNA or L-*a*TNA as complementary strands of [PV]A-SNA, the reversible photo-crosslinking reaction also proceeds efficiently. In other words, not only SNA/RNA duplex but also SNA/XNA duplexes can be photo-controlled based on our novel strategy.

This is the first example of reversible photo-switching of XNA duplexes formation at constant temperature, and this is also virtually the first example of reversible photo-control of the duplex using only photo-cycloaddition and cycloreversion reaction.[13] In addition, it should also note that [PV]A and its crosslinked adduct have extremely high thermal stability. This property allowed duplex with [PV]A-SNA to respond only by photo-stimulus, unlike azobenzene-based photo-regulation methods which suffer from *cis*-to-*trans* isomerization induced by heat.

This versatile strategy should be applicable to another acyclic XNA such as PNA and L-*a*TNA for their photo-regulation. The reported approach using [PV]A makes SNAs candidates for use as various photo-regulated biological tools and in photon-fueled nanomachines.

2-6. Experimental section

Materials

Reagents for the synthesis of the ^{PV}A phosphoramidite monomer were purchased from Tokyo Kasei Co., Ltd., Wako Pure Chemical Industries, Ltd., and Aldrich. Reagents for oligomer synthesis and Poly-Pak II cartridges were purchased from Glen Research. Column for HPLC purification was purchased from Kanto Chemical Co., Ltd. RNAs were purchased from Hokkaido System Science Co., Ltd.

Photo-irradiation

A xenon light source (MAX-301, Asahi Spectra) equipped with interference filters centered at 340 nm (6.85 mW cm^{-2}) and 455 nm light-emitting diodes (LEDs; Mightex, 203 mW cm^{-2}) were used for photoirradiation. The sample solution was added to a cuvette, and the temperature of light irradiation was controlled by using a programmable temperature controller. All photoirradiation was conducted at 20 °C

Spectroscopic measurements

UV/Vis spectra were measured using a JASCO model V-560 spectrometer equipped with a programmable temperature controller; 10-mm quartz cells were used. Fluorescence spectra were measured on a JASCO model FP-6500 spectrometer equipped with a microcell holder. Wavelength of excitation laser was 400 nm for ^{PV}A and 530 nm for Cy3. CD spectra were measured on JASCO model J-820 instrument equipped with a programmable temperature controller. The sample solutions contained 100 mM NaCl, 10 mM phosphate buffer (pH 7.0). The concentration of duplex was 5.0 μM, and experiments were performed in a 10-mm quartz cell. HPLC analyses: A Mightysil RP-18GP II column

heated to 50 °C was used for HPLC analyses. The flow rate was 0.5 mL min^{-1}. A solution of 50 mm ammonium formate (solution A) and a mixture of 50 mm ammonium formate and acetonitrile (50:50, v/v; solution B) were used as mobile phases. HPLC chromatograms were monitored at 260 nm. Spectra of peaks at each retention time were recorded on JASCO EXTREMA HPLC system.

Melting-temperature measurements

Melting curves of all nucleic acid duplexes were obtained using a JASCO model V-560 spectrometer equipped with a programmable temperature controller by measuring the change in absorbance at 260 nm versus temperature. The temperature ramp was 1.0 °C min^{-1}. The melting temperature (T_m) was determined from the maximum in the first derivative of the melting curve. Both the heating and cooling curves were measured, and the Tm measurements obtained agreed within 2.0 °C. The solution conditions were (unless otherwise noted) 100 mM NaCl, 10 mM phosphate buffer (pH 7.0), 5.0 μM oligonucleotide.

Computer simulation of structures of SNA/RNA duplex

MacroModel, version 10.4 (Schrödinger) was used for conformational energy minimization. First, a canonical A-form DNA/RNA duplex was constructed. The DNA strand was displaced with SNA scaffold and minimized. After that ^{PV}A was inserted instead of natural adenine base. The amber* force field was used for the calculation.

Melting-temperature measurements:

Synthesis of 2 (step a):

A solution of 1[3a] (5.00 g, 22.6 mmol) in 80 mL 1,4-dioxane was added to an 80 mL solution of 10% disodium hydrogen phosphate in water. Bromine (5.0 g, 31 mmol) was added to this solution dropwise. After 10 min of stirring at ambient temperature, 50 mL of sodium thiosulfate aqueous solution was added dropwise. The reaction mixture was neutralized by addition of a saturated aqueous solution of $NaHCO_3$. After extraction with $CHCl_3$ twice, the collected organic phase was dried in vacuo. The residue was purified by silica gel column chromatography ($CHCl_3$: MeOH, 50:1 to 50:3) to obtain the desired 2 (3.11 g, 10.4 mmol; yield: 46%). ^{1}H-NMR [$CDCl_3$, 500 MHz] δ = 8.32 (s, 1H), 5.62 (br, 2H), 4.95 (s, 2H), 4.27 (q 2H), 1.30 (t, 3H). ^{13}C-NMR [$CDCl_3$, 125 MHz] δ = 166.3, 154.1, 153.4, 151.6, 127.7, 119.8, 62.4, 44.7, 14.1. HRMS (FAB) Calcd for $C_9H_{11}BrN_5O_2$ ($M+H^+$) 300.0096. Found 300.0104.

Synthesis of 3 (step b):

2 (3.10 g, 10.3 mmol) was dissolved in 20 mL dry pyridine under the nitrogen atmosphere. To the solution was slowly added 3.3 mL benzoyl chloride (28 mmol) with stirring at room temperature. After 1 h, 2.5 mL benzoyl chloride was added to complete the reaction, and the solution was stirred 30 min. The reaction was quenched by the addition of 10 mL MeOH. After 10 min stirring, the solution was dried in vacuo. The residue was recrystallized in 100 mL EtOH, and filtered with cold EtOH to obtain 3 (4.06 g, 7.99 mmol; yield: 77%). ^{1}H-NMR [$CDCl_3$, 500 MHz] δ = 8.60 (s, 1H), 7.85 (m, 4H), 7.50 (m, 2H), 7.38 (m, 4H), 5.01 (s, 2H), 4.28 (q 2H), 1.29 (t, 3H). ^{13}C-NMR [$CDCl_3$, 125 MHz] δ = 172.1, 165.8, 154.3, 152.3, 150.5, 134.0, 133.8, 133.0, 129.5, 128.7, 127.5, 62.6, 45.0,

14.1. HRMS (FAB) Calcd for $C_{23}H_{19}BrN_5O_4$ (M+H$^+$) 508.0620. Found 508.0584.

Synthesis of 4 (step c):

To a solution of 3 (2.20 g, 4.33 mmol) and tetrakis (triphenylphosphine) palladium (0) (0.50 g, 0.43 mmol) in 8 mL dry NMP, 2.52 mL tributylvinyltin (8.66 mmol) was added under the nitrogen atmosphere. The reaction mixture was placed in an oil bath at 110 ºC and stirred 10 min. To the solution was added chloroform and distilled water. The precipitated solid was collected by filtration, and the organic layer was dried in vacuo. The obtained solid and the residue after the organic phase was dried were purified by silica gel column chromatography (CHCl$_3$: ethyl acetate, 20:1 to 5:1) to obtain 4 (1.72 g, 3.78 mmol; yield: 87%) ^{1}H-NMR [CDCl$_3$, 500 MHz] δ = 8.61 (s, 1H), 7.87 (d, 4H), 7.47 (t, 2H), 7.35 (m, 4H), 6.60 (m, 2H), 5.80 (dd, 1H), 5.02 (s 2H), 4.25 (q, 2H), 1.27 (t,3H). ^{13}C-NMR [CDCl$_3$, 125 MHz] δ = 172.3, 166.6, 154.4, 152.5, 151.8, 150.8, 134.4, 132.8, 129.4, 128.6, 127.4, 127.3, 121.8, 62.5, 43.5, 14.1. HRMS (FAB) Calcd for $C_{25}H_{22}N_5O_4$ (M+H$^+$) 456.1672. Found 456.1657.

Synthesis of 5 (step d):

To a solution of 4 (1.72 g, 3.78 mmol), 1-bromopyrene (1.07 g, 3.81 mmol), palladium (II) acetate (0.12 g, 0.53 mmol), and triphenylphosphine (0.24 g, 0.92 mmol) in 30 mL dry DMF was added 15 mL dry triethylamine. The solution was refluxed 30 min at 110 ºC. After cooling to room temperature, 100 mL of 1N HCl and CHCl$_3$ were added. The organic phase was washed with saturated aqueous NaCl solution twice and dried in vacuo. The residue was purified by silica gel column chromatography (CHCl$_3$: ethyl acetate, 100:1 to 20:1) to obtain 5 (1.32 g, 2.01 mmol; yield: 53%). ^{1}H-NMR [CDCl$_3$, 500 MHz]

δ = 9.04 (d, 1H), 8.64 (s, 1H), 8.42 (m, 1H), 8.29 (m, 1H), 8.22 (m, 2H), 8.13 (m, 3H), 8.07-7.96 (m, 6H), 7.52 (m, 2H), 7.41 (m, 4H), 7.12 (d, 1H), 5.15 (s, 2H), 4.29 (q, 2H), 1.29 (t,3H). ^{13}C-NMR [CDCl$_3$, 125 MHz] δ = 172.3, 166.6, 154.4, 152.5, 151.8, 150.8, 134.4, 132.8, 129.4, 128.6, 127.4, 127.3, 121.8, 62.5, 43.5, 14.1. HRMS (FAB) Calcd for C$_{41}$H$_{30}$N$_5$O$_4$ (M+H$^+$) 656.2298. Found 657.7440.

Synthesis of 6 (step e):

5 (1.32 g, 2.01 mmol) was suspended in 24 mL 1,4-dioxane and 12 mL MeOH. The mixture of 0.96 g NaOH, 6.0 mL distilled water, and 6 mL MeOH was added to the stirred solution. After 20 min, the pH was adjusted to between 2 and 3 by the addition of 1 N HCl. The solution was dried in vacuo. The residue was suspended in 25 mL MeOH and precipitated with 200 mL diethyl ether. The precipitate was collected by filtration and washed with diethyl ether to obtain compound 6 (0.54 g, 1.03 mmol; yield: 51%). NMR signals were not observed due to insolubility of 6. HRMS (FAB) Calcd for C$_{32}$H$_{22}$N$_5$O$_3$ (M) 523.1644. Found 523.1473.

Synthesis of 8 (step f):

To a stirred solution of 6 (0.50 g, 0.96 mmol), triethylamine (0.10 mL), and 7[3] (0.43 g, 1.1 mmol) in 10 mL DMF was added 4-(4,6-dimethoxy-1,3,5-triazin-2-yl)-4-methylmorpholinium chloride (DMT-MM) (0.40 g, 1.4 mmol), and the mixture was vigorously stirred. After 1 h, 20 mL of CHCl$_3$ was added, and the reaction was stirred for 10 min. The mixture was washed with saturated aqueous solutions of NaHCO$_3$ three times. The organic layer was added to 150 mL diethyl ether with stirring. The precipitate was collected by filtration and purified by silica gel column chromatography (CHCl$_3$: MeOH,

20:1) to yield compound 8 (0.71 g, 0.79 mmol; yield: 82%). ^{1}H-NMR [CDCl$_3$, 500 MHz] δ = 11.27 (br, 1H), 8.96 (d, 1H), 8.73 (s, 1H), 8.54 (m, 3H), 8.39-8.10 (m, 9H), 7.74-7.61 (m, 4H), 7.39 (m, 2H), 7.26 (m, 7H), 7.17 (m, 1H), 6.82 (m, 4H), 5.38 (s, 2H), 4.85 (t, 1H), 4.13 (m, 1H), 3.68 (s, 3H), 3.67 (s, 3H), 3.61 (m, 2H), 3.18-3.04 (m, 2H). ^{13}C-NMR [CDCl$_3$, 125 MHz] δ = 166.5, 166.2, 162.8, 158.4, 154.5, 152.8, 151.5, 149.4, 145.5, 136.2, 134.2, 133.9, 132.8, 132.0, 131.4, 130.7, 130.1, 129.7, 129.2, 129.0, 128.9, 128.6, 128.2, 127.8, 127.0, 126.9, 126.5, 126.1, 125.7, 124.6, 124.4, 122.8, 117.0, 113.5, 85.0, 79.7, 63.0, 61.2, 55.5, 55.4, 52.0, 44.9, 36.2, 31.2. HRMS (FAB) Calcd for C$_{56}$H$_{46}$N$_6$O$_6$ (M) 898.3479. Found 898.4057.

Synthesis of 9 (step g):

In dry dichloromethane under nitrogen, 7 (0.45 g, 0.50 mmol) and triethylamine (0.60 mL, 4.4 mmol) were added to 2-cyanoethyl diisopropylchlorophosphoramidite (0.30 mL, 0.75 mmol) at 0 °C. After stirring at room temperature for 30 min, the reaction mixture was subjected to silica gel column chromatography (CHCl$_3$ containing 3% triethylamine). After column chromatography, products were dissolved in small amount of dry CHCl$_3$ and re-precipitated twice from hexane to yield compound 8 (0.42 g, 0.38 mmol; yield: 76%). Before the synthesis of SNA on a DNA synthesizer, 8 was dried by co-evaporation with dry acetonitrile. ^{1}H-NMR [CDCl$_3$, 500 MHz] δ = 9.14-9.06 (m, 2H), 8.71 (m, 1H), 8.58 (m, 1H), 8.30 (m, 1H), 8.23-8.01 (m, 9H), 7.66-7.56 (m, 3H), 7.32-7.10 (m, 10H), 6.73-6.59 (m, 5H), 4.99 (m, 2H), 4.38-4.27 (m, 1H), 3.87-3.52 (m, 10H), 3.44 (m, 2H), 3.30 (m, 1H), 3.09 (m, 1H), 2.45 (m, 2H), 1.12-0.99 (m, 12H). ^{13}C-NMR [CDCl$_3$, 125 MHz] δ = 166.5, 166.2, 162.8, 158.4, 154.5, 152.8, 151.5, 149.4, 145.5, 136.2, 134.2, 133.9, 132.8, 132.0, 131.4, 130.7, 130.1, 129.7, 129.2, 129.0, 128.9, 128.6, 128.2, 127.8,

127.0, 126.9, 126.5, 126.1, 125.7, 124.5, 124.4, 122.8, 117.0, 113.5, 85.7, 79.7, 63.0, 61.2, 55.5, 55.4, 52.0, 44.9, 36.2, 31.2. ^{31}P-NMR [CDCl$_3$, 121 MHz] δ = 148.1, 148.0. HRMS (FAB) Calcd for C65H64N8O7P (M+H$^+$) 1099.4636. Found 1099.0155.

Synthesis and purification of oligonucleotides:

SNA phosphoramidite monomers involving T, G, A, C, anthraquinone, and Cy3 were synthesized following reported procedures.2 All SNAs were synthesized using an ABI 3400 DNA/RNA synthesizer using phosphoramidite chemistry. For the coupling of all SNA monomers, incubation time was extended to 600 s. The concentrations of SNA phosphoramidite monomers were adjusted to 0.1 M for 9 (^{PV}A) and G and 0.75 M for T, A, and C. Synthesized oligonucleotides were purified using Poly-Pak cartridges. The collected residue was further purified by reversed-phase HPLC (Kanto Chemical, Mightysil RP-18 GPII column). After purification, synthesized oligonucleotides were characterized by MALDI-TOF MS.

The MALDI-TOFMS data for the SNA

SNA-P: Obsd. m/z 2755 (Calcd. for [SNA-P + H$^+$]: m/z 2756)

SNA-P2P: Obsd. m/z 2981 (Calcd. for [SNA-P2P + H$^+$]: m/z 2982)

SNA-P1P: Obsd. m/z 3005 (Calcd. for [SNA-P1P + H$^+$]: m/z 3006)

SNA-P0P: Obsd. m/z 2981 (Calcd. for [SNA-P0P + H$^+$]: m/z 2982)

SNA-P0P-Dab: Obsd. m/z 3386 (Calcd. for [SNA-P0P-Q + H$^+$]: m/z 3386)

SNA-P0P-Q: Obsd. m/z 3369 (Calcd. for [SNA-P0P-Q + H$^+$]: m/z 3369)

2-7. Appendixes

Table. S2-1 Sequences of synthesized SNA and complementary strands.

	Sequence[a]
SNA-P2P / RNA	(*S*)-GC^{PV}**A**TT^{PV}**A**GC-(*R*) / 5'-AA<u>GCUAAUGC</u>AA-3'
SNA-P1P / RNA	(*S*)-TCG^{PV}**A**T^{PV}**A**GA-(*R*) / 5'-AA<u>UCUAUCGA</u>AA-3'
SNA-P0P / RNA	(*S*)-GCT^{PV}**A**^{PV}**A**TGC-(*R*) / 5'-AA<u>GCAUUAGC</u>AA-3'
SNA-P / RNA	(*S*)-GCT^{PV}**A**ATGC-(*R*) / 5'-AA<u>GCAUUAGC</u>AA-3'
SNA-N / RNA	(*S*)-GCATCAGT-(*R*) / 5'-ACUGAUGC-3'
SNA-P0P-Dab / RNA-Cy3	(*S*)-**Dab**-GCT^{PV}**A**^{PV}**A**TGC-(*R*) / 5'-AA<u>GCAUUAGC</u>-**Y**-3'
SNA-P0P-Q / RNA-Cy3	(*S*)-**Q**-GCT^{PV}**A**^{PV}**A**TGC-(*R*) / 5'-AA<u>GCAUUAGC</u>-**Y**-3'
SNA-P2P / SNA	(*S*)-GC^{PV}**A**TT^{PV}**A**GC-(*R*) / (*S*)-<u>GCTAATGC</u>-(*R*)
SNA-P1P / SNA	(*S*)-TCG^{PV}**A**T^{PV}**A**GA-(*R*) / (*S*)-<u>UCTATCGA</u>-(*R*)
SNA-P0P / SNA	(*S*)-GCT^{PV}**A**^{PV}**A**TGC-(*R*) / (*S*)-<u>GCATTAGC</u>-(*R*)
SNA-P / SNA	(*S*)-GCT^{PV}**A**ATGC-(*R*) / (*S*)-<u>GCATTAGC</u>-(*R*)
SNA-N / SNA	(*S*)-GCATCAGT-(*R*) / (*S*)-<u>ACTGATGC</u>-(*R*)
SNA-P0P / L-*a*TNA	(*S*)-GCT^{PV}**A**^{PV}**A**TGC-(*R*) / 3'-<u>GCATTAGC</u>-1'

[a] Some duplexes contain an RNA overhang region due to synthetic reasons. This overhang should not significantly affect hybridization.
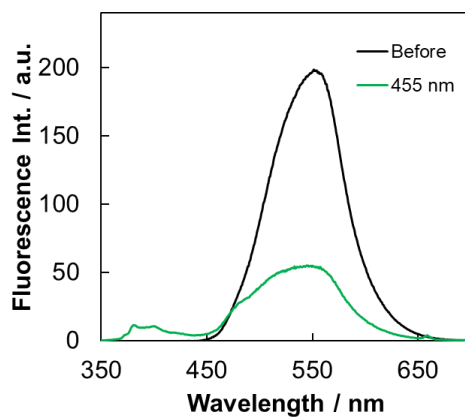
Figure. 2-1 Fluorescence spectra and of SNA-P2P before irradiation (black lines), PSS at 455 nm light (green lines). λ_{ex} = 330 nm. Solution conditions were 5.0 μM duplex, 100 mM NaCl, 10 mM phosphate buffer (pH 7.0) at 20 °C. PSS was attained by irradiation with 455 nm for 4 min or 300 nm for 6 min.
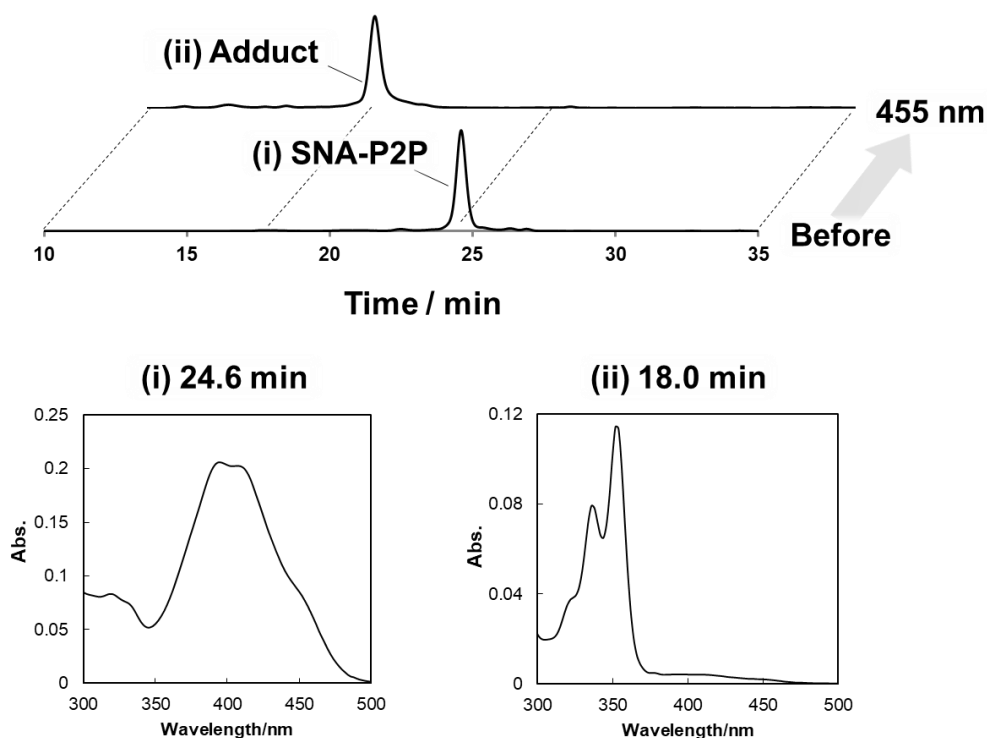
Figure. S2-2 HPLC profiles of SNA-P2P before and after irradiation with 455 nm for 120 s, and absorption spectra corresponding to the peaks at (i) 26.3 min and (ii) 30.4 min. Conditions: 100 mM NaCl, 10 mM phosphate buffer (pH 7.0), 20 °C, Concentration of SNA was 5.0 ☐M.
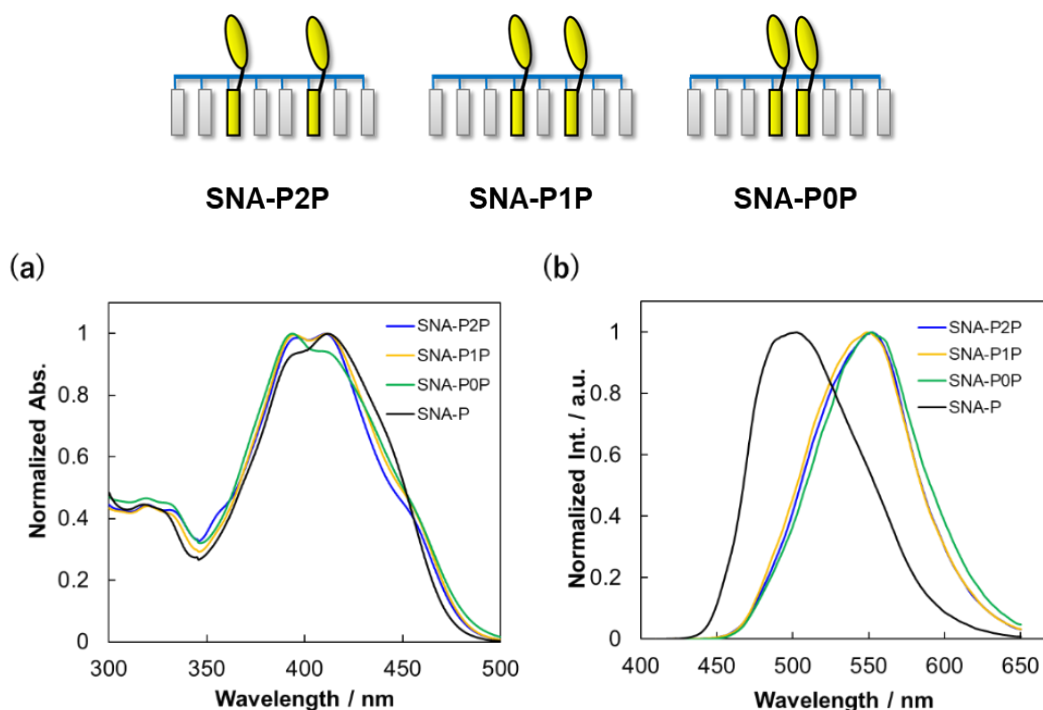
Figure. S2-3 (a) Normalized absorption spectra and (b) fluorescence spectra of single stranded SNAs without photo-irradiation. Conditions: 100 mM NaCl, 10 mM phosphate buffer (pH 7.0), 20 °C. The concentration of SNA was 5.0 μM. λ_{ex} = 400 nm
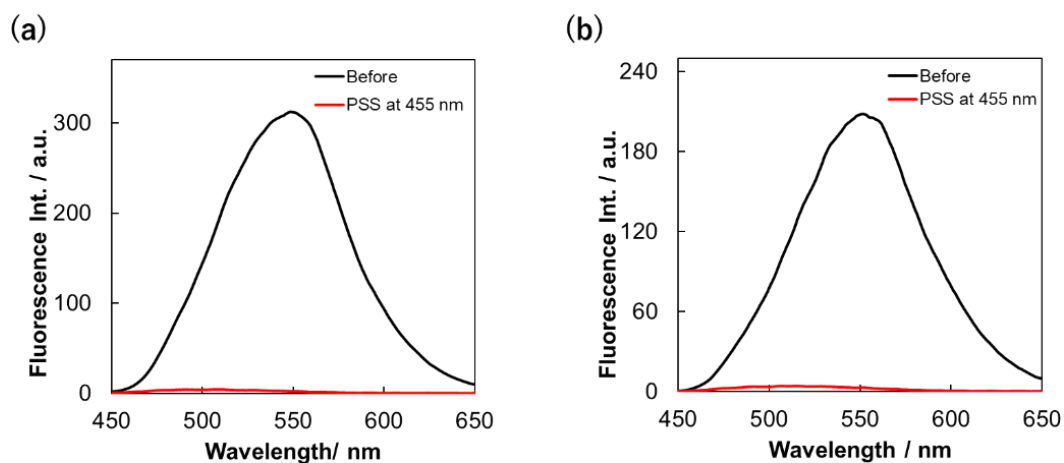
Figure. S2-4 Fluorescence spectra of (a) SNA-P1P, and (b) SNA-P0P before irradiation with 455 nm light (black line) and at PSS (red line). Conditions: 100 mM NaCl, 10 mM phosphate buffer (pH 7.0), 20 °C. The concentration of SNA was 5.0 μM. λ_{ex} = 400 nm
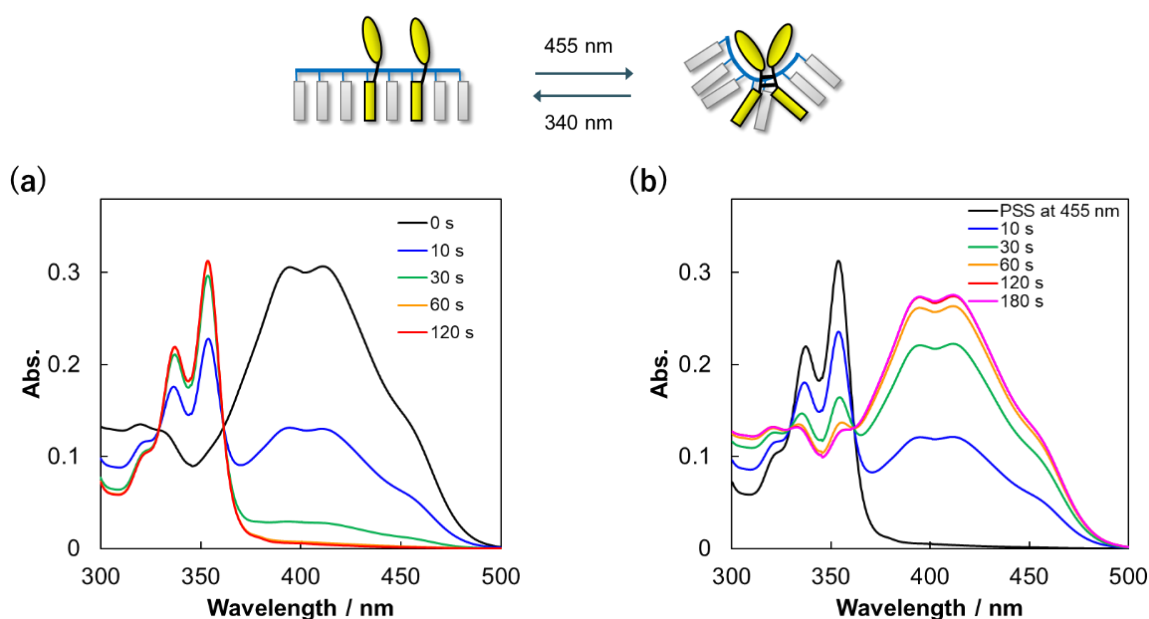
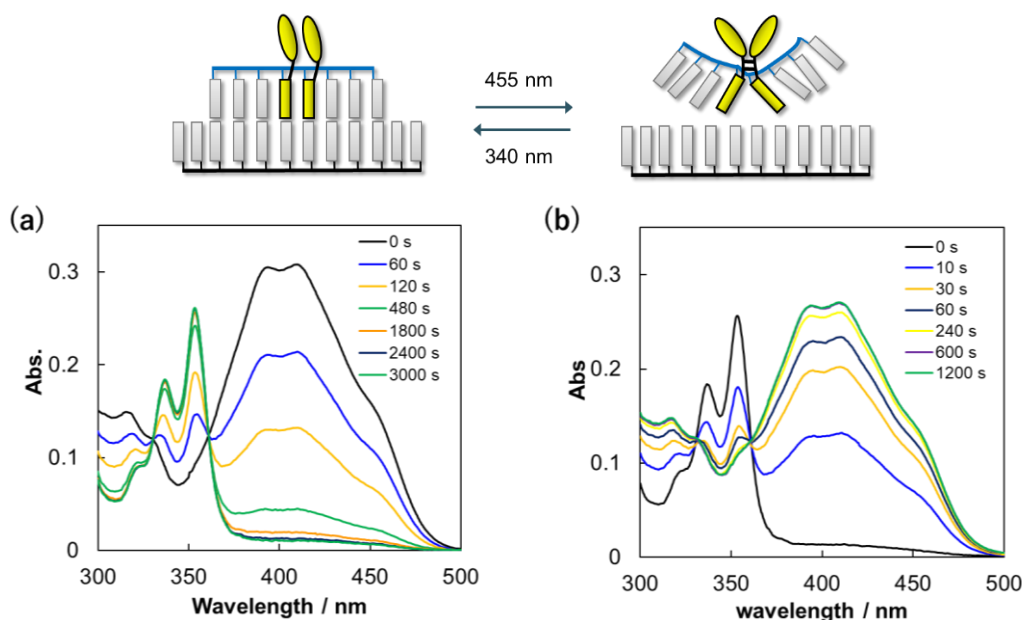**Figure S2-5**. (a) Absorption spectra of SNA-P1P after indicated times of irradiation with 455 nm light. (b) Absorption spectra of at photo-stationary state (PSS) at 455 nm and after irradiation for the indicated times with 340 nm light. Irradiation was performed at 20 °C. Conditions: 100 mM NaCl, 10 mM phosphate buffer (pH 7.0), 20 °C. Concentration of SNA was 5.0 M.
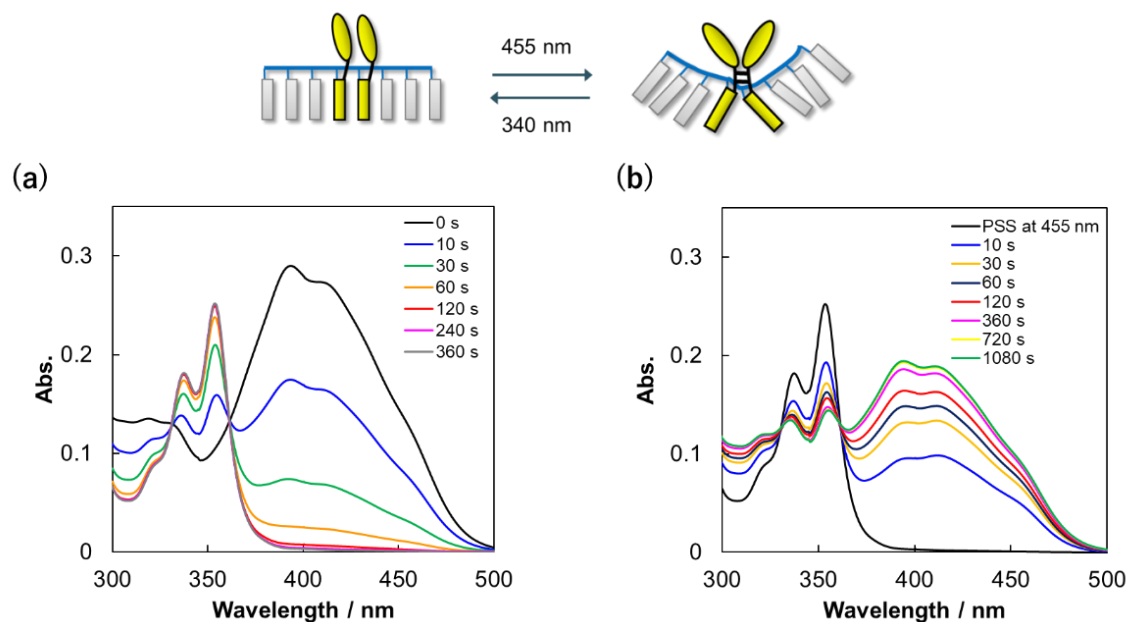
Figure. S2-6 (a) Absorption spectra of SNA-P0P after indicated times of irradiation with 455 nm light. (b) Absorption spectra of at photo-stationary state (PSS) at 455 nm and after irradiation for the indicated times with 340 nm light. Irradiation was performed at 20 °C. Conditions: 100 mM NaCl, 10 mM phosphate buffer (pH 7.0), 20 °C. Concentration of SNA was 5.0 M.
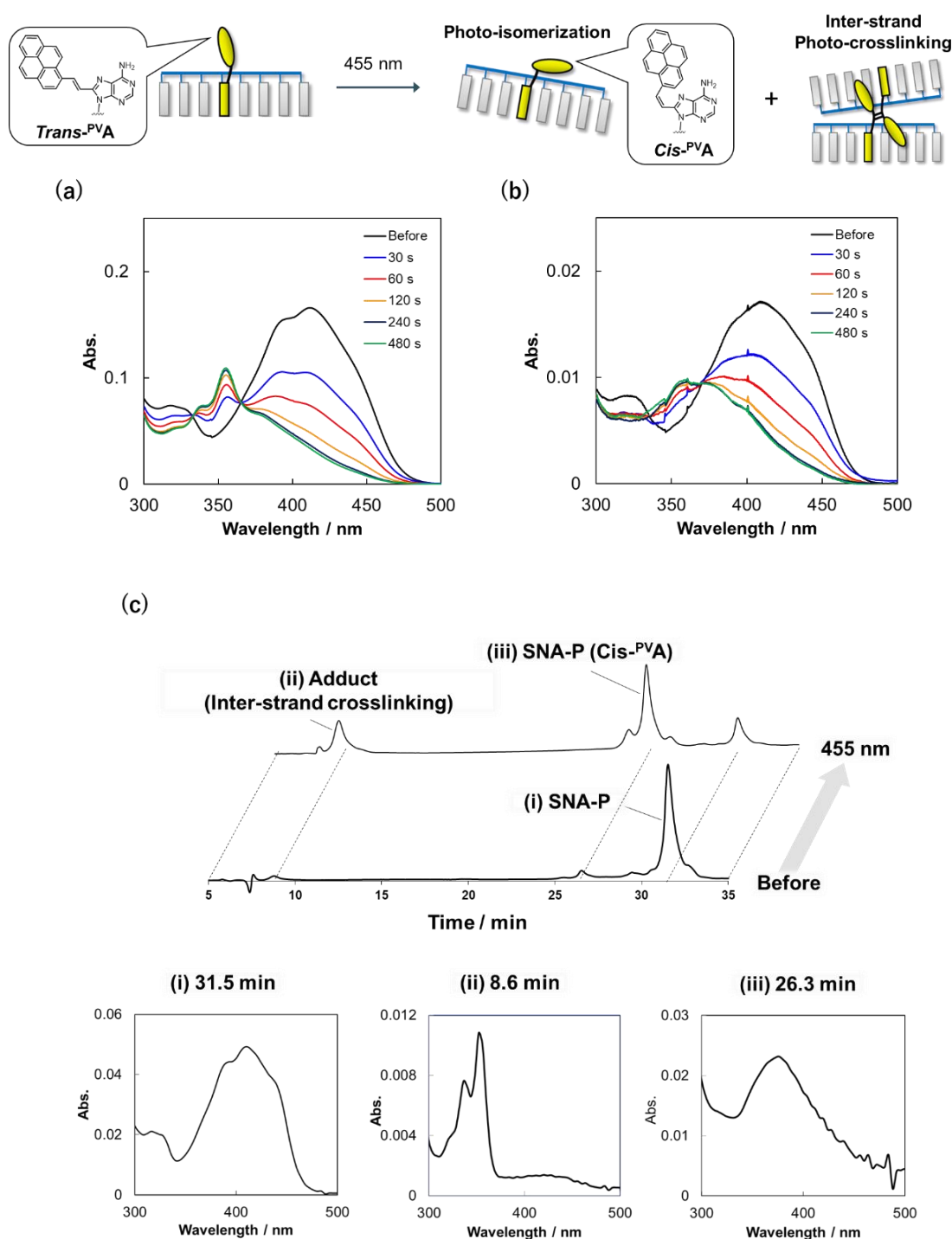
Figure. S2-7 (a, b) Absorption spectra of SNA-P at (a) 5.0 µM and (b) 0.5 µM upon irradiation with 455 nm light for indicated times. In this experiment, the power of the light source was reduced to 10%, because *cis*-isomerization was rapid. (c) HPLC chromatogram of 5.0 µM SNA-P before and after irradiation with 455 nm for 480 s. UV-Vis spectrum at 8.6 min, 26.3 min and 31.5 min were recorded. The small peak appeared 8.6 min exhibited alkyl pyrene-like spectrum and was attributed to inter-strand crosslinking. The peak at 26.3 min showed absorption at $\lambda_{max} = 376$ nm, attributed to *cis*-^{PV}A.
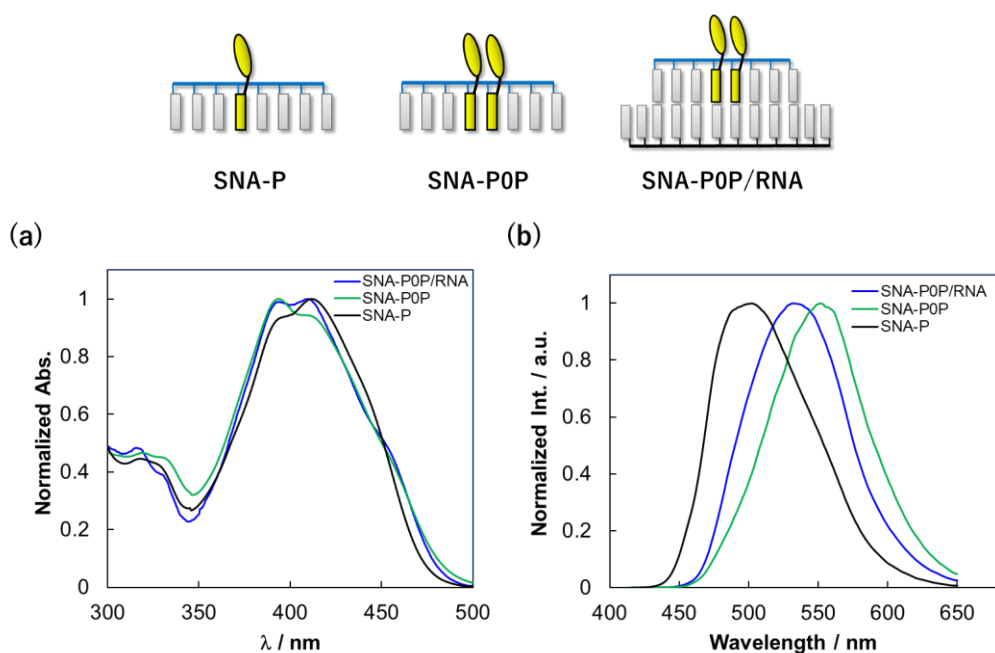
Figure. S2-8 (a) Normalized absorption spectra and (b) fluorescence spectra of SNA-P, SNA-P0P, and SNA-2P0P/RNA before photoirradiation. Conditions: 100 mM NaCl, 10 mM phosphate buffer (pH 7.0), 20 °C. The concentration of SNA was 5.0 μM. λ_{ex} = 400 nm.

Figure. S2-9 Absorption spectra of SNA-P0P/RNA upon irradiation with (a) 455 nm light followed by (b) 340 nm light. Conditions: 100 mM NaCl, 10 mM phosphate buffer (pH 7.0), 20 °C. The concentration of duplex was 5.0 μM.
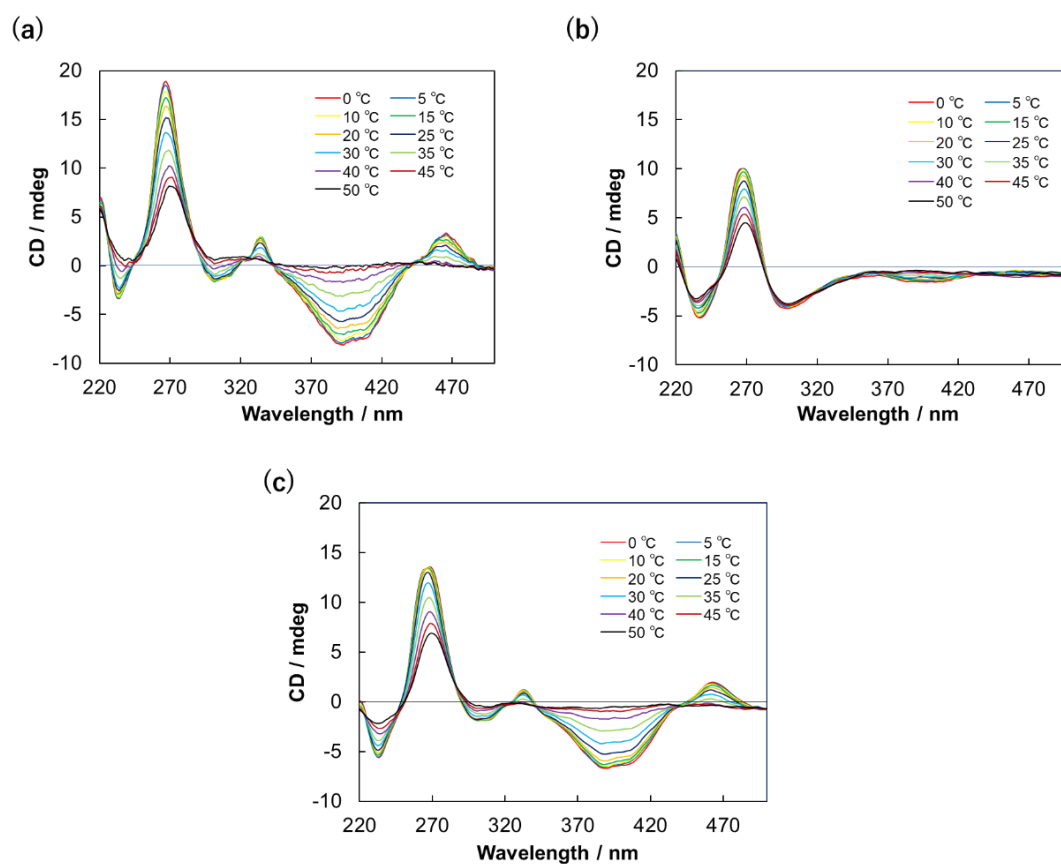
Figure. S2-10 CD spectra of (a-c) SNA-P0P/RNA at indicated temperatures. (a) before irradiation, (b) PSS at 455 nm, and (c) PSS at 340 nm. Conditions: 100 mM NaCl, 10 mM phosphate buffer (pH 7.0). For the PSS experiments, irradiation time was 60 min at 455 nm and 15 min at 340 nm. Conditions: 100 mM NaCl, 10 mM phosphate buffer (pH 7.0), 20 °C. The concentration of duplex was 5.0 μM
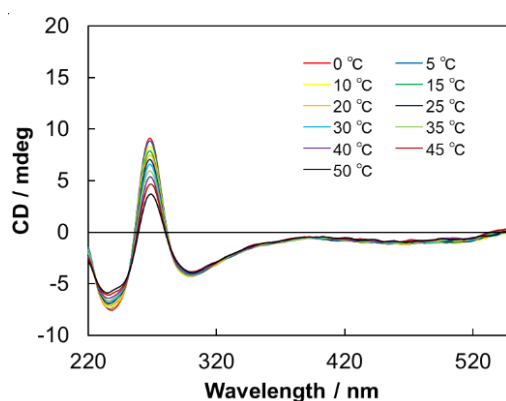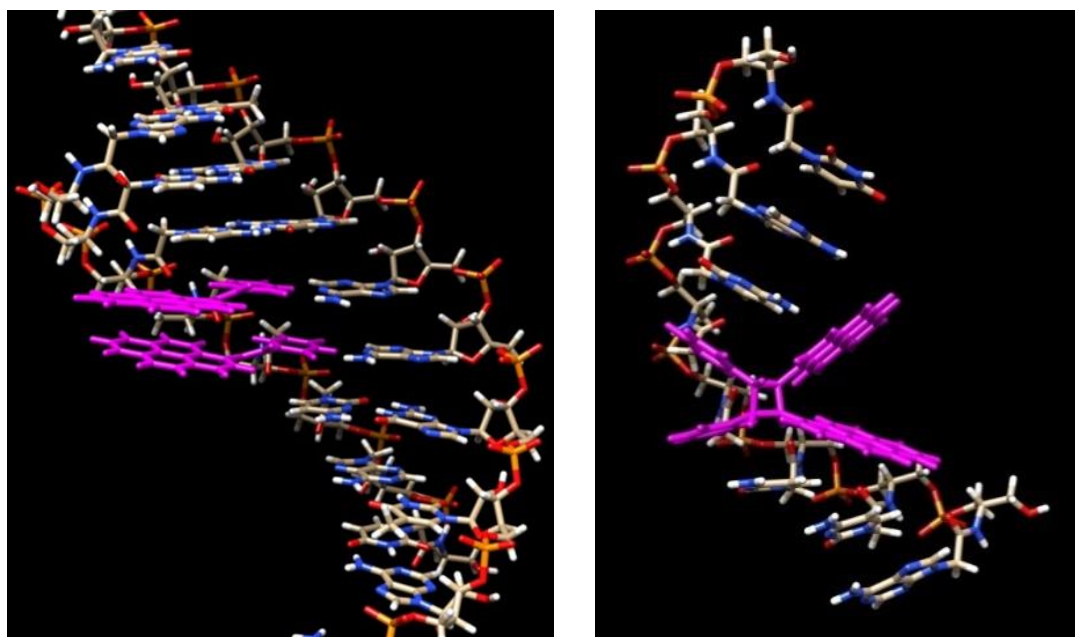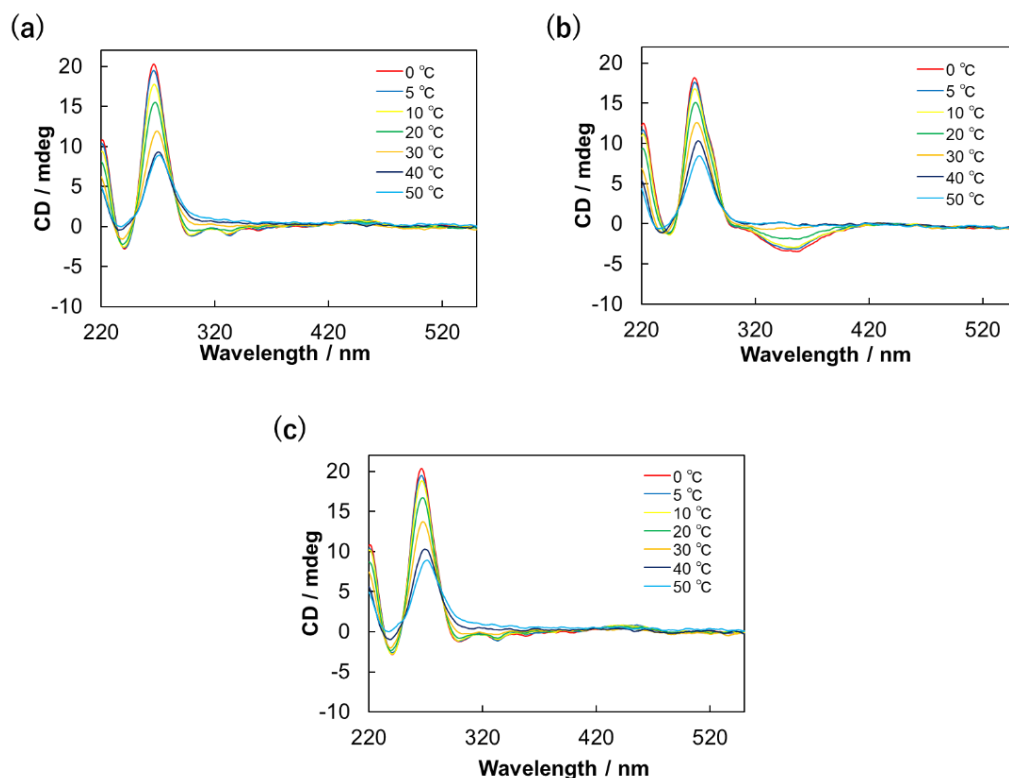

Figure S2-11. CD spectra of single stranded RNA (complementary strand of SNA-P0P) at indicated temperatures. Conditions: 100 mM NaCl, 10 mM phosphate buffer (pH 7.0). Conditions: 100 mM NaCl, 10 mM phosphate buffer (pH 7.0), 20 °C. The concentration of duplex was 5.0 μM
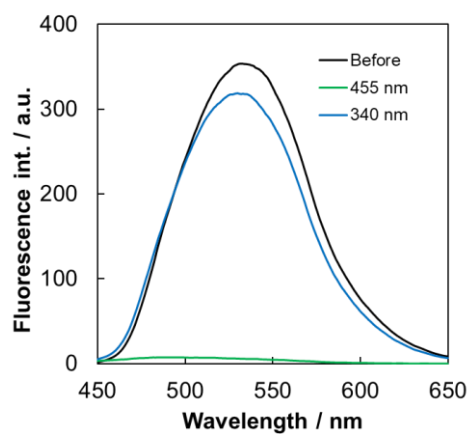
Figure. S2-12 Fluorescence spectra of SNA-P0P / RNA before irradiation, at PSS at 455 nm, and at PSS at 340 nm measured by 400 nm excitation. For the PSS experiments, irradiation time was 60 min at 455 nm and 15 min at 340 nm. Conditions: 100 mM NaCl, 10 mM phosphate buffer (pH 7.0), 20 °C. The concentration of duplex was 5.0 μM.


Figure. S2-13. Energy minimized structures of (a) SNA-P0P/RNA duplex and (b) single stranded SNA-P0P containing [PV]A photo-dimer. [PV]A residues are presented as magenta.

Figure. S2-14 CD spectra of (a-c) SNA-P/RNA at indicated temperatures. (a) before irradiation, (b) PSS at 455 nm, and (c) PSS at 340 nm. Conditions: 100 mM NaCl, 10 mM phosphate buffer (pH 7.0). For the PSS experiments, irradiation time was 5 min at 455 nm and 1 min at 340 nm. Conditions: 100 mM NaCl, 10 mM phosphate buffer (pH 7.0), 20 °C. The concentration of duplex was 5.0 μM
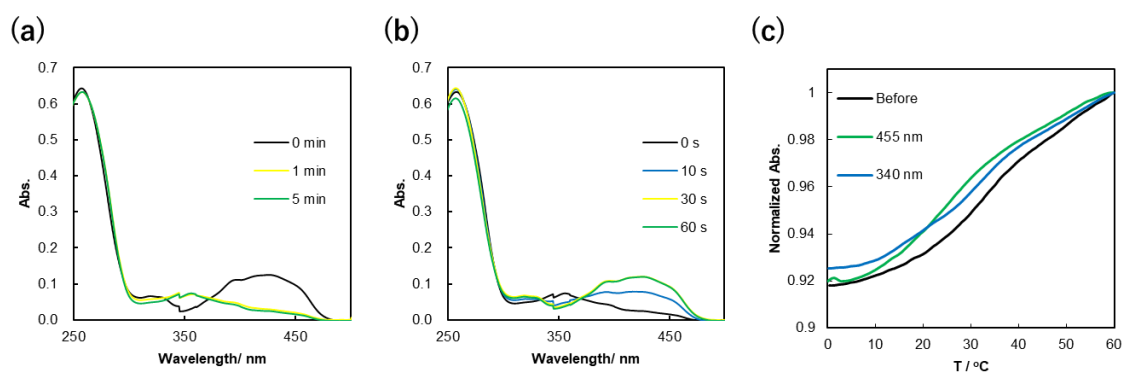
Figure. S2-15 Absorption spectra of SNA-P/RNA upon irradiation with (a) 455 nm light followed by (b) 340 nm light. (c) Melting temperature of SNA-P/RNA duplex before (black lines) and after irradiation with 455 nm light (green lines) and 340 nm light (blue lines). Conditions: 100 mM NaCl, 10 mM phosphate buffer (pH 7.0), 20 °C. The concentration of duplex was 5.0 μM.

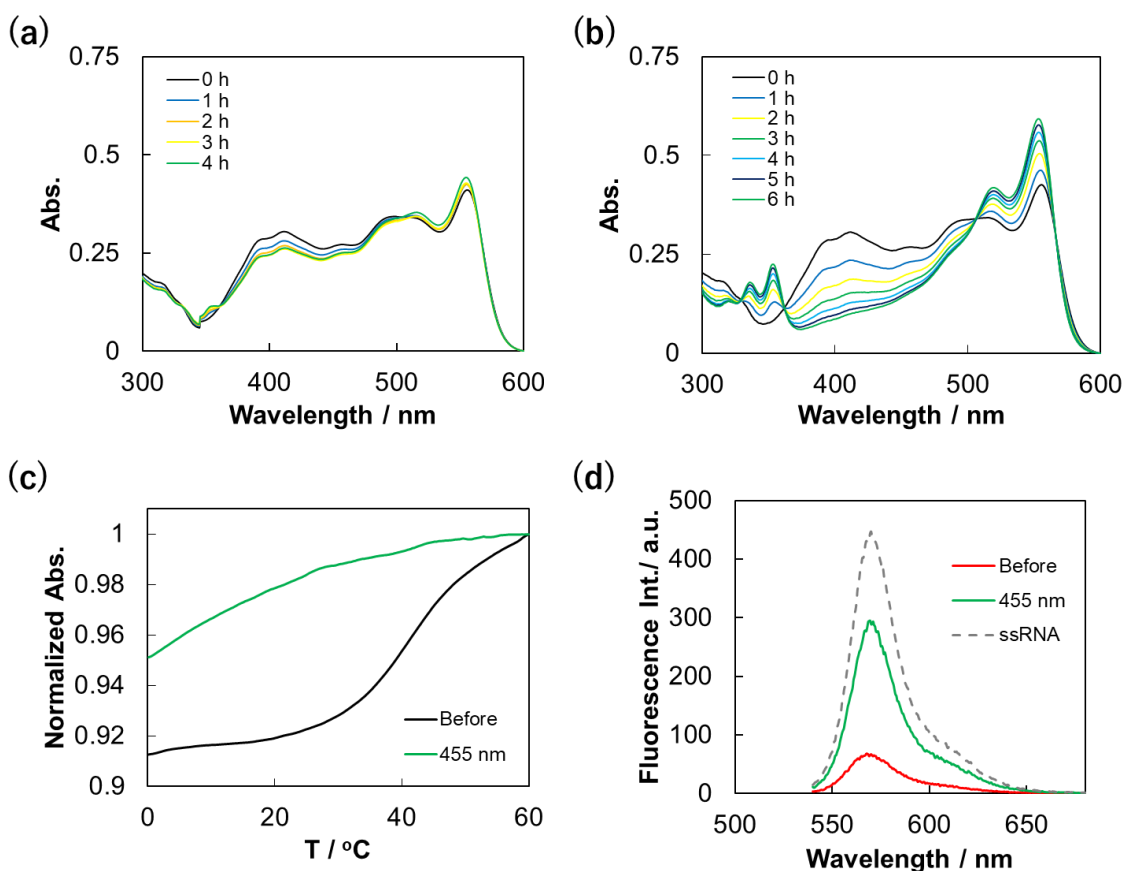| T_m with complementary RNA	
455 nm	24.6 °C
340 nm	30.0 °C

Figure. S2-16 (a, b) Absorption spectra of SNA-P0P-Dab/RNA-Cy3 after irradiation with 455 nm light at (a) 20 °C and (b) 60 °C. (d) Melting profiles at before and after 455 nm irradiation for 6 h at 60 °C. (c) Fluorescence spectra of single stranded RNA-Cy3 and SNA-P0P-Dab/RNA-Cy3 before and after 455 nm irradiation for 6 h at 60 °C. Conditions: 100 mM NaCl, 10 mM phosphate buffer (pH 7.0), 20 °C. The concentration of oligomer or duplex was 5.0 μM. The reactivity of [PV]A in the SNA-P0P-Dab/RNA-Cy3 duplex was even lower than that in single-stranded SNA-P0P-Dab: almost no cross-linking reaction proceeded through 4 h of visible light irradiation. In this system, the cross-linking reaction proceeded only at high temperatures that the duplexes were dissociated.
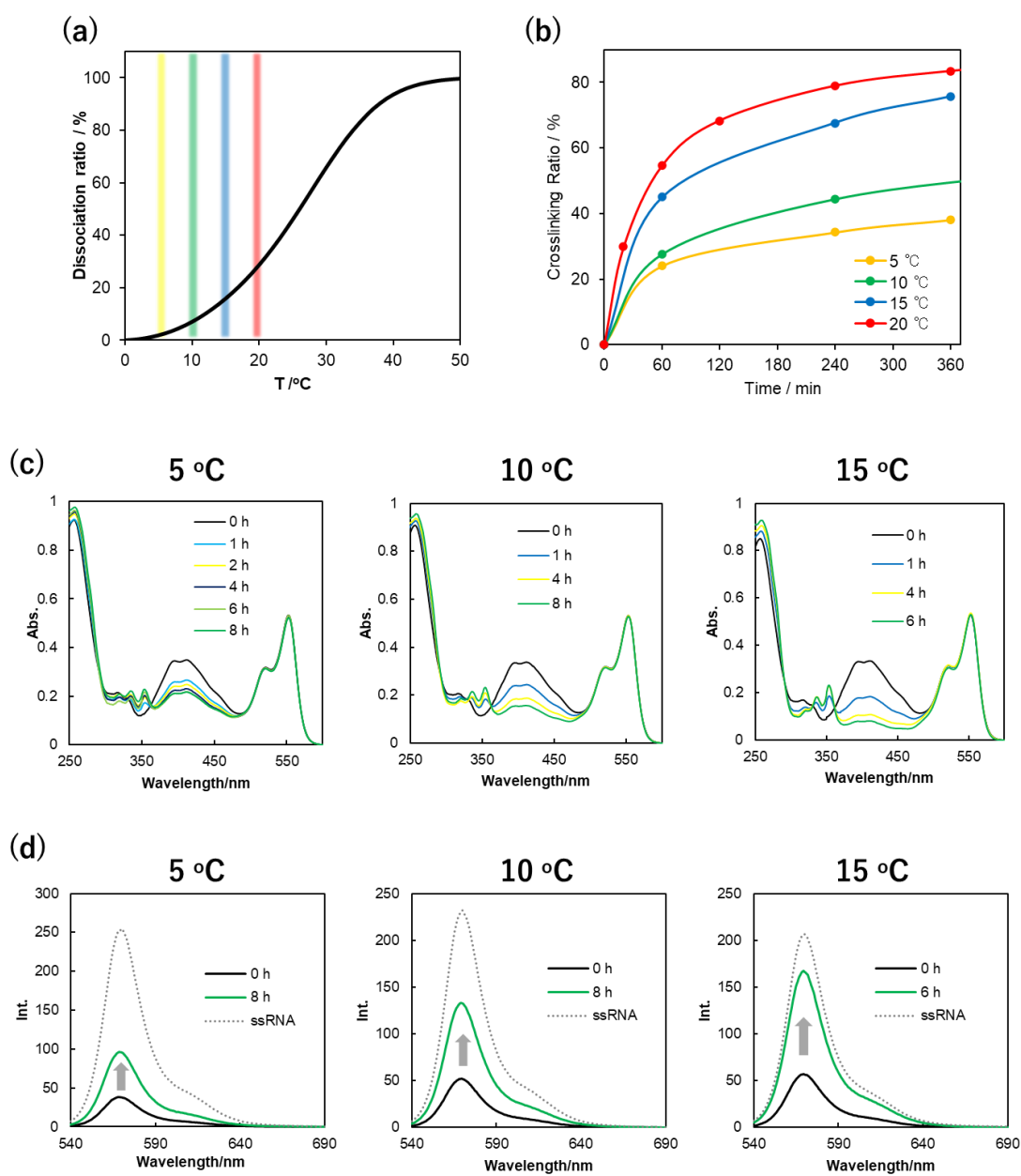
Figure. S2-17 (a) Dissociation ratio of SNA-P0P-Q/RNA-Cy3 duplex at before irradiation. (b) percent crosslink of [PV]As in SNA-P0P-Q/RNA on the time of irradiation with 455 nm light at 5 °C, 10 °C, 15 °C and 20 °C. Percent crosslink was calculated from absorbance at 400 nm. (c) Absorption spectra of SNA-P0P-Q/RNA-Cy3 upon irradiation with 455 nm light 5 °C, 10 °C and 15 °C (d) Fluorescence spectra of SNA-P0P-Q/RNA-Cy3 after irradiation with 455 nm light at 5 °C, 10 °C and 15 °C. Conditions: 100 mM NaCl, 10 mM phosphate buffer (pH 7.0), The concentration of oligomer or duplex was 5.0 μM.
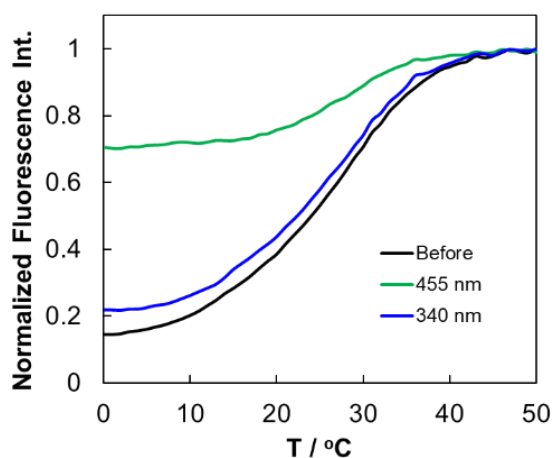
Figure. S2-18 Melting profiles monitored by fluorescent change before and after photo-irradiation. Melting curves were obtained by difference of profiles between single-stranded RNA-Cy3 and the duplex. Conditions: 100 mM NaCl, 10 mM phosphate buffer (pH 7.0), 20 °C. The concentration of oligomer or duplex was 5.0 μM.
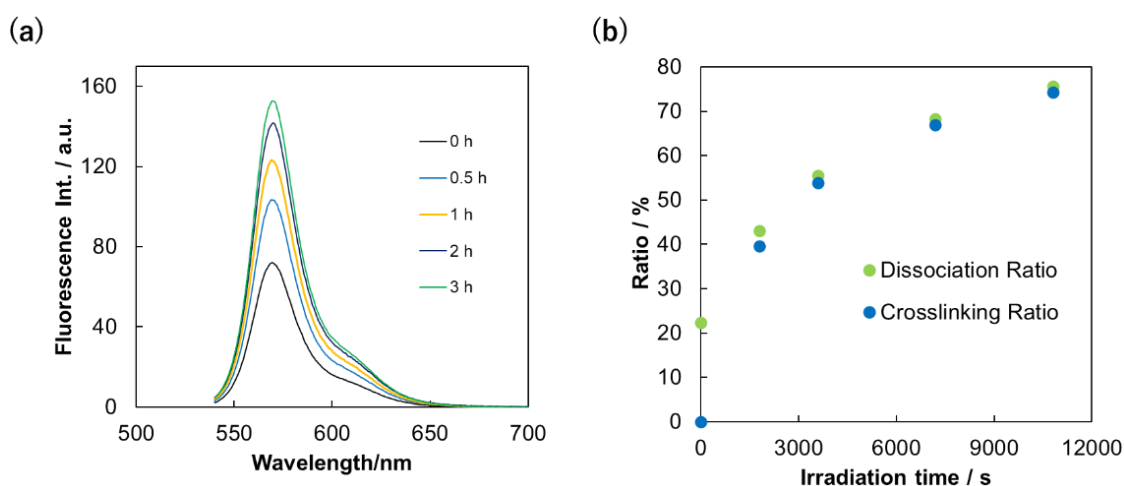

Figure. S2-19 (a) Fluorescence spectra of SNA-P0P-Q/RNA-Cy3 after irradiation with 455 nm light. Conditions: 100 mM NaCl, 10 mM phosphate buffer (pH 7.0), 20 °C. The concentration of oligomer or duplex was 5.0 μM. (b) Crosslinking ratio of [PV]As and dissociation ratio of SNA-P0P-Q/RNA at each irradiation time. Crosslinking ratio was calculated from absorbance at 400 nm and dissociation ratio was calculated from fluorescence of Cy3.
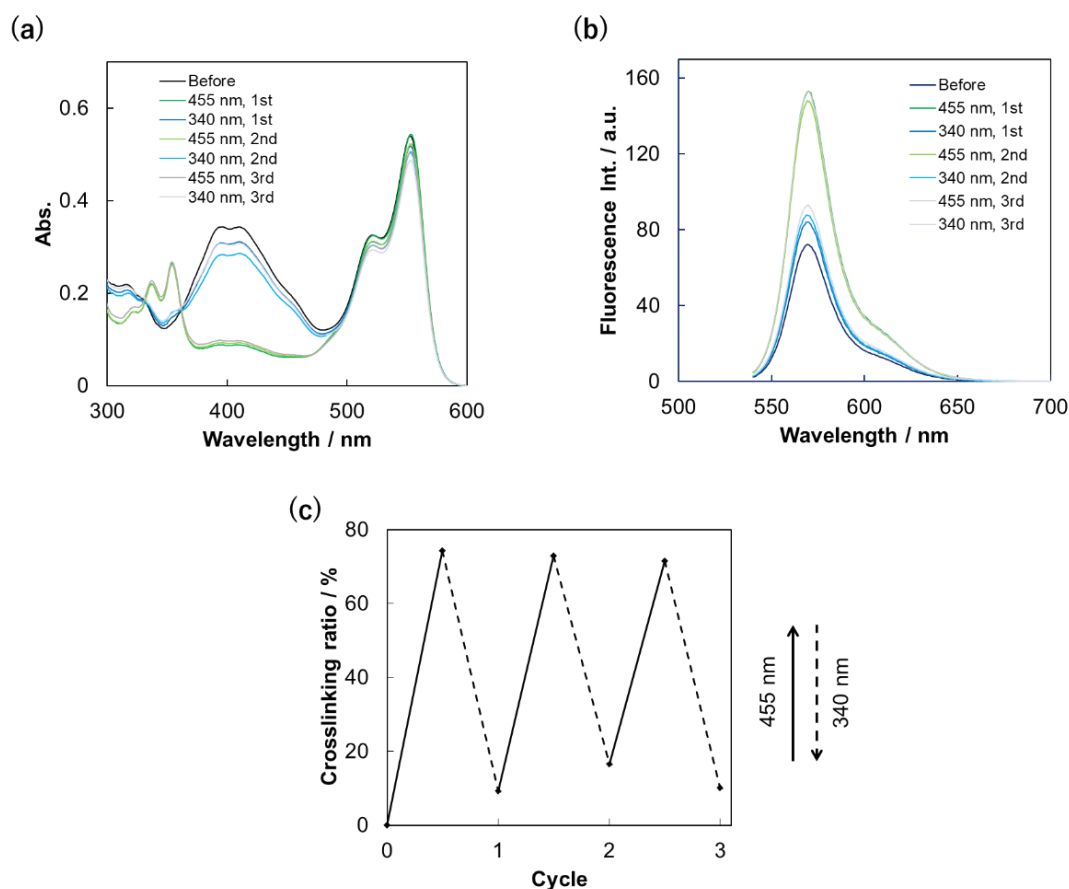
Figure. S2-20 (a) Absorption spectra and (b) Fluorescence spectra of SNA-P0P-Q/RNA-Cy3 after repeated irradiation cycles. (c) Percent crosslink of SNA-P0P-Q/RNA-Cy3 after multiple photo-switching cycles. Samples were irradiated at 455 nm for 3 h and at 340 nm for 50 min. The reaction ratios were calculated by using absorption spectra recorded after each irradiation. Conditions: 100 mM NaCl, 10 mM phosphate buffer (pH 7.0), 20 °C. The concentration of oligomer or duplex was 5.0 μM
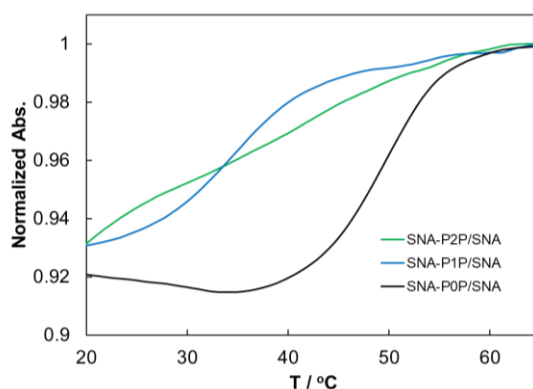

Figure. S2-21 Melting profiles of ^{PV}A-SNAs with complementary SNA. Conditions: 5.0 μM oligonucleotide, 100 mM NaCl, 10 mM phosphate buffer (pH 7.0).

Table. 2-1 Melting temperature (T_m) of SNA-PnP/SNA duplexes and SNA-P/SNA duplex

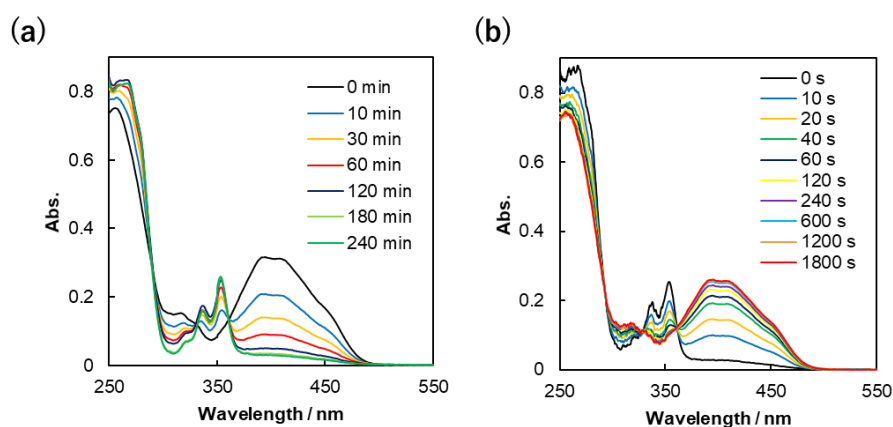|	T_m with complementary SNA
SNA-P2P/SNA	14.0 °C.
SNA-P1P/SNA	35.5 °C
SNA-P0P/SNA	49.5 °C
SNA-P/SNA	46.1 °C
SNA-N/SNA	51.1 °C

Figure. S2-22 Absorption spectra of SNA-P0P/SNA upon irradiation with (a) 455 nm light followed by (b) 340 nm light. Conditions: 100 mM NaCl, 10 mM phosphate buffer (pH 7.0), 40 °C. The concentration of duplex was 5.0 μM.

Figure. S2-23 Absorption spectra of SNA-P0P/L-aTNA upon irradiation with (a) 455 nm light followed by (b) 340 nm light. Conditions: 100 mM NaCl, 10 mM phosphate buffer (pH 7.0), 40 °C. The concentration of duplex was 5.0 μM.
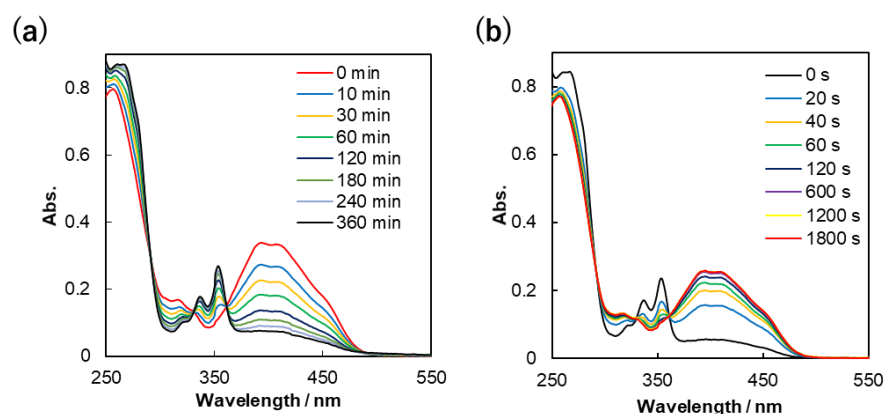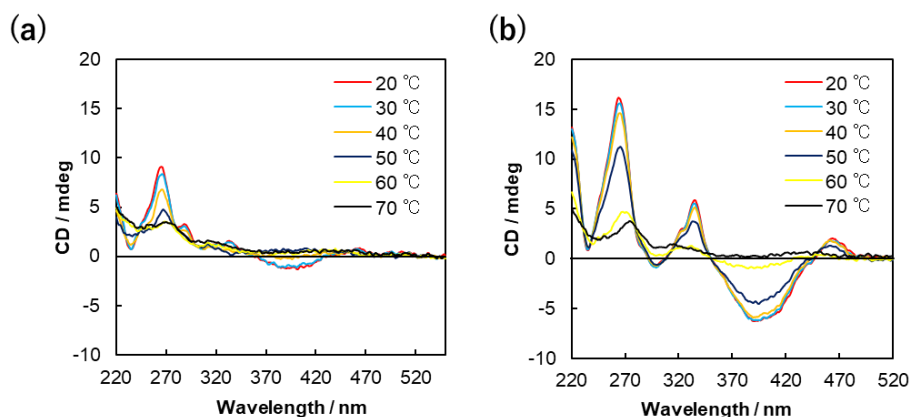
Figure. S2-24 CD spectra of (a) SNA-P0P/SNA and (b) SNA-P0P/L-aTNA duplexes at indicated temperatures before irradiation. Conditions: 100 mM NaCl, 10 mM phosphate buffer (pH 7.0). Conditions: 100 mM NaCl, 10 mM phosphate buffer (pH 7.0). The concentration of duplex was 5.0 μM
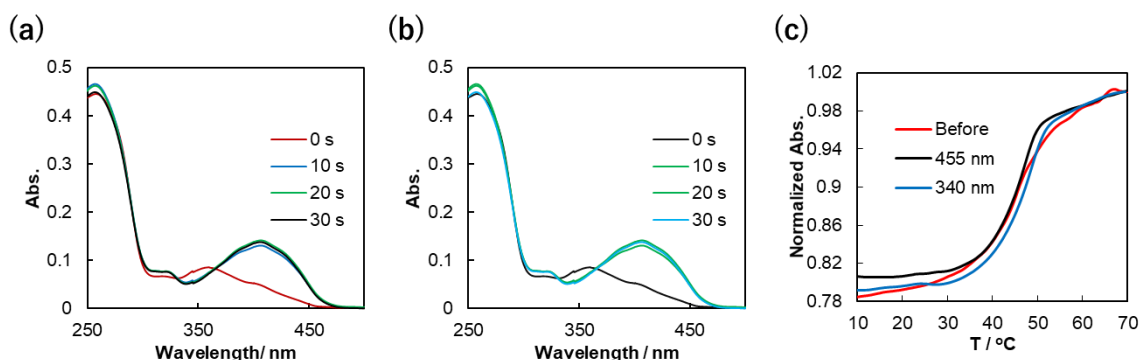

Figure. S2-25 Absorption spectra of SNA-P/SNA upon irradiation with (a) 455 nm light followed by (b) 340 nm light. (c) Melting temperature of SNA-P/SNA duplex before (black lines) and after irradiation with 455 nm light (green lines) and 340 nm light (blue lines). Conditions: 100 mM NaCl, 10 mM phosphate buffer (pH 7.0), 20 °C. The concentration of duplex was 5.0 μM. One ^{PV}A in the SNA/SNA duplex was also isomerized by irradiation with Vis/UV-A light. However, the melting temperature did not change significantly before and after irradiation, indicating that photo-control using this reaction is impossible.

Table. S2-2 Melting temperature (T_m) of SNA-P/SNA after 455 nm and 340 nm irradiation.

T_m with complementary SNA	
455 nm	44.6 °C
340 nm	46.2 °C

2-8. References

[1] (a) C. J. Leumann, *Bioorg. Med. Chem.* **2002**, 10, 841−854; (b) J. K. Watts, D. R. Core, *J. Pathol.* **2012**, 226, 365−379; (c) P. E. Nielsen, M. Egholm, R. H. Berg, O. Buchardt, *Science* **1991**, *254*, 1497-1500 (d) S. K. Singh, P. Nielsen, A. A. Koshkin, J. Wengel, *Chem. Commun.* **1998**, 455-456; (e) S. Obika, D. Nanbu, Y. Hari, J. Andoh, K. Morio, T. Doi, T. Imanishi, *Tetrahedron Lett.* **1998**, *39*, 5401-5404; (f) T. Vilaivan, C. Srisuwannaket, *Org. Lett.* **2006**, *8*, 1897−1900.

[2] (a) U. Wenge, J. Wengel, H.-A. Wagenknecht, *Angew. Chem., Int. Ed.* **2012**, *51*, 10026−10029. (b) R. S. Zhang, E. O. McCullum, J. C. Chaput, *J. Am. Chem. Soc.* **2008**, *130*, 5846−5847. (c) W.-C. Hsieh, G. R Martinez, A. Wang, S. F. Wu, R. Chamdia, D. H. Ly, *Communications Chemistry* **2018**, *1*, 89. (d) M. Rana, M. Balcioglu, N. Robertson, M. V. Yigit, *Analyst* **2014**, *139*, 714−720.

[3] (a) H. Kashida, K. Murayama, T. Toda, H. Asanuma., *Angew. Chem. Int. Ed.* **2011,** *50*, 1285-1288; (b) K. Murayama, Y. Tanaka, T. Toda, H. Kashida, H. Asanuma, *Chem. Eur. J.* **2013,** *19*, 14151-14158.

[4] (a)Y. Kamiya, Y. Donoshita, H. Kamimoto, K. Murayama, J. Ariyoshi, H. Asanuma, *ChemBioChem* **2017**, *18*, 1917– 1922; (b) B. T. Le, K. Murayama, F. Shabanpoor, H. Asanuma, R. N. Veedu, *RSC Adv.* **2017**, *7*, 34049–34052. (c) K. Murayama, R. Nagao, H. Asanuma, *ChemistrySelect* **2017**, *2*, 5624– 5627; (d) K. Murayama, Y. Kamiya, H. Kashida, H. Asanuma, *ChemBioChem* **2015**, *16*, 1298-1301.

[5] (a) T. Kaewsomboon, S. Nishizawa, T. Kanamori, H. Yuasa, A. Ohkubo, *J. Org. Chem.* **2018**, *83*, 1320−1327; (b) T. Wada, N. Minamimoto, Y. Inaki, Y. Inoue, J. Am. Chem. Soc. **2000**, *122*, 6900−6910; (c) A. Ohkubo, R. Kasuya, K. Miyata, H. Tsunoda, K. Seio, M. Sekine, *Org. Biomol. Chem.* **2009**, *7*, 687−694; (d) P. Scharf, J. Müller *ChemPlusChem* **2013**, *78*, 20−34.

[6] (a) C. Brieke, F. Rohrbach, A. Gottschalk, G. Mayer, A. Heckel, *Angew. Chem., Int. Ed*. **2012**, *51*, 8446−8476. (b) Q. Liu, A. Deiters, *Acc. Chem. Res*. **2014**, *47*, 45−55. (c) B. K. Ruble, S. B. Yeldell, *J. Inorg. Biochem*. **2015**, *150*, 182−188. (d) S. Mori, K. Morihiro, S. Obika, *Molecules* **2014**, *19*, 5109−5118. (c) A. S. Lubbe, W. Szymanski, B. L. Feringa, *Chem. Soc. Rev*. **2017**, *46*, 1025−1079. (d) A. S. Lubbe, Q. Liu, S. J. Smith, J. W. Vries, J. C. M. Kistemaker, A. H. Vries, I. Faustino, Z. Meng, W. Szymanski, A. Herrmann, B. L. Feringa, *J. Am. Chem. Soc.* **2018**, *140*, 5069−5076.

[7] (a) R. Wang, C. Jin, X. Zhu, L. Zhou, W. Xuan, Y. Liu, Q. Liu, W. Tan, *J. Am. Chem. Soc.* **2017**, *139*, 9104−9107. (b) T. Goldau, K Murayama, C. Brieke, S. Steinwand, P. Mondal, M. Biswas, I. Burghardt, J. Wachtveitl, H. Asanuma, H.; A. Heckel, *Chem. Eur. J.* **2015**, *21*, 2845−2854. (c) T. Goldau, K. Murayama, C. Brieke, H. Asanuma, A. Heckel, *Chem. Eur. J.* **2015**, *21*, 17870−17876. (d) S. Barrois, H.-A. Wagenknecht, Beilstein *J.Org. Chem*. **2012**, *8*, 905−914. (e) H. Cahová, A. Jäschke, *Angew. Chem., Int. Ed.* **2013**, *52*, 3186−3190.

[8] Y. Kamiya, H. Asanuma, *Acc. Chem. Res*. **2014**, *47*, 1663−1672.

[9] (a) G. T. Hwang, Y. J. Seo, B. H. Kim, *Tetrahedron Lett*. **2005**, *46*, 1475-1477; (b) M. V.

Skorobogatyi, A. D. Malakhov, A. A. Pchelintseva, A. A. Turban, S. L. Bondarev, V. A. Korshun, *ChemBioChem* **2006**, *7*, 810-816; (c) K.-Y. Lin, R. J. Jones, M. Matteucci, *J. Am. Chem. Soc*. **1995**, *117*, 3873-3874.

[10] (a) Y. Saito, K. Matsumoto, Y. Takeuchi, S. S. Bag, S. Kodate, T. Morii, I. Saito, *Tetrahedron Lett.* **2009**, *50*, 1403– 1406; (b) S. Ogasawara, I. Saito, M. Maeda, *Tetrahedron Lett*. **2008**, *49*, 2479-2482; (c) S. Ogasawara, M. Maeda, *Angew. Chem. Int. Ed*. **2008**, *47*, 8839-8842; (d) S. Ogasawara, *ACS Synth. Biol.* **2018**, 7, 2507−2513.

[11] (a) Y. Yoshimura, K. Fujimoto, K. *Org. Lett.* **2008**, *10*, 3227−3230; (b) U. Pieles, U. Englisch, *Nucleic Acids Res.* **1989**, *17*, 285−299. (c) H. Kashida, T. Doi, T. Sakakibara, T. Hayashi, H. Asanuma, *J. Am. Chem. Soc.* **2013**, *135*, 7960-7966. (d) L. Antusch, N. Gaß, H.-A. Wagenknecht, *Angew. Chem., Int. Ed.* **2017**, *56*, 1385−1389.

[12] (a) T. Doi, H. Kawai, K. Murayama, H. Kashida, H. Asanuma, *Chem. Eur. J.* **2016**, *22*, 10533-10538; (b) D.E. Marschner, H. Frisch, J. T. Offenloch, B. T. Tuten, C. R. Becer, A. Walther, A. S. Goldmann, P. Tzvetkova, C. Barner-Kowollik, *Macromolecules* **2018**, *51*, 3802−3807; (c) V. X. Truong, F. Li, F. Ercole, J. S. Forsythe, *ACS Macro Lett*. **2018**, *7*, 464−469; (d) N. P. Kovalenko, A. T. Abdukadyrov, V. I. Gerko, M. V. J. Alfimov, *Photochem.* **1980**, *12*, 59−65.

[13] Tucker's group has provided photo-control of hybridization by using photo-crosslinking of anthracene incorporated into DNA strand. However, it was limited to irradiation in the single stranded state, and only for one-way reaction by light. J. Manchester, D. M. Bassani, J.-L. H. A. Duprey, L. Giordano, J. S. Vyle, Z.-y. Zhao, J. H. R. Tucker, *J. Am. Chem. Soc.* **2012**, *134*, 10791−10794.

Chapter 3. Orthogonal photo-control of SNA/RNA duplexes by dual crosslink type photo-switches

3-1. Abstract

Wavelength-selective photo-regulation by multiple chromophores responding to different wavelength can expand the variation of photo-manipulating system.

In this study, we demonstrated orthogonal photo-control of dual duplexes formation between serinol nucleic acid (SNA) and RNA using light-induced crosslinking reactions mediated by a new photo-reactive nucleobase 8-naphthylvinyladenine (^{NV}A) and previously described ^{PV}A. We newly synthesized SNA oligomers containing adjacent ^{NV}As or adjacent ^{PV}A and ^{NV}A as orthogonal photo-switches. ^{NV}As in SNA strand were caused intra-strand crosslinking reaction by 340-405 nm light, whereas ≤ 300 nm light caused cycloreversion. Crosslinking of adjacent ^{PV}A and ^{NV}A in SNA was induced with 465-405 nm light, which was reversed by irradiation with ≤ 340 nm light. Each crosslinking caused dissociation of corresponding SNA/RNA duplex, whereas the cycloreversion resulted in re-formation of duplexes. It should be noted that these crosslink type photo-switches enabled the selective photo-regulation of dual SNA/RNA duplexes, orthogonally. With these ^{NV}A/^{NV}A and ^{NV}A/^{PV}A photo-switches, four hybridization states of two SNA/RNA duplexes could be orthogonally photo-controlled only by irradiation with a suitable wavelength of light.

This technology should expand use of acyclic XNAs including SNA in applications such as construction of complex photo-driven nanomachines.

3-2. Introduction

Manipulating molecules using external stimuli is important for construction of molecular robots, nano-devices, nano-machines, and other biological tools.[1] Light is suitable for this purpose, since it does not contaminate the reaction system and enables spatiotemporal control.[2] Use of different wavelengths of light allows simultaneous use of multiple photo-switches. With multiple photo-switches, sophisticated nanodevices have been developed that allow selective uncaging of caged compounds,[3] simultaneous monitoring of multiple enzymatic reactions,[4] polymer linkage and extension,[5] and photo-therapy.[6]

Photo-responsive DNAs have also been employed in bio- and nano-technology applications, and two photo-switches have been used to enable orthogonal control. Heckel et al. established a wavelength-selective uncaging system for DNA manipulation in which two caged molecules responded to different wavelength.[7] Fujimoto's group developed photo-crosslinkers based on pyranocarbazole and 3-cyanovinylcarbazole that orthogonally and reversibly react with nucleobases when irradiated with different wavelengths of light.[8] Reversible and orthogonal photo-regulation of DNA hybridization,[9] DNAzyme activity[10], and a DNA walker have also orthogonally controlled using two azobenzene derivatives.[11]

Recently, we incorporated photo-responsive moieties into serinol nucleic acid (SNA) which is a xeno nucleic acid with a non-ribose scaffold that can hybridize with complementary RNA, DNA, and SNA.[12] SNA has potential for use in biological tools and nucleic acid medicines that target RNA in cells, therefore photo-responsive SNA is expected to expand its performance. For the photo-regulation of SNA's duplex forming ability, we selected 8-pyrenylvinyladenine (^{PV}A, Figure. 3-1a), which undergoes [2+2] cycloaddition upon visible light irradiation that is reversed upon UV-A irradiation. Unlike

azobenzene-based photo-regulation, which can be induced thermally, the cycloaddition and cycloreversion reactions of ^{PV}A proceed only photochemically.[13]
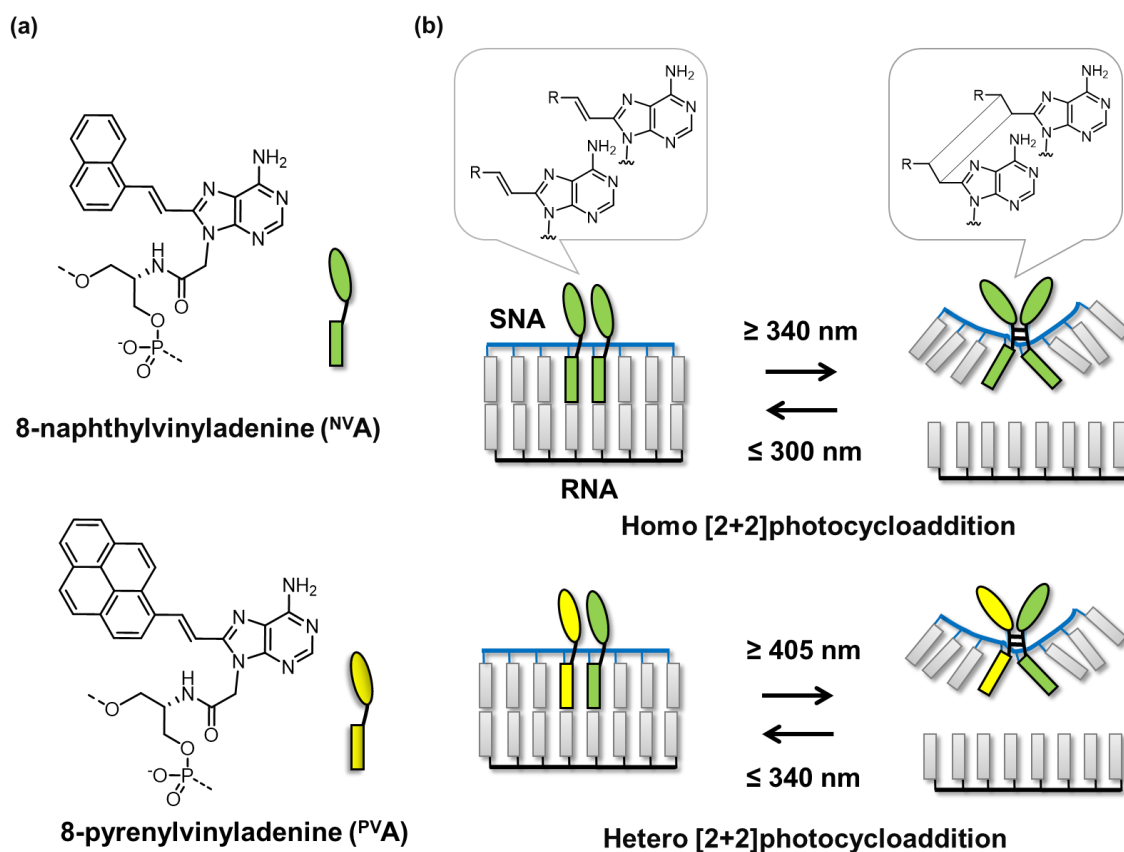
3-3. Method

(a)

8-naphthylvinyladenine (^{NV}A)

8-pyrenylvinyladenine (^{PV}A)

(b)

SNA

RNA

≥ 340 nm

≤ 300 nm

Homo [2+2]photocycloaddition

≥ 405 nm

≤ 340 nm

Hetero [2+2]photocycloaddition

Figure. 3-1 (a) Chemical structures of 8-naphthylvinyl adenine (^{NV}A) and 8-pyrenylvinyl adenine (^{PV}A). (b) Schematic illustration of reversible photo-control of SNA/RNA duplex formation via photo-crosslinking and cycloreversion when the SNA strand contains two adjacent ^{NV}A residues or ^{NV}A adjacent to ^{PV}A.

In this study, we designed and synthesized a new modified nucleobase: 8-naphthylvinyl adenine (^{NV}A, Figure. 3-1a) that responds to defferent wavelength of light from ^{PV}A. Adjacent ^{NV}A residues in SNA strand should be crosslinked by 340-405 nm light irradiation, whereas 300 nm light should cause cycloreversion of this crosslinked adduct.

The goal of our design was orthogonal photo-control of four different hybridization states by selection of suitable wavelengths of light. The first photo-responsive SNA contained adjacent ^{NV}A residues. The second photo-responsive SNA contained adjacent ^{PV}A and ^{NV}A residues because with this hetero pair cycloaddition and cycloreversion are induced by wavelengths derived from both pyrene and naphthalene absorptions. Partial overlap of the reacting wavelengths of ^{NV}A/^{NV}A and ^{PV}A/^{NV}A ensures both cooperativity and orthogonality of light sources. These two photo-responsive SNAs enabled orthogonal photo-control of SNA/RNA hybridization (Figure. 3-1b).

3-4. Results and Discussion

3-4-1. Synthesis of ^{PV}A and ^{NV}A introduced SNA oligomer
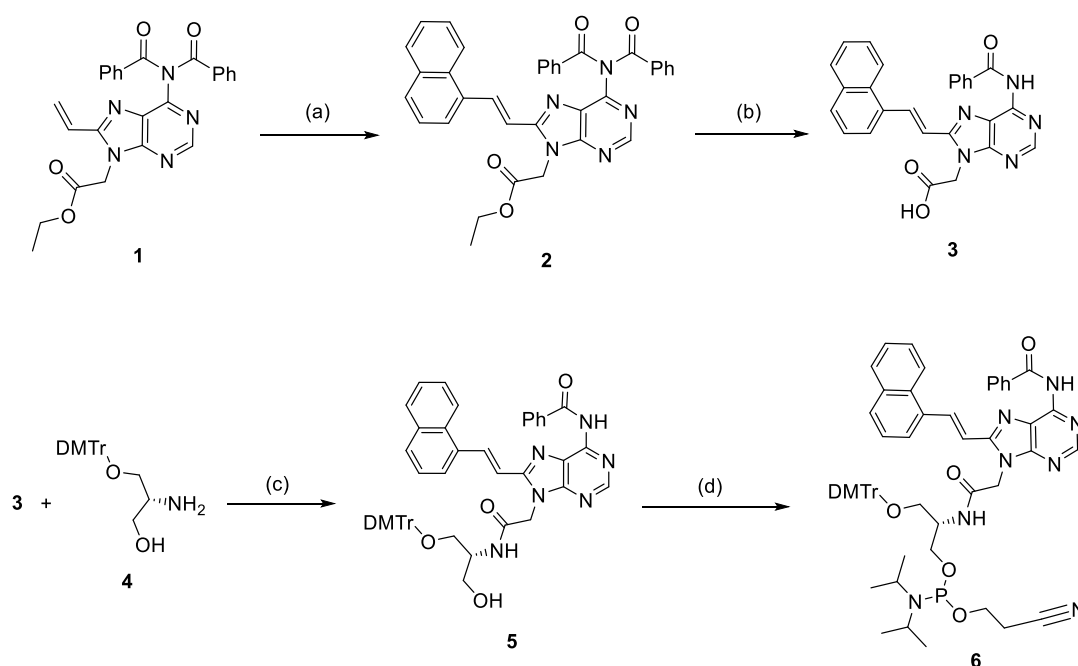
Scheme. 3-1 Synthesis of the phosphoramidite monomer of SNA-^{NV}A. Reagents and conditions: a) 1-bromonaphthalene, Pd(OAc)$_2$, triphenylphosphine, triethylamine, dry DMF, 110 °C, 30 min.; b) NaOH aq, MeOH, room temperature, 20 min.; c) DMT-MM, triethylamine, DMF, room temperature, 30 min.; d) 2-cyanoethyl diisopropylchlorophosphoramidite, Et$_3$N, dry CH$_2$Cl$_2$, room temperature, 30 min.

The phosphoramidite monomer of SNA-^{NV}A was synthesized by similar procedure to that of SNA-^{PV}A (Scheme 1). For orthogonal photo-control of hybridization, SNA oligomers containing two ^{NV}A residues (SNN) and one ^{NV}A and one ^{PV}A residue (SPN) were synthesized. In addition, SNA including only one ^{NV}A or ^{PV}A residue (SN, SP) were also prepared for comparison of reactivity (Table. 3-1).

Table. 3-1 SNA Sequences containing photo-responsive modified nucleobases (^{NV}A, ^{PV}A)

	Sequence
SNN	(*S*)-GCT^{NV}**A**^{NV}**A**TGC-(*R*)
SPN	(*S*)-GCT^{PV}**A**^{NV}**A**TGC-(*R*)
SN	(*S*)-GCT^{NV}**A**ATGC-(*R*)
SP	(*S*)-GCT^{PV}**A**ATGC-(*R*)

3-4-2. Effect of modified nucleobases on the stability of SNA/RNA duplex

First, in order to evaluate the effect of modified nucleobases on the stability of a duplex with RNA, melting temperatures (T_ms) were measured; the sequences and T_ms are listed in Table. 3-2.

Table. 3-2 Melting temperature (T_m) of SNA/ RNA duplex containing ^{NV}A and ^{PV}A

T_m with complementary RNA	
SNN/RNA	39.6 °C
SPN/RNA	39.5 °C
SN/RNA	37.9 °C
SP/RNA	30.0 °C

The modification with a single ^{NV}A (SN/RNA) slightly increased T_m relative to the duplex with the unmodified SNA ($T_m = 35.5 \,^\circ C$) (Figure. S3-1). The melting temperatures of both SNN/RNA and SPN/RNA with tandem modified adenines were significantly higher than that of SN/RNA (Figure.3-8b and 3-13b black lines). We also calculated the thermodynamic parameters of the SNN/RNA duplex (Table. S3-2). As a result, SNN/RNA duplex showed much smaller ΔH° values and $-T\Delta S^\circ$ values than those of unmodified SNA/RNA duplex, indicating that stabilization of SNN/RNA duplexes relative to the duplexes formed from unmodified strands was caused by favorable entropic contributions: stacking between ^{NV}As presumably made the single stranded SNA (SNN) rigid and reduced the entropy loss associated with duplex formation. This result is in agreement with our previous report that demonstrated that stacking interactions between adjacent chromophore-modified nucleobases result in duplex stabilization.[14, 15]

3-4-3. Interaction of modified nucleobases introduced into SNA/RNA duplex

Next, in order to investigate the interaction of ^{NV}As in SNA, absorption and fluorescence spectra of SNN/RNA and SN/RNA were measured prior to irradiation. The absorption spectra of the SNN/RNA duplex showed a hypsochromic shift with an absorption maximum at 363 nm, respect to SN/RNA (λ_{max} = 369 nm) (Figure. 3-2a). Fluorescent emission of the SNN/RNA appeared around 473 nm showing obvious bathochromical shift compared with the SN/RNA duplex (λ_{max} = 452 nm) (Figure. 3-2b). These results suggested excimer formation of ^{NV}As introduced into SNA similar to ^{PV}As in SNA.
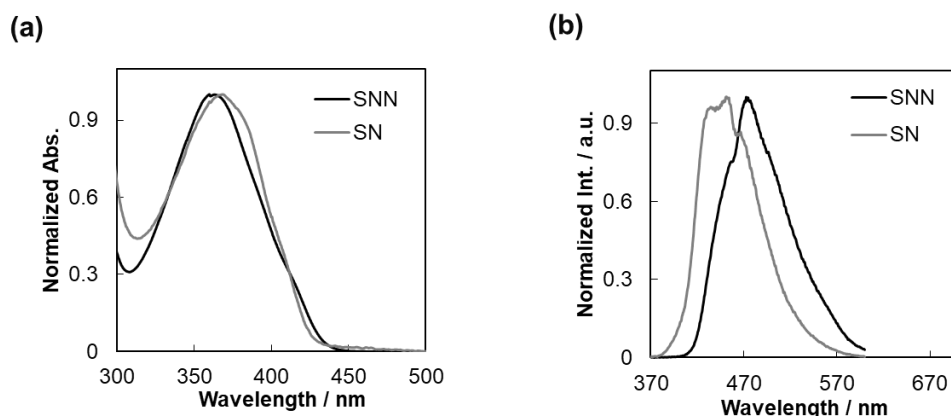
Figure. 3-2 (a) Normalized absorption spectra of SNN/RNA and SN/RNA duplexes. (b) Fluorescence spectra of SNN/RNA and SN/RNA duplexes. λ_{ex} = 360 nm. Conditions: 100 mM NaCl, 10 mM phosphate buffer (pH 7.0), 20 °C. Concentration of SNA was 5.0 mM..

We also investigated the interaction between ^{NV}A and ^{PV}A in the SPN/RNA duplex.The absorption spectra of the SPN/RNA duplex was not identical with sum of SP/RNA and SN/RNA: slight hypsochromic shift and the formation of a weak shoulder band at the long wavelength (Figure. 3-3a). Also emission of the SPN/RNA duplex (around 512 nm) was red-shifted relative to both SP/RNA and SN/RNA. These results was suggested exciplex formation of ^{NV}A and ^{PV}A in SNA (Figure. 3-3b).
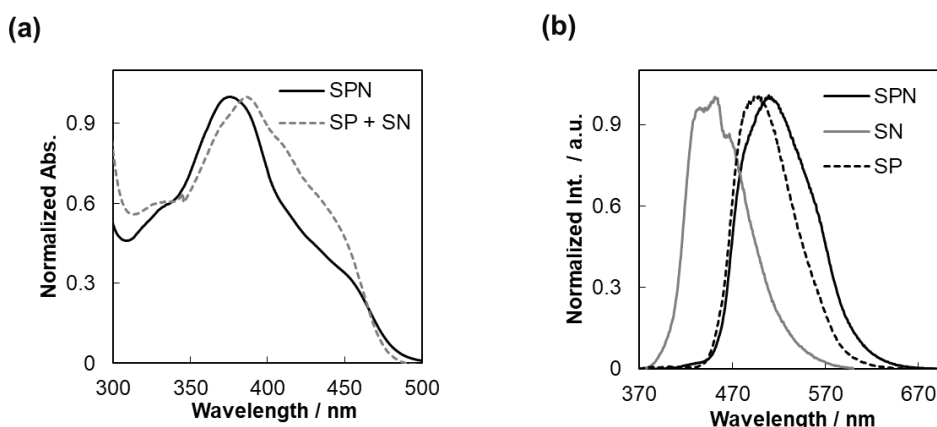
Figure. 3-3 (a) Normalized absorption spectra of SPN/RNA, SN/RNA, and SP/RNA duplexes without photoirradiation. (b) Fluorescence spectra of SPN/RNA, SN/RNA, and SP/RNA duplexes without photoirradiation. λ_{ex} = 400 nm. Conditions: 100 mM NaCl, 10 mM phosphate buffer (pH 7.0), 20 °C. Concentration of SNA was 5.0 mM..

Furthermore, induced CD derived from exciton coupling of adjacent modified nucleobases was observed on each SNA/RNA duplex prior to light irradiation, which also means their strong stacking (Figure 3-8a and Figure 3-13a black lines). It should also be noted that the CDs near 260 nm, which correspond to the nucleobases of each duplex, showed a shape very similar to that of the unmodified duplex. In other words, their strong interaction also did not significantly affect not only the duplex stability but also the overall structure of the duplex at before irradiation.[13, 14]

3-4-4. Photo-reactivity of [NV]As in SNA/RNA duplex

The SNN/RNA duplex was exposed to Vis/UV light at 20 °C firstly to evaluate the photo-reaction of [NV]A residues in SNA.
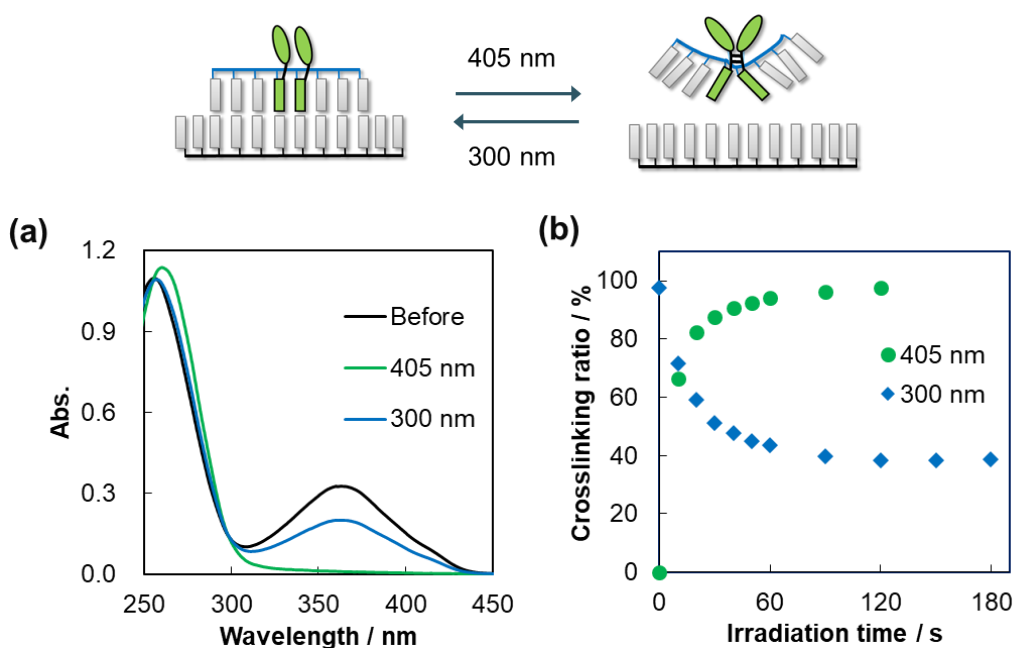
Figure. 3-4 (a) Absorption spectra of SNN/RNA before (black lines) and after irradiation with 405 nm light (green lines) and 300 nm light (blue lines). Solution conditions were 5.0 μM oligonucleotide, 100 mM NaCl, 10 mM phosphate buffer (pH 7.0). (b) Percent of crosslinked [NV]A in SNN/RNA as a function of irradiation time at 405 nm (green circles) and 300 nm (blue squares). The percentages of crosslinked products were calculated from absorbance at 368 nm.
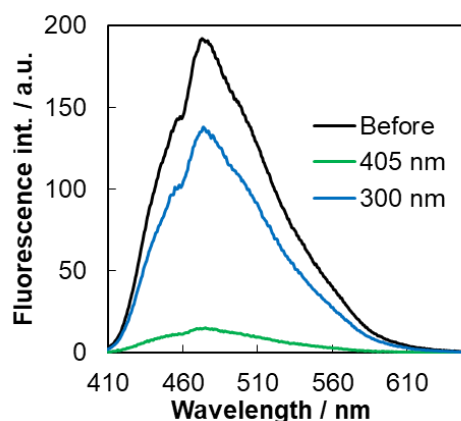
Figure. 3-5 Fluorescence spectra of SNN/RNA before irradiation (black lines), PSS at 405 nm light (green lines), and PSS at 300 nm light (blue lines). Solution conditions were 5.0 μM duplex, 100 mM NaCl, 10 mM phosphate buffer (pH 7.0) at 20 °C. PSS was attained by irradiation with 405 nm for 2 min or 300 nm for 3 min.

Upon irradiation with 405 nm light for 60 s, the absorption band due to ^{NV}A at around 360 nm completely disappeared from the spectrum of the SNN/RNA duplex due to quantitative photo-cycloaddition between ^{NV}A residues (Figure.3-4 green line and green circle, and S3-2a). An increasing absorbance at around 250-300 nm would be partly contributed by appearance of 1-alkylnaphtalene in photo-dimer of ^{NV}A, not only hyperchromic effect by the dissociation of the duplex. Upon irradiation with 300 nm light to this photo-adduct, photo-cycloreversion occurred, and 61% of the initial absorption band was restored within 120 s (Figure.3-4 blue line and blue circle, and S3-2b). An isosbestic point at 298 nm was indicative of a 1:1 selective reaction.

Elimination and recovery of the fluorescence of ^{NV}A by the irradiation with 405 nm and 300 nm, respectively, also suggesting the progression of the reversible photo-cycloaddition (Figure.3-5).

The photo-reaction in SNN/RNA was further analyzed by reversed phase HPLC (Figure. 3-6 and S3-4). A peak at 26 min present in the chromatogram of the initial SNN duplex sample almost completely disappeared after irradiation with 405 nm light and

concurrently a new peak corresponding to the photo-adduct appeared at 31 min. Subsequent irradiation with 300 nm light restored the initial peak. These results clearly demonstrate reversible and selective intra-strand photo-crosslinking reaction of ^{NV}A residues in the SNA strand.
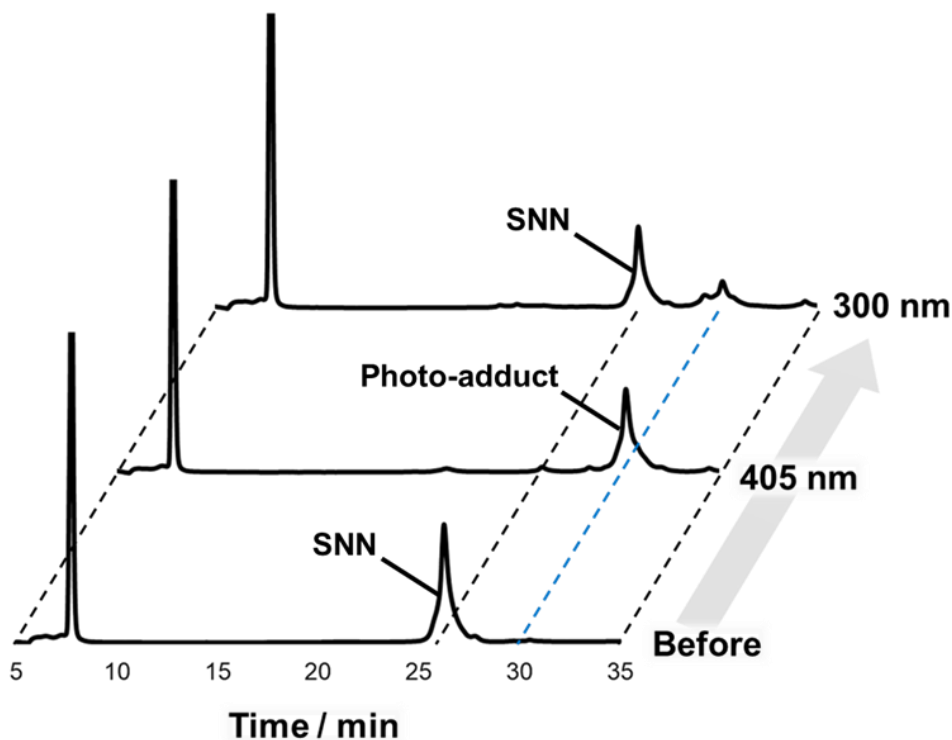

Figure. 3-6 Reversed-phase HPLC profiles of SNN/RNA duplex monitored at 260 nm before and after irradiating with 405 nm light for 120 s and 300 nm for 300 s at 20 °C.

Furthermore, we also confirmed that reversible photo-switching of these cycloaddition in SNN was achieved by at least 5 cycles of repetitive irradiation, with only little photo-bleaching (Figure 3-7).

On the other hand, one ^{NV}A residue in SNA/RNA duplex (SN/RNA) primarily caused the isomerization reaction (Figure. S3-6). Presumably the strong stacking of ^{NV}As in SNN also worked favorably to induce the cycloaddition reaction by suppressing the isomerization reaction.
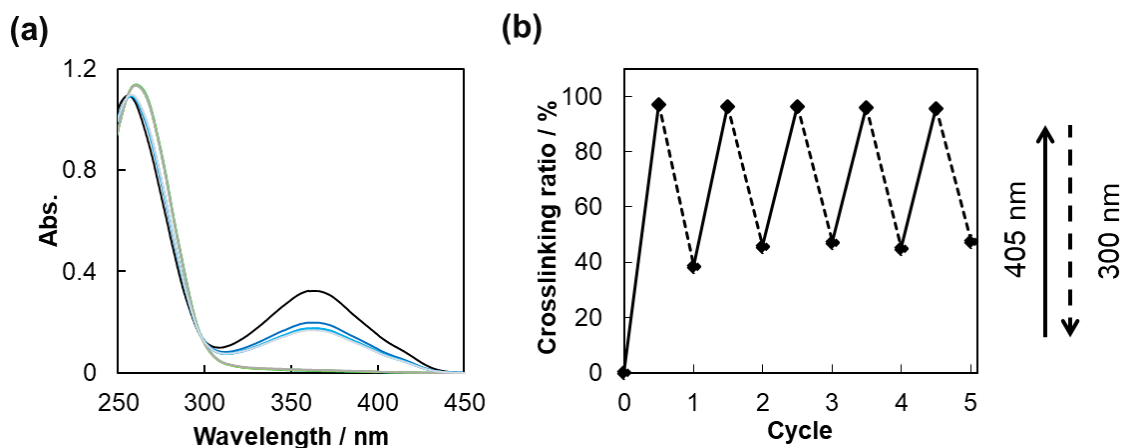
Figure. 3-7 (a) Absorption spectra of SNN/RNA after repeated irradiation cycles. Conditions: 100 mM NaCl, 10 mM phosphate buffer (pH 7.0), 20 °C. Concentration of duplex was 5.0 μM. (b) Percent crosslinking of chromophores in SNN after indicated number of photo-switching cycles. Samples were irradiated at 405 nm for 2 min and at 300 nm for 3 min. The percent crosslinking was determined from the absorption spectra.

3-4-5. Evaluation of photo-control of SNA/RNA duplex formation by using reversible photo-crosslinking of ^{NV}A

Next, we measured T_{m}s of SNN/RNA duplex after irradiation. Photo-crosslinking of the SNA in the SNN/RNA duplex by irradiation with 405 nm light significantly decreased the T_{m}s (Figure. 3-8b green line and Table. 3-3). This severe destabilization resulted in a single-stranded state at around room temperature (20 °C). Subsequent irradiation of the photo-adducts with 300 nm light restored sigmoidal melting curves with T_{m}s close to those observed pre-irradiation (Figure. 3-8b blue line), demonstrating photo-control of duplex formation. The induced circular dichroism CD derived from excitonic coupling between modified nucleobases in duplex also disappeared upon visible light irradiation and was restored by UV light irradiation (Figure. 3-8a). The CD signal at around 260 nm also changed reversibly, confirming the synchronization of reversible cycloaddition with duplex formation.
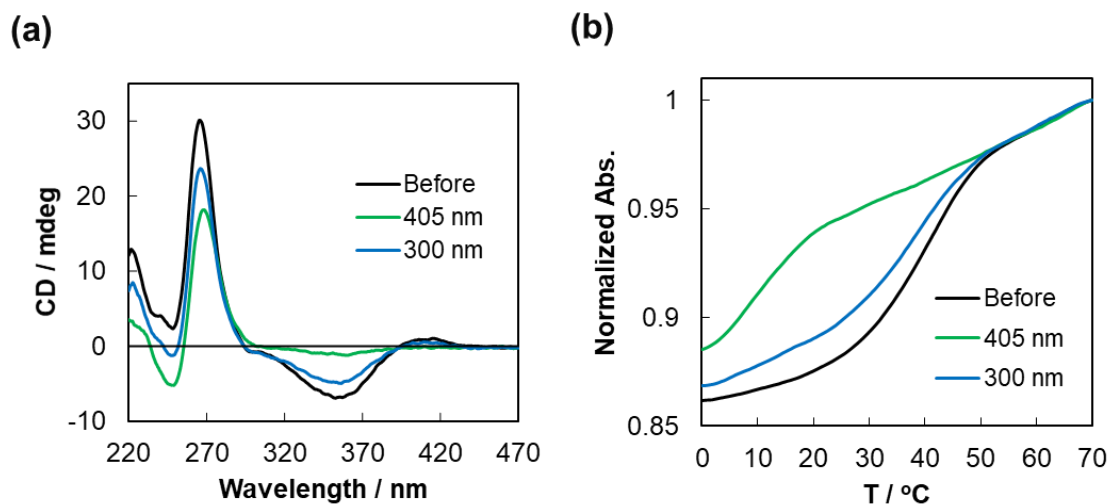
(a)

(b)

Figure. 3-8 (a) CD spectra and (b) Melting profile of SNN/RNA before (black lines) and after irradiation with 405 nm light (green lines), respectively, followed by irradiation with 300 nm light (blue lines) at 20 °C. Solution conditions were 5.0 μM oligonucleotide, 100 mM NaCl, 10 mM phosphate buffer (pH 7.0).

Table. 3-3 Melting temperature (T_m) of SNN/RNA at PSS at 405 nm and 300 nm.

T_m with complementary RNA	
PSS at 405 nm	<10 °C
PSS at 340 nm	36.2 °C

3-4-6. Photo-reactivity of ^{NV}A and ^{PV}A in SNA/RNA duplex

To verify that the second photo-switch, which is based on photo-crosslinking reaction of adjacent ^{PV}A and ^{NV}A residues, works properly, the SPN/RNA duplex was also exposed to Vis/UV light at 20 °C.

Irradiation with 465 nm resulted in disappearance of the peak at around 380nm corresponding both ^{NV}A and ^{PV}A, with appearance of a peak assignable to alkylpyrene appeared at around 310-360 nm: proceeding of heterologous crosslinking reaction was suggested (Figure. 3-9 green line and green circle, and S3-3a). The reverse occurred upon

irradiation with 300 nm light (Figure. 3-9 blue line and blue circle, and S3-3b). A significant decrease in emission intensity ($\lambda_{ex} = 360$ nm) by 465 nm irradiation also suggested that both ^{NV}A and ^{PV}A in SNA were consumed: progression of this "hetero" crosslinking (Figure. 3-10).
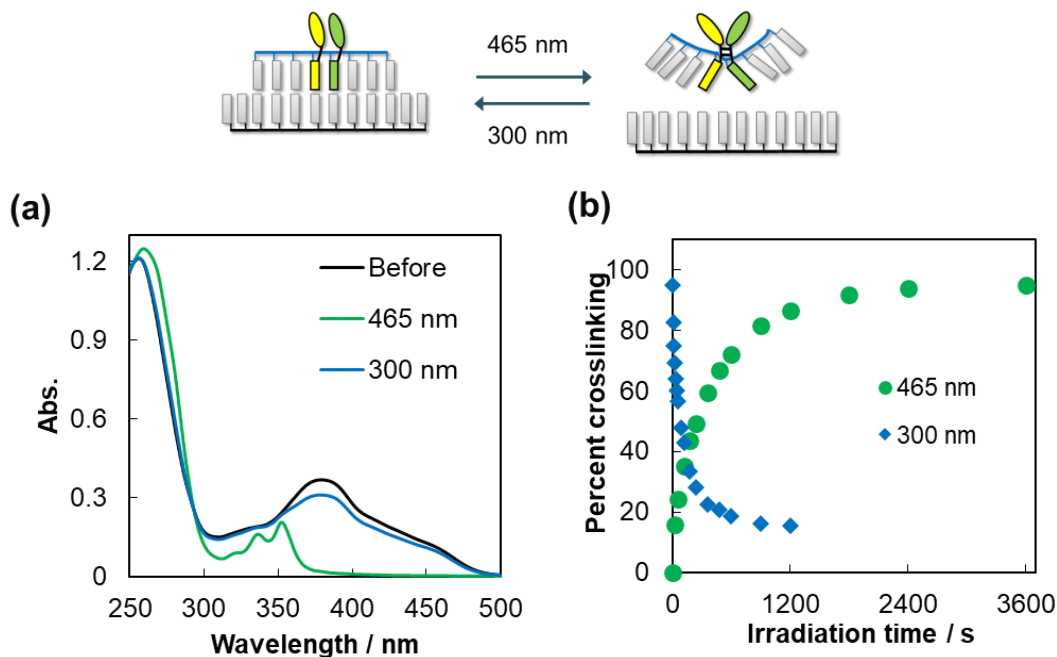

Figure. 3-9 (a) Absorption spectra of SPN/RNA before (black lines) and after irradiation with 465 nm light (green lines) and subsequent irradiation with 300 nm light (blue lines). Solution conditions were 5.0 μM oligonucleotide, 100 mM NaCl, 10 mM phosphate buffer (pH 7.0) (b) Percent of crosslinked chromophores as a function of irradiation time at 465 nm (green circles) and 300 nm (blue squares). The percentages of crosslinked products were calculated from absorbance at 383 nm recorded after each irradiation.

HPLC analyses revealed that irradiation with 465 nm light resulted in loss of the peak at 27 min corresponding to SPN accompanied by appearance of a main peak at 31 min and several minor peaks at shorter retention times (Figure. 3-11). Since all of these peaks showed both alkylpyrene and alkylnaphthalene absorptions (Figure. S3-7), they were assigned to diastereomers of hetero-cycloaddition adducts or the interstrand crosslinking product. Subsequent irradiation with 300 nm light resulted in the disappearance of all

photo-adduct peaks and the recovery of the peak with a retention time of 27 min (Figure. 3-11 and S3-7). These results clearly demonstrated that a hetero-cycloaddition reaction occured between ^{NV}A and ^{PV}A in SNA strand and that the reaction was reversible.
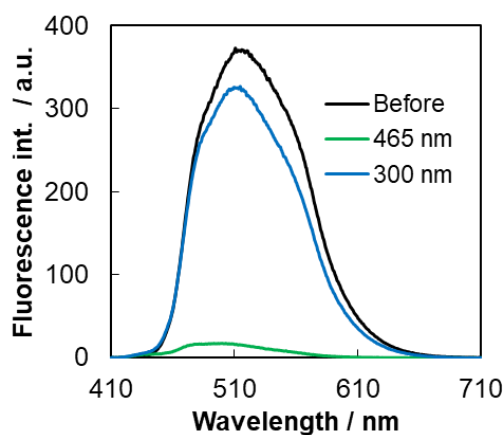

Figure. 3-10 Fluorescence spectra of SPN/RNA before irradiation (black lines), PSS at 465 nm light (green lines), and PSS at 300 nm light (blue lines). Solution conditions were 5.0 μM oligonucleotide, 100 mM NaCl, 10 mM phosphate buffer (pH 7.0) at 20 °C. PSS was attained by irradiation with 465 nm for 60 min and 300 nm for 20 min.
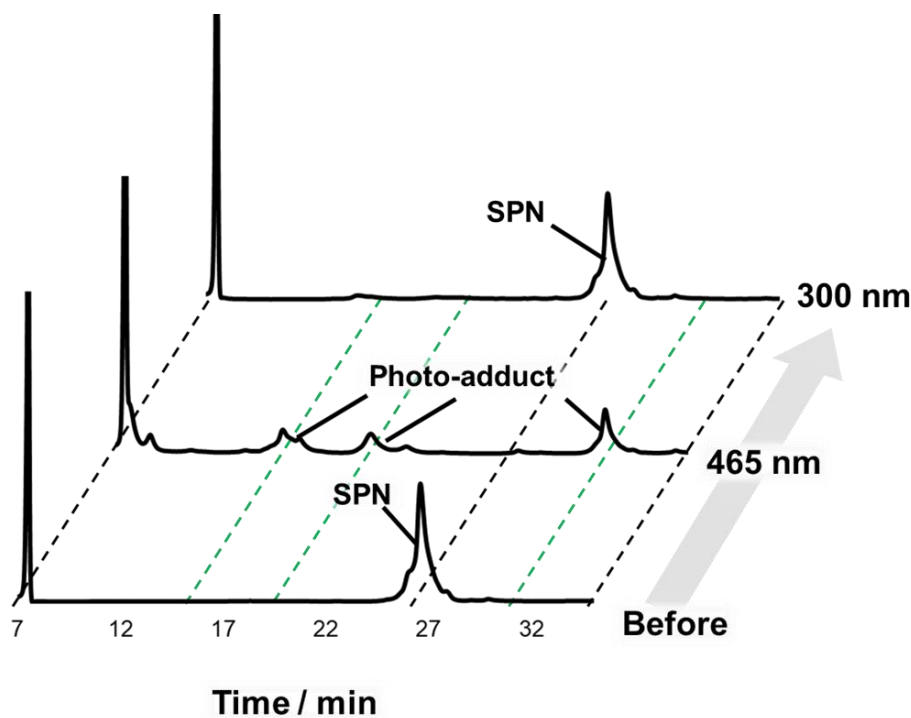
Figure. 3-11 Reversed-phase HPLC profilesof SPN/RNA duplex at 260 nm before and after irradiating with 465 nm light for 3600 sec and with 300 nm for 1800 sec.

In addition, this photo-cycloaddition/cycloreversion reaction could also be induced repeatedly by alternating irradiation with Vis/UV light (Figure. 3-12).
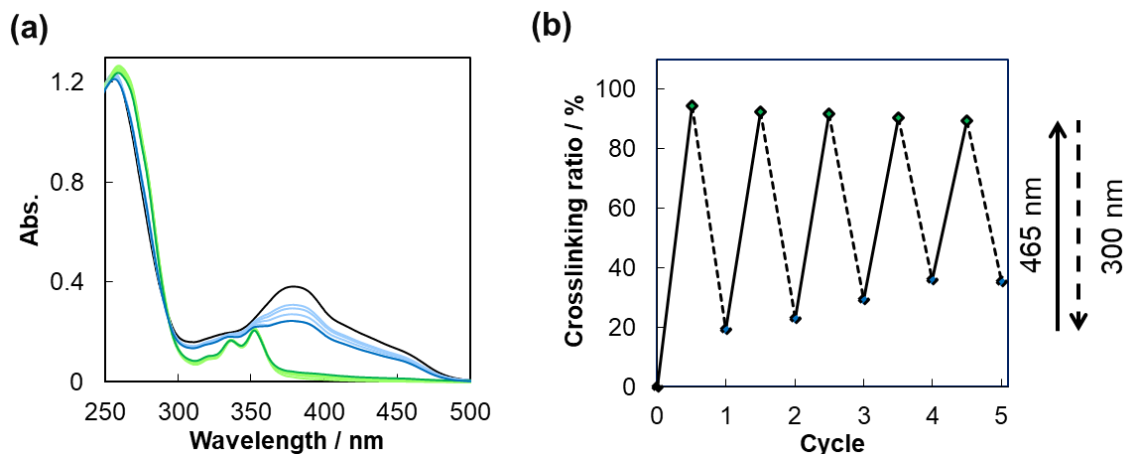
Figure. 3-12 (a) Absorption spectra of SPN/RNA after repeated irradiation cycles. Conditions: 100 mM NaCl, 10 mM phosphate buffer (pH 7.0), 20 $^{\circ}$C. The concentration of duplex was 5.0 μM. (b) Percent crosslinking of chromophores in SPN after multiple photo-switching cycles. Sample of SPN/RNA duplex was irradiated with 465 nm for 60 min and with 300 nm for 20 min. The reaction ratios were calculated by using absorption spectra recorded after each irradiation.

3-4-7. Evaluation of photo-control of SNA/RNA duplex formation by using reversible photo-crosslinking of ^{NV}A and ^{PV}A

We examined whether it is possible to control duplex formation based on the hetero-photo-crosslinking reaction of ^{NV}A/^{PV}A in SPN/RNA. At photo-stationary state at 465 nm, the induced CD derived from the modified nucleobases eliminated, and the CD corresponding to the nucleobase also changed significantly (Figure. 3-13a green line). Moreover, T_m of duplex also decreased significantly (Figure. 3-13b green line and Table. 3-4), indicating double-strand dissociation. At photo-stationary state at 300 nm, the initial CD and sigmoidal melting were restored (Figure. 3-13a blue line and Table. 3-4), demonstrating duplex re-formation at room temperature. These results ensured that this photo-switch can also be applied to regulate duplex forming.
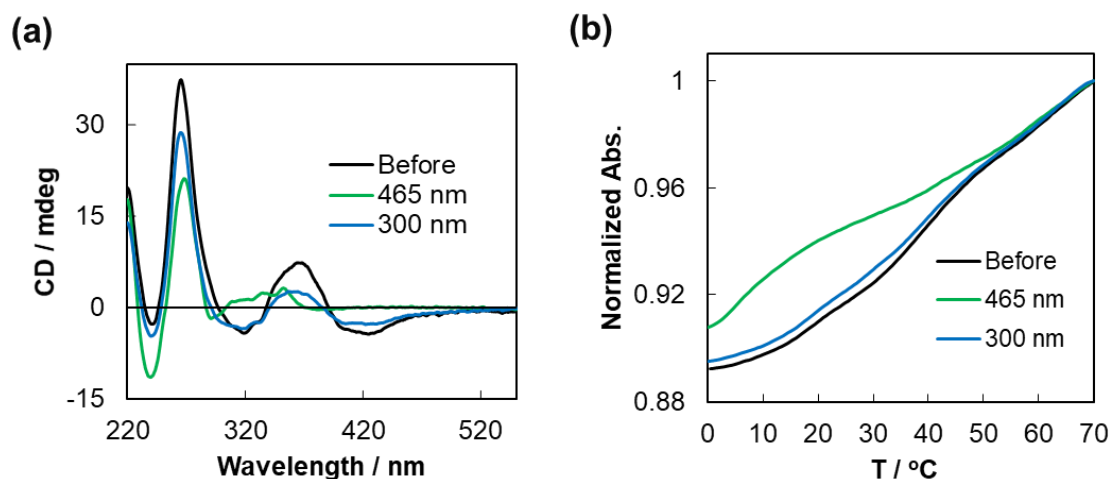
81

Figure. 3-13 (a) CD spectra and (b) Melting profile of SPN/RNA before (black lines) and after irradiation with 465 nm light (green lines), followed by irradiation with 300 nm light (blue lines) at 20 °C. Solution conditions were 5.0 μM oligonucleotide, 100 mM NaCl, 10 mM phosphate buffer (pH 7.0).

Table. 3-4 Melting temperature (T_m) of SPN/RNA at PSS at 465 nm and 300 nm.

T_m with complementary RNA	
PSS at 465 nm	N.A.
PSS at 340 nm	36.2 °C

3-4-8. Effect of wavelength on photo-crosslinking of dual photo-switches

We next examined the effect of wavelength on photo-crosslinking of chromophores in SNN and SPN. The absorption of SNN/RNA and SPN/RNA at before and after crosslinking, and the wavelengths of the irradiated light are shown in Figure. 3-14a.

Photo-irradiation at 405 nm that both ^{NV}A and ^{PV}A have absorption, allowed efficient cross-linking of both modified SNA strand. Whereas irradiation at 254-300 nm, correspond to alkyl naphthalene, caused cycloreversion of both adducts (Figure. S3-8 and S3-10). 465 nm LED light much more efficiently induced crosslinking in SPN (^{PV}A/^{NV}A) than in SNN (^{NV}A/^{PV}A) (Figure. S3-12 and S3-13). This was expected as ^{PV}A has a

considerably higher absorption coefficient than [NV]A.[15] In contrast, 340 nm light accelerated crosslinking only in SNN and not SPN (Figure. S3-9a and S3-11b). Moreover, 340 nm light induced cycloreversion of the photo-adduct in SPN (Figure. S3-11a) and reformation of SPN/RNA duplex (Figure. S3-11d), because crosslinked [NV]A/[PV]A had clear absorption at around 340 nm, whereas the [NV]A/[NV]A photo-adduct had no absorption at this wavelength.
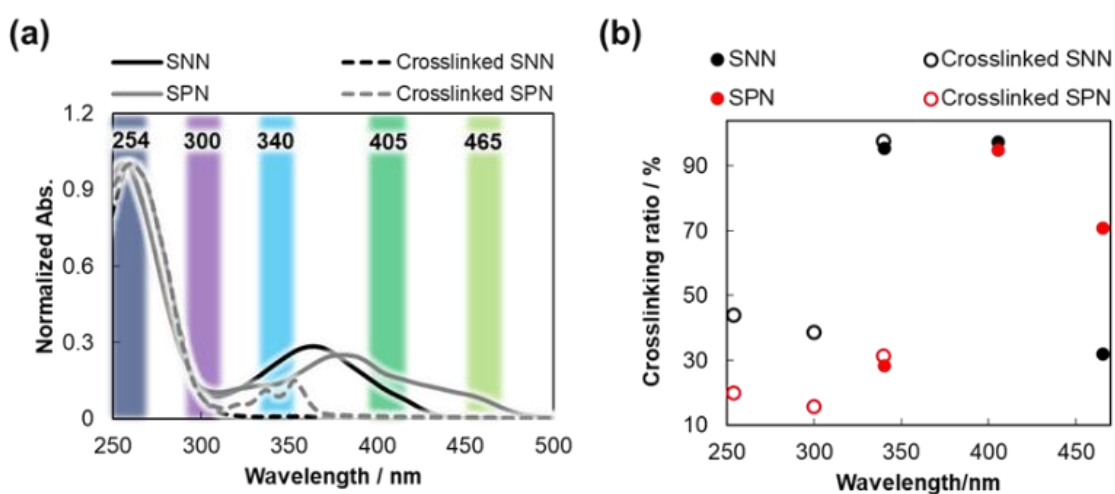

Figure. 3-14 (a) Relationship between the wavelength of photo-irradiation and absorption spectra of SNN and SPN before and after crosslinking. (b) Relationship between the percent of crosslinked chromophores of SNN (black) and SPN (red) and irradiation wavelength. Open circles are percent crosslinking of chromophores in SNN and SPN first irradiated with 405 nm light and then with the indicated light of wavelength. Solution conditions were 5.0 µM oligonucleotide, 100 mM NaCl, 10 mM phosphate buffer (pH 7.0). For 465 nm irradiation, a longpass optical filter was used to remove the light below 450 nm.

The percent crosslinking of SNN and SPN after light irradiation at each wavelength are shown in Figure 3-14b. These results mean that the reactivity of both modified SNAs can be regulated individually by only switching the irradiation wavelength.

3-4-9. Orthogonal photo-control of hybridization between SNA and RNA

Based on the above results, we expected that orthogonal photo-control of SNN/RNA and SPN/RNA duplexes formation is possible by selecting suitable wavelengths of light (Figure. 3-15). Both modified SNA strands should form duplexes with complementary RNA strand before irradiation and after irradiation with 300 nm light (State 1). When 405 nm light is irradiated for State1, State3 or State4, both duplexes should dissociate by photo-cycloaddition reactions induced by irradiating with this wavelength (State 2). In contrast, 465 nm irradiation of duplexes in State1 should induce preferential dissociation of the SPN/RNA duplex than the SNN/RNA duplex and allow transition to State3. Irradiation of 340 nm for each state should allow both dissociation of the SNN/RNA duplex and formation of SPN/RNA duplex and result in State 4.
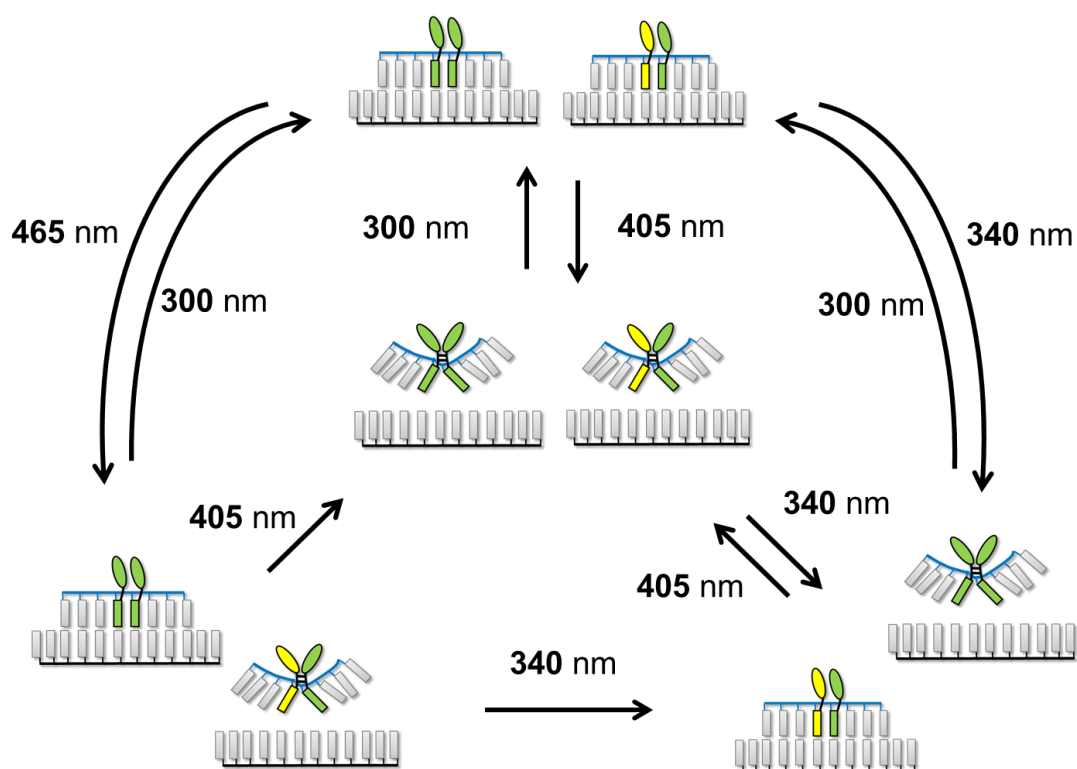
Figure. 3-15 Illustration of controlled hybridization of two SNA/RNA duplexes. Four possible states of SNA/RNA duplexes can be realized by irradiating with four different wavelengths of light (465 nm, 405 nm, 340 nm, and 300 nm).

To demonstrate photo-control of the four states, we analyzed both HPLC and absorption spectra.

We first sought to demonstrate transition from State 1 to State 2 to State 1 by irradiating with 405 nm and 300 nm light (Figure. 3-16 and S3-14). We started with a sample containing both SNN/RNA duplex and SPN/RNA duplex that had not been irradiated (State 1). Irradiation of 405 nm light to state 1 (before irradiation) eliminated the absorption band of modified nucleobases around 310-490 nm and appeared a new peak corresponding to alkylpyrene (Figure. 3-16a green line and S3-14a). Also, this irradiation resulted in almost completely disappearance of peaks corresponding to both modified SNA accompanied by appearance of new peaks from each photo-adduct in the HPLC chromatogram (Figure.3-16b). In addition, after 405 nm irradiation, the percent crosslinking of both SNN and SPN reached more than 90% (Figure. 3-16c). These results clearly indicated transition to State 2 induced by photo-cycloaddition in both SNN and SPN. Subsequent irradiation with 300 nm restored initial absorption of modified nucleobases and the HPLC peak corresponding to both SNA strands (Figure.3-16a purple line, S3-14b). After this irradiation, the percent crosslinking was reduced to 55% for SNN and 12% for SPN (Figure. 3-16c), indicated return, although not completely, to State 1.

Next, we examined the pathway from State 2 to State 4 to State 1, in order to confirm whether the re-formation of SPN/RNA duplex and SNN/RNA can be orthogonally photo-controlled (Figure. 3-17 and S3-15). For this purpose, the sample containing both dissociated duplexes (State 2) was prepared. Irradiation with 340 nm for this sample restored the HPLC peak corresponding to the SPN/RNA duplex without reduction of photo-crosslinked SNN (State 4) (Figure. 3-17b). Selective cycloreversion in SPN was confirmed by analysis of the absorption spectrum due to the disappearance of the

absorption peak assigned to alkylpyrene (Figure. 3-17a blue line and S3-15). Over 90% of modified nucleobases were crosslinked for SNN and less than 20% for SPN, indicative of high selectivity (Figure. 3-17c). Final irradiation with 300 nm light restored both SNN related absorption and HPLC peaks (Figure. 3-17a, b and S3-15b), the percent crosslinking was reduced to 45% for SNN and 15% for SPN (Figure. 3-17c). These results suggest that 300 nm irradiation for state 4 also results in State 1. In other words, we confirmed that the selection of the wavelength of the irradiation light allowed either simultaneous or selective formation of the two SNA/RNA duplexes.
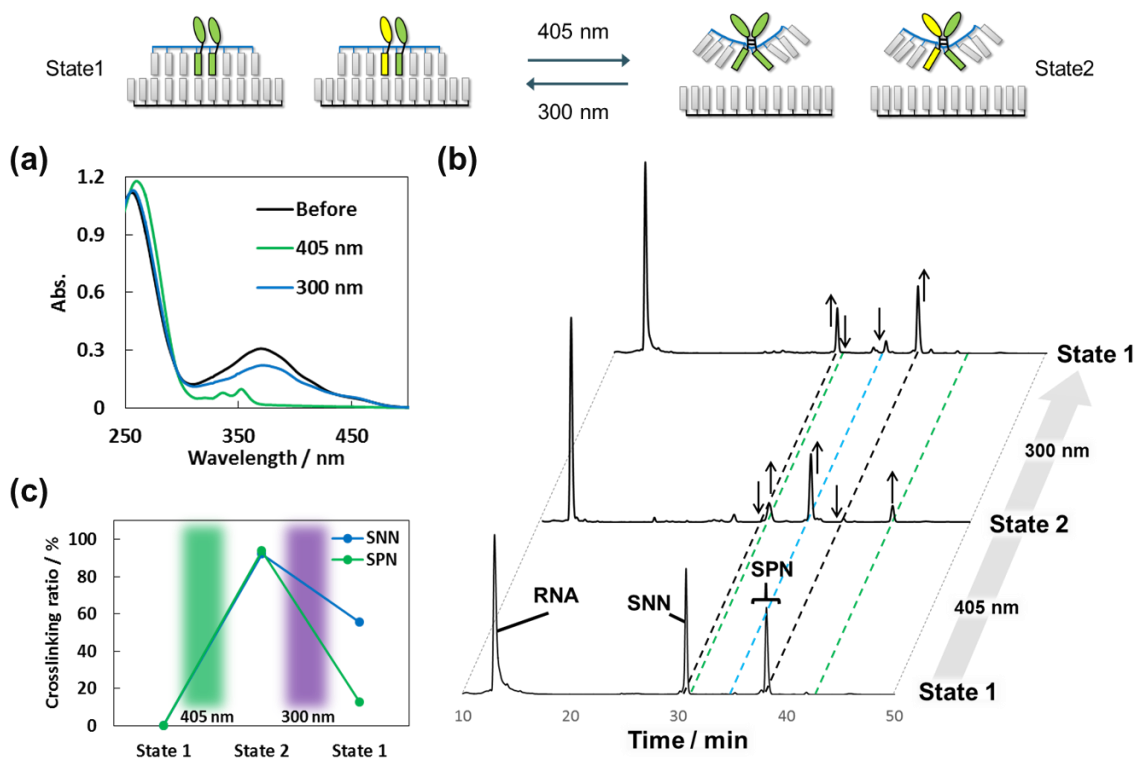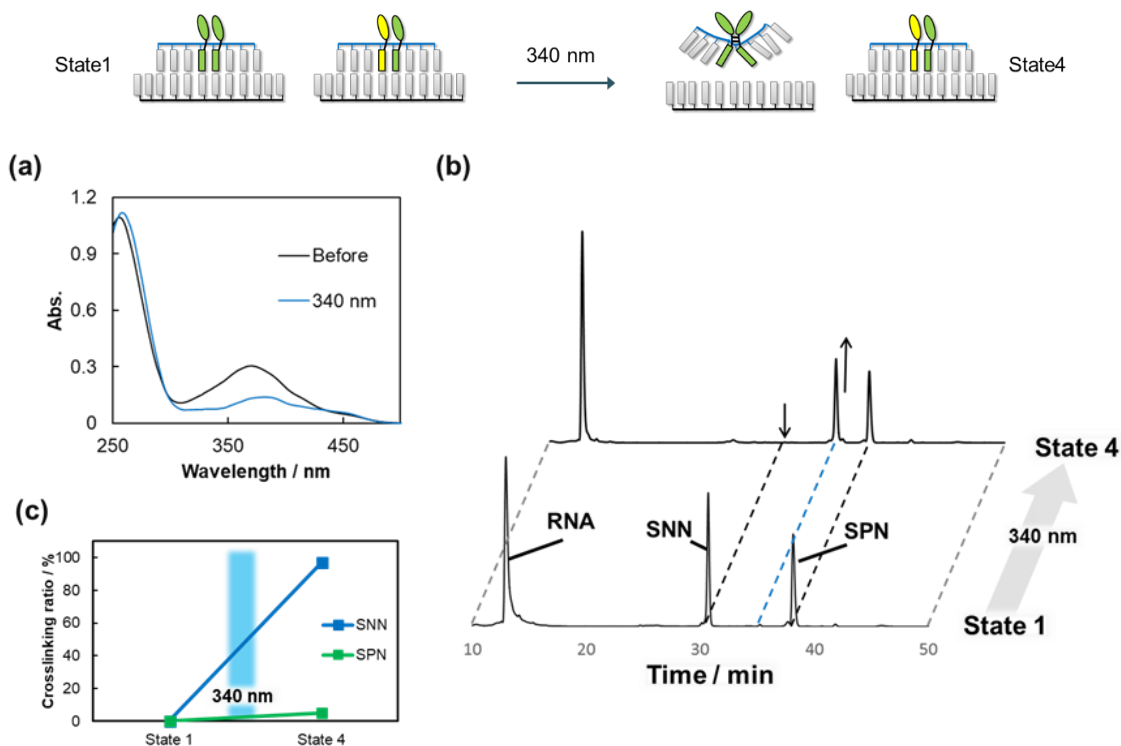

Figure 3-16. Controlled transition of two SNA/RNA duplexes from State 1 to State 2 to State 1. (a) Absorption spectra of SNA/RNA duplexes at before irradiation (State 1, black line), after 405 nm irradiation (State 2, green line) and after 300 nm irradiation (State 1, purple line). (b) HPLC profiles at each state. Absorption was monitored at 260 nm. (c) Percent of crosslinked $^{NV}A/^{NV}A$ in SNN (blue) and $^{NV}A/^{PV}A$ in SPN (green) at each state. The percentages of crosslinked products were calculated from decrease of HPLC peak areas corresponding SNN and SPN. Light irradiation was carried out for 60 min at 405 nm and 30 min at 300 nm. Solution conditions were 2.5 μM SNA, 5.0 μM RNA, 100 mM NaCl, 10 mM phosphate buffer (pH 7.0), 20 °C
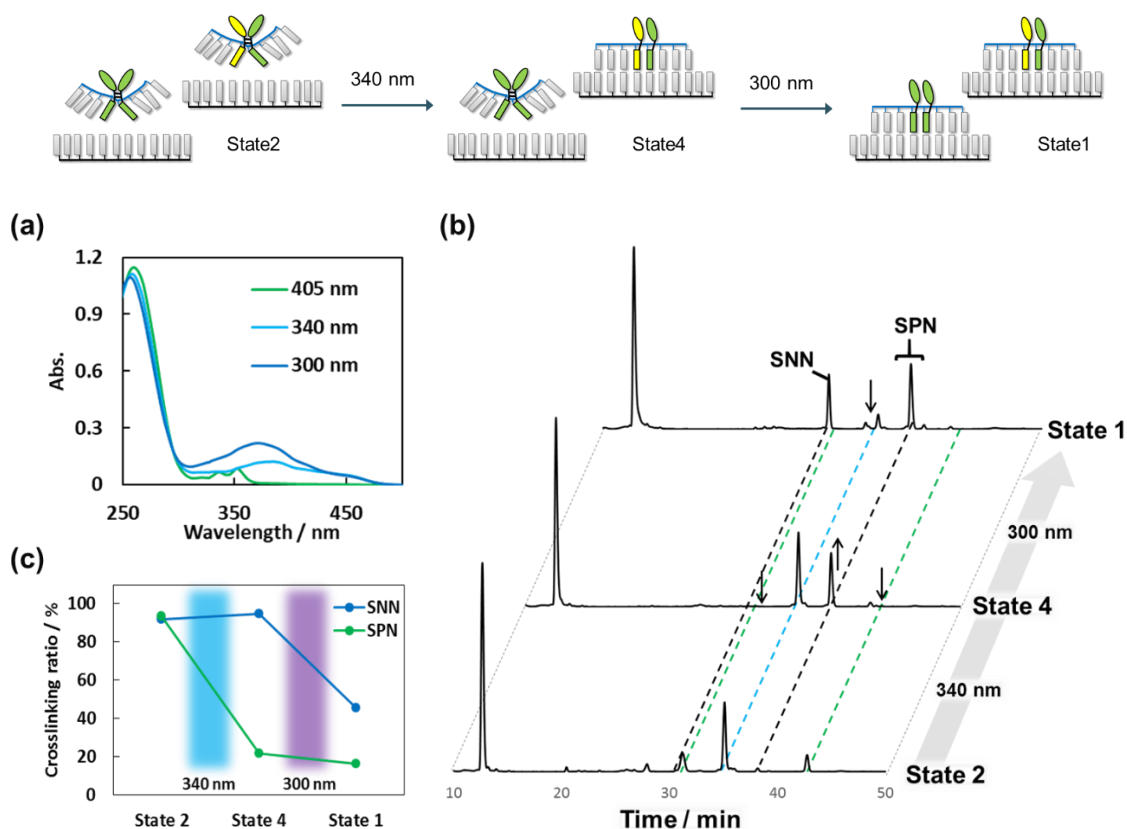
Figure. 3-17 Controlled transition of two SNA/RNA duplexes from State 2 to State 4 to State 1. (a) Absorption spectra of SNA/RNA duplexes after 405 nm irradiation (State 2, green line), after 340 nm irradiation (State 4, blue line) and after 300 nm irradiation (State 1, purple line). (b) HPLC profiles at each state. Absorption was monitored at 260 nm. (c) Percent of crosslinked $^{NV}A/^{NV}A$ in SNN (blue) and $^{NV}A/^{PV}A$ in SPN (green) at each state. The percentages of crosslinked products were calculated from decrease of HPLC peak areas corresponding SNN and SPN. Light irradiation was carried out for 30 min at 340 nm, and 5 min at 300 nm. Solution conditions were 2.5 μM SNA, 5.0 μM RNA, 100 mM NaCl, 10 mM phosphate buffer (pH 7.0), 20 ºC

Selective dissociation of SNN/RNA duplexes by 340 nm light irradiation, direct transition from State 1 to State 4, was also examined. Irradiation with 340 nm light for State 1 reduced both absorption and HPLC peak of SNN strand, while SPNs were retained (Figure. 3-18 and S3-16 the percent crosslinking was increased to 97% for SNN and 5% for SPN). These results were in good agreement with dataset after light irradiation for State 2 with this wavelength, suggesting a transition to State 4. In other words, it was

demonstrated that formation of dual SNA/RNA duplexes was photo-controlled orthogonally regardless of the order of photo-irradiation.

Figure. 3-18 Controlled transition of two SNA/RNA duplexes from State 1 to State 4. (a) Absorption spectra of SNA/RNA duplexes at before irradiation (State 1, green line), after 340 nm irradiation (State4, blue line).   (b) HPLC profiles at each state. Absorption was monitored at 260 nm. (c) Percent of crosslinked $^{NV}A/^{NV}A$ in SNN (blue) and $^{NV}A/^{PV}A$ in SPN (green) at each state. The percentages of crosslinked products were calculated from decrease of HPLC peak areas corresponding SNN and SPN. Light irradiation was carried out for 30 min at 340 nm. Solution conditions were 2.5 μM SNA, 5.0 μM RNA, 100 mM NaCl, 10 mM phosphate buffer (pH 7.0), 20 °C

Finally, we investigated two pathways including State3: transitions from State 1 to State 3 to State 1 (induced by 465 nm and 300 nm light, Figure. 3-19) and transitions from State 3 to State 4 to State 1 (induced by 340 nm and 300 nm light, Figure. 3-20).

When a sample of SNN/RNA and SPN/RNA (State 1) was irradiated with 465 nm light, most of the peak corresponding to uncrosslinked SPN was converted into two peaks corresponding to photo-adducts, [16] whereas the intensity of the uncrosslinked SNN peak

was only partially reduced, indicating selective crosslinking of ^{PV}A to ^{NV}A (Figure. 3-19b and S3-17a). In addition, absorption after irradiation also suggested the coexistence of alkylpyrene (crosslinked SPN) and ^{NV}A (uncrosslinked SNN) (Figure.3-19a and S3-Xb). Thus, conversion to State 3 was successful. Upon irradiation with 300 nm light for state 3 regenerated the uncrosslinked SPN peak (Figure. 3-19 and S3-17b), indicating the transition to State 1.
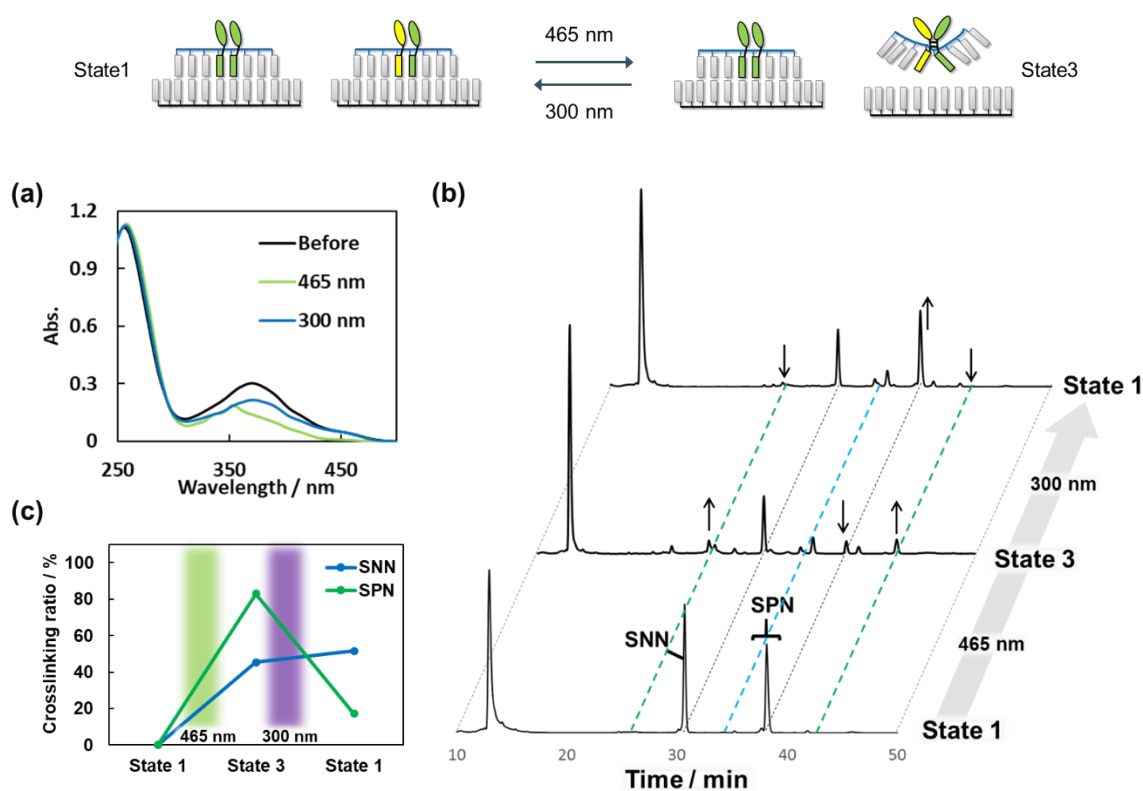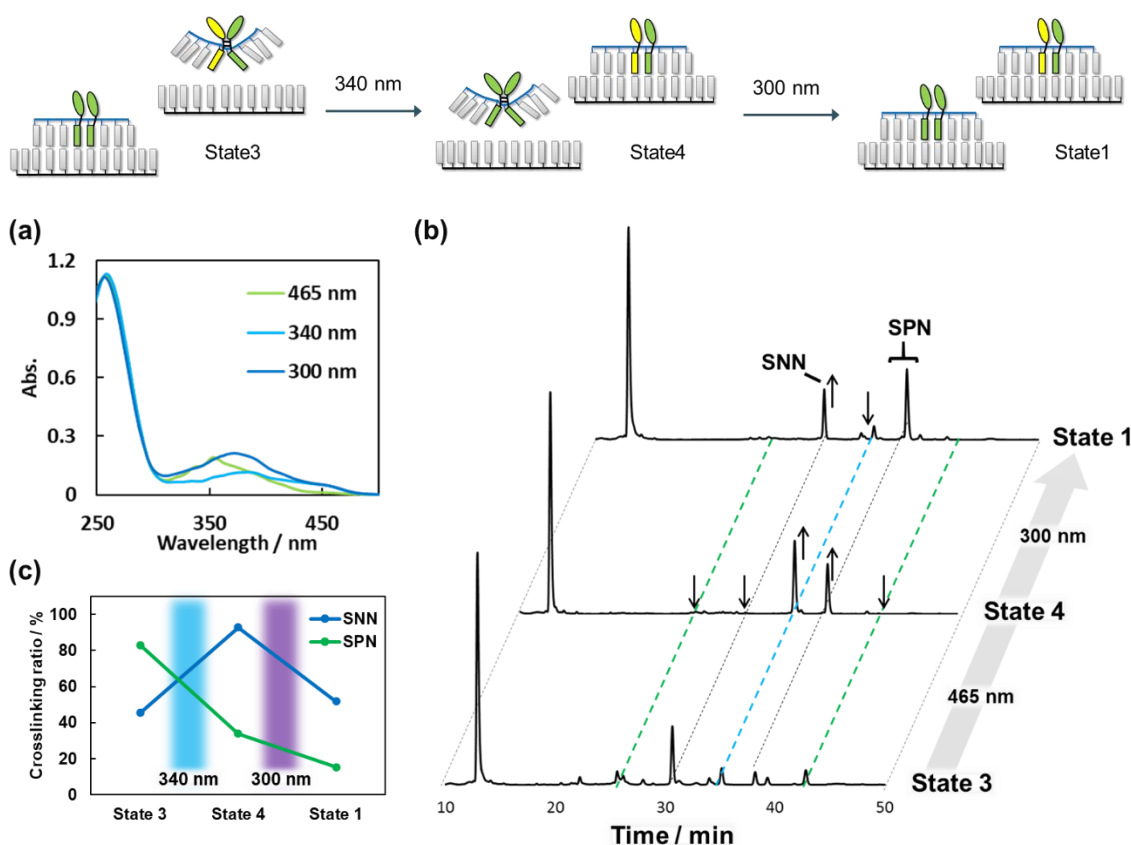

Figure. 3-19 Controlled transition of two SNA/RNA duplexes from State 2 to State 4 to State 1. (a) Absorption spectra of SNA/RNA duplexes after 405 nm irradiation (State 2, green line), after 340 nm irradiation (State 4, blue line) and after 300 nm irradiation (State 1, purple line). (b) HPLC profiles at each state. Absorption was monitored at 260 nm. (c) Percent of crosslinked ^{NV}A/^{NV}A in SNN (blue) and ^{NV}A/^{PV}A in SPN (green) at each state. The percentages of crosslinked products were calculated from decrease of HPLC peak areas corresponding SNN and SPN. Light irradiation was carried out for 30 min at 340 nm, and 5 min at 300 nm. Solution conditions were 2.5 μM SNA, 5.0 μM RNA, 100 mM NaCl, 10 mM phosphate buffer (pH 7.0), 20 °C

Figure. 3-20 Controlled transition of two SNA/RNA duplexes from State 2 to State 4 to State 1. (a) Absorption spectra of SNA/RNA duplexes after 405 nm irradiation (State 2, green line), after 340 nm irradiation (State 4, blue line) and after 300 nm irradiation (State 1, purple line). (b) HPLC profiles at each state. Absorption was monitored at 260 nm. (c) Percent of crosslinked $^{NV}A/^{NV}A$ in SNN (blue) and $^{NV}A/^{PV}A$ in SPN (green) at each state. The percentages of crosslinked products were calculated from decrease of HPLC peak areas corresponding SNN and SPN. Light irradiation was carried out for 30 min at 340 nm, and 5 min at 300 nm. Solution conditions were 2.5 μM SNA, 5.0 μM RNA, 100 mM NaCl, 10 mM phosphate buffer (pH 7.0), 20 °C

On the other hand, when State 3 was irradiated with 340 nm light instead of 300 nm light, the absorption and HPLC peak corresponding to SNN was eliminated and those corresponding to uncrosslinked SPN was recovered (Figure. 3-20 and S3-18a): light of this wavelength should mediate the dissociation of SNN/RNA duplexes and the re-formation of SPN/RNA duplexes simultaneously and enable transition from State 3 to State 4. Finally, 300 nm light irradiation also allowed the return to state 1 (Figure. 3-20

and S3-18b).

These results clearly demonstrate selective photo-regulation of the formation of two different SNA/RNA duplexes by irradiating with specific wavelengths of light.

3-5. Conclusion

We designed and synthesized a novel photo-crosslinkable nucleobase: 8-naphthylvinyl adinine (^{NV}A). When two consecutive ^{NV}A residues were incorporated into an SNA (SNN), intra-strand photo-crosslinking resulted upon irradiation with 405-340 nm light. This crosslinking resulted in dissociation of an SNA/RNA duplex. Irradiation with light of wavelength below 300 nm resulted in cycloreversion of the ^{NV}A/^{NV}A adduct and re-formation of the SNA/RNA duplex. Adjacent ^{NV}A and ^{PV}A residues in the SPN strand were also reversibly crosslinked: irradiation with 465-405 nm light generated a "hetero" photo-dimer of ^{NV}A/^{PV}A. Intra-strand crosslinking of the modified nucleobases in SPN also caused dissociation of the SNA/RNA duplex, and irradiation with light at wavelength below 340 nm reversed the crosslink and allowed duplex formation.

Photo-irradiation for the solution containing both SNN/RNA and SPN/RNA with suitable wavelengths of light selectively generated four possible hybridization states. It should be noted that this orthogonal photo-control of dual SNA/RNA duplex is not possible with ^{PV}A/^{PV}A, since simultaneous cycloreversion of ^{PV}A/^{PV}A and ^{NV}A/^{NV}A would be impossible due to poor absorbance at 300 nm of the ^{PV}A/^{PV}A photo-adduct.

This technology should expand use of acyclic XNAs including SNA in applications such as construction of complex photo-driven nanomachines.

3-6. Experimental section

Materials

Reagents for the synthesis of the ^{NV}A phosphoramidite monomer were purchased from Tokyo Kasei Co., Ltd., Wako Pure Chemical Industries, Ltd., and Aldrich. Reagents for oligomer synthesis and Poly-Pak II cartridges were purchased from Glen Research. The column used for HPLC analyses was purchased from Kanto Chemical Co., Ltd. RNAs were purchased from Hokkaido System Science Co., Ltd.

Photo-irradiation

A xenon light source (MAX-301, Asahi Spectra) equipped with interference filters centered at 254 nm, 300 nm, 340 nm, and 465 nm, 405 nm light-emitting diodes (LEDs, CCS) were used for photo-irradiation. When 465 nm irradiated for mixed solution of SNN / RNA and SPN / RNA, a longpass optical filter (LVX450, Asahi Spectra) that cuts out wavelengths below 450 nm was also used. The sample solution was added to a cuvette, and the temperature during irradiation was maintained at 20 ºC using a programmable temperature controller.

Spectroscopic measurements

UV/Vis spectra were measured using a JASCO model V-560 spectrometer equipped with a programmable temperature controller. Fluorescence spectra were measured on a JASCO model FP-6500 spectrometer equipped with a microcell holder. The wavelength of the excitation laser was 360 nm for ^{NV}A and 400 nm for ^{PV}A. CD spectra were measured on JASCO model J-820 instrument equipped with a programmable temperature controller. The sample solutions contained 100 mM NaCl, 10 mM phosphate buffer (pH 7.0). The

concentration of duplex was 5.0 µM, and experiments were performed in a 10-mm quartz cell.

HPLC analyses

A Mightysil RP-18GP II column heated to 50 °C was used for HPLC analyses. The flow rate was 0.5 mL min^{-1}. A solution of 50 mM ammonium formate (solution A) and a mixture of 50 mM ammonium formate and acetonitrile (50:50, v/v; solution B) were used as mobile phases. HPLC chromatograms were monitored at 260 nm. Spectra of peaks at each retention time were recorded on JASCO EXTREMA HPLC system.

Melting-temperature measurements

Melting curves of duplexes were obtained using a JASCO model V-560 spectrometer equipped with a programmable temperature controller by measuring the change in absorbance at 260 nm versus temperature. The temperature ramp was 0.5 °C min^{-1}. The T_m was determined from the maximum in the first derivative of the melting curve. Both the heating and cooling curves were measured, and the T_m measurements obtained agreed within 2.0 °C. The solution conditions were (unless otherwise noted) 100 mM NaCl, 10 mM phosphate buffer (pH 7.0), 5.0 µM oligonucleotide.

Synthesis of ^{NV}A-Serinol phosphoramidite

Synthesis of 2 (Scheme. 3-1, step a):

To a solution of 1[13] (1.36 g, 2.99 mmol), 1-bromonaphthalene (0.5 mL, 3.57 mmol), palladium (II) acetate (0.10 g, 0.45 mmol), and triphenylphosphine (0.20 g, 0.92 mmol) in 30 mL dry DMF was added 15 mL dry triethylamine. The solution was refluxed 30 min

at 110 °C. After cooling to room temperature, 100 mL of 1 N HCl in CHCl$_3$ was added. The organic phase was washed with saturated aqueous NaCl solution twice and dried in vacuo. The residue was purified by silica gel column chromatography (CHCl$_3$: ethyl acetate, 100:1 to 20:1) to obtain **2** (0.85 g, 1.46 mmol; yield: 49%). ^{1}H-NMR [CDCl$_3$, 500 MHz] δ = 8.72 (d, 1H), 8.61 (s, 1H), 8.16 (d, 1H), 7.95-7.87 (m, 6H), 7.75 (d, 1H), 7.58-7.47 (m, 5H), 7.38 (m, 4H), 6.94 (d, 1H), 5.08 (s, 2H), 4.26 (q, 2H), 1.29 (t, 3H). ^{13}C-NMR [CDCl$_3$, 125 MHz] δ = 172.4, 166.7, 154.7, 153.2, 151.6, 150.3, 138.3, 134.5, 133.7, 132.8, 131.4, 130.3, 129.5, 128.7, 128.6, 127.9, 127.8, 126.9, 126.3, 125.5, 124.6, 123.6, 114.3, 62.5, 43.6, 14.1.   HRMS (FAB) Calcd for C$_{35}$H$_{28}$N$_5$O$_4$ (M+H$^+$) 582.2136. Found 582.1967.

Synthesis of 3 (Scheme. S3-1, step b):

Compound **2** (0.85 g, 1.46 mmol) was suspended in 12 mL 1,4-dioxane and 6 mL MeOH. A solution of 0.48 g NaOH, 3.0 mL distilled water, and 3 mL MeOH was added to the stirred solution. After 20 min, the pH was adjusted to between 2 and 3 by the addition of 1 N HCl. The solution was dried under vacuum. The residue was suspended in 10 mL MeOH and precipitated with 120 mL diethyl ether. The precipitate was collected by filtration and washed with diethyl ether to obtain **3** (0.58 g, 1.30 mmol; yield: 89%). NMR signals were not observed due to insolubility of **3**. HRMS (FAB) Calcd for C$_{26}$H$_{20}$N$_5$O$_3$ (M+H$^+$) 450.1561. Found 450.1571.

Synthesis of 5 (Scheme. 3-1, step c):

To a stirred solution of **3** (0.75 g, 1.6 mmol), triethylamine (3.0 mL), and **4**[12] (0.43 g, 1.1 mmol) in 6 mL DMF was added 4-(4,6-dimethoxy-1,3,5-triazin-2-yl)-4-

methylmorpholinium chloride (DMT-MM; 0.40 g, 1.4 mmol), and the mixture was vigorously stirred. After 30 min, 10 mL of $CHCl_3$ was added, and the reaction was stirred for 10 min. A 10-mL aliquot of $CHCl_3$ was added, and the mixture was washed with saturated aqueous $NaHCO_3$ three times. The organic layer was added to 150 mL diethyl ether with stirring. The precipitate was collected by filtration and purified by silica gel column chromatography ($CHCl_3$: MeOH, 20 : 1) to yield **5** (0.63 g, 0.76 mmol; yield: 48%). ^{1}H-NMR [$CDCl_3$, 500 MHz] δ = 9.06 (br, 1H), 8.78 (m, 1H), 8.62 (br, 1H), 8.26 (m, 3H), 8.02 (m, 3H), 7.91 (m, 2H), 7.83 (m, 1H), 7.58-7.48 (m, 6H), 7.23 (m, 3H), 7.15 (m, 5H), 6.74 (m, 4H), 5.03 (s, 2H), 4.16 (br, 1H), 3.79 (m, 1H), 3.70 (m, 7H), 3.31-3.24 (m, 2H). ^{13}C-NMR [$CDCl_3$, 125 MHz] δ = 165.4, 164.5, 158.5, 152.9, 152.4, 151.7, 144.5, 136.9, 135.6, 134.2, 133.8, 132.7, 131.5, 130.3, 129.9, 129.0, 128.8, 128.0, 127.9, 127.8, 126.9, 126.3, 125.6, 124.7, 123.6, 122.8, 118.0, 113.2, 113.1, 86.1, 58.5, 55.2, 50.4, 43.1, 43.0, 24.6, 24.5. HRMS (FAB) Calcd for $C_{50}H_{45}N_6O_6$ (M+H$^+$) 825.3395. Found 825.1210

Synthesis of 6 (Scheme. 3-1, step d):

In dry CH_2Cl_2 under nitrogen, **5** (0.90 g, 1.09 mmol) and triethylamine (0.60 mL, 4.4 mmol) were added to 2-cyanoethyl diisopropylchlorophosphoramidite (0.30 mL, 0.75 mmol) at 0 °C. After stirring at room temperature for 30 min, the reaction mixture was subjected to silica gel column chromatography ($CHCl_3$: ethyl acetate, 1:1 containing 3% triethylamine). After column chromatography, products were dissolved in small amount of dry $CHCl_3$ and re-precipitated twice from hexane to yield **6** (0.42 g, 0.41 mmol; yield: 38%). ^{1}H-NMR [$CDCl_3$, 500 MHz] δ = 9.07(m, 1H), 8.85 (m, 1H), 8.71 (m, 1H), 8.31 (m, 1H), 8.07 (m, 2H), 7.91-7.89 (m, 2H), 7.64-7.53 (m, 4H), 7.46 (m, 1), 7.29 (m, 2H), 7.23-7.14 (m, 8H), 6.74 (m, 4H), 6.59 (m, 1H), 5.00 (m, 2H), 4.41 (m, 1H), 3.84 (m, 1H),

3.74-3.59 (m, 9H), 3.46 (m, 2H), 3.28 (m, 1H), 3.09 (m, 1H), 2.45 (m, 2H), 1.12-1.02 (m, 12H). ^{13}C-NMR [CDCl$_3$, 125 MHz] δ = 165,4 164.5, 158.5, 152.9, 152.4, 151.7, 151.6, 148.5, 144.5, 136.9, 135.8, 135.6, 134.2, 133.8, 132.7, 132.6, 132.5, 131.5, 130.3, 129.9, 129.8, 128.9, 128.8, 128.0, 127.9, 127.8, 126.9, 126.8, 126.3, 125.6, 124.7, 124.6, 123.6, 122.8, 118.1, 118.0, 114.7, 114.6, 113.1, 113.1, 86.1, 62.1, 61.8, 61.4, 61.2, 58.5, 58.4, 58.3, 58.2, 55.2, 46.0, 43.1, 43.0, 24.6, 24.5, 20.4. ^{31}P-NMR [CDCl$_3$, 121 MHz] δ = 148.1, 148.0. HRMS (FAB) Calcd for C$_{59}$H$_{61}$N$_8$O$_7$P (M) 1024.4401. Found 1024.4285.

Synthesis and purification of oligonucleotides

SNA phosphoramidite monomers functionalized with bases T, G, A, and C were synthesized following reported procedures.[12] All SNAs were synthesized using an H-8-SE DNA/RNA synthesizer using phosphoramidite chemistry. For the coupling of all SNA monomers, incubation time was 600 s. The concentrations of SNA phosphoramidite monomers were 0.15 M for ^{NV}A and ^{PV}A (CH$_2$Cl$_2$ solution), 0.1 M for G, and 0.075 M for T, A, and C (acetonitrile solution). Synthesized oligonucleotides were purified using Poly-Pak cartridges. The collected residue was further purified by reversed-phase HPLC (Kanto Chemical, Mightysil RP-18 GPII column). After purification, synthesized oligonucleotides were characterized by MALDI-TOF MS.

The MALDI-TOFMS data for the SNA

SN: Obsd. m/z 2681 (Calcd. for [SN + H$^+$]: m/z 2681)

SNN: Obsd. m/z 2832 (Calcd. for [SNN + H$^+$]: m/z 2833)

SPN: Obsd. m/z 2907 (Calcd. for [SPN + H$^+$]: m/z 2907)

3-7. Appendixes

Table. S3-1 Sequences of synthesized SNA and complementary strands.

Sequence[a]
SNN / RNA   (*S*)-GCT^{NV}**A**^{NV}**A**TGC-(*R*) / 5'-AA<u>GCAUUAGC</u>AA-3'
SPN / RNA   (*S*)-GCT^{PV}**A**^{NV}**A**TGC-(*R*) / 5'-AA<u>GCAUUAGC</u>AA-3'
SN / RNA   (*S*)-GCT^{NV}**A**ATGC-(*R*) / 5'-AA<u>GCAUUAGC</u>AA-3'
SP / RNA   (*S*)-GCT^{PV}**A**ATGC-(*R*) / 5'-AA<u>GCAUUAGC</u>AA-3'

[a] Some duplexes contain an RNA overhang region due to synthetic reasons. This overhang should not significantly affect hybridization.
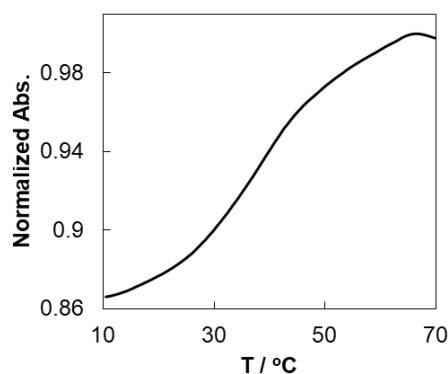
Figure. S3-1 Melting profile of **SN/RNA** before irradiation with light. Solution conditions were 5.0 μM oligonucleotide, 100 mM NaCl, 10 mM phosphate buffer (pH 7.0).

Table. S3-2 Thermodynamic parameters of SNN/RNA, SNA/RNA and RNA/RNA duplexes.

	T / °C	$-\Delta G^{\circ}_{37}$ / kcal mol^{-1}	$-\Delta H$ / kcal mol^{-1}	$-T\Delta S^{\circ}$ /kcal mol^{-1}
SNA / RNA	35.0	8.2	70.6	62.4
SNN / RNA	39.6	8.7	46.6	37.9
RNA / RNA	38.9	8.8	65.2	56.4
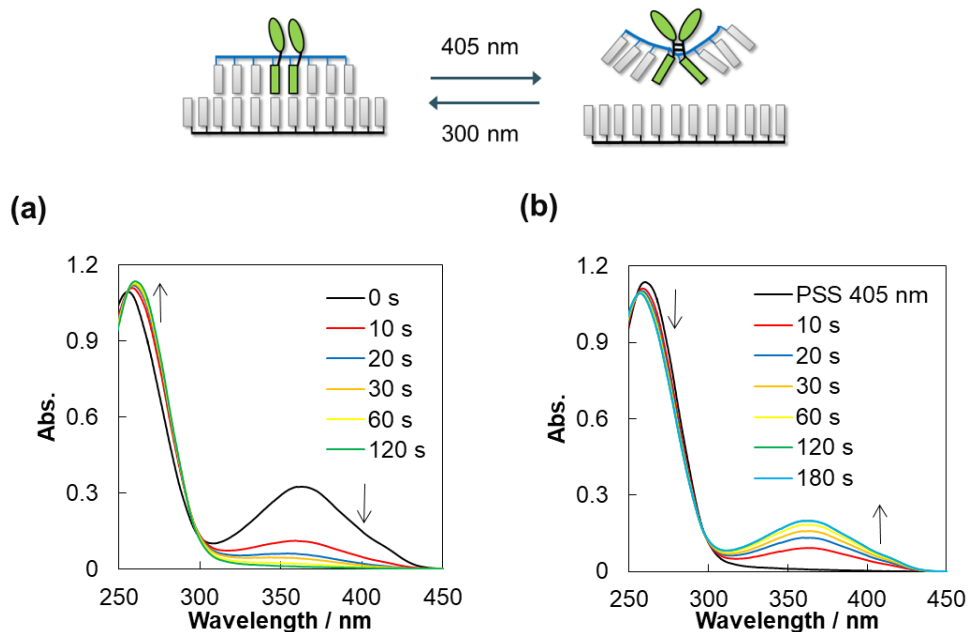
Figure. S3-2 (a) Absorption spectra of SNN/RNA after indicated times of irradiation with 405 nm light. (b) Absorption spectra of SNN/RNA at photo-stationary state (PSS) at 405 nm and after irradiation for the indicated times with 300 nm light. Irradiation was performed at 20 °C. Conditions: 100 mM NaCl, 10 mM phosphate buffer (pH 7.0), 20 °C. Concentration of SNA was 5.0 μM.
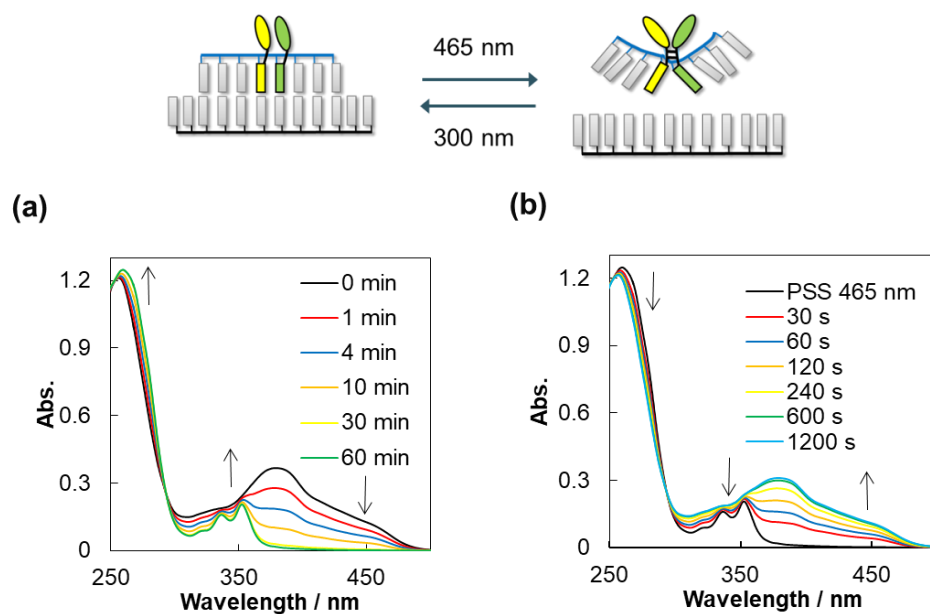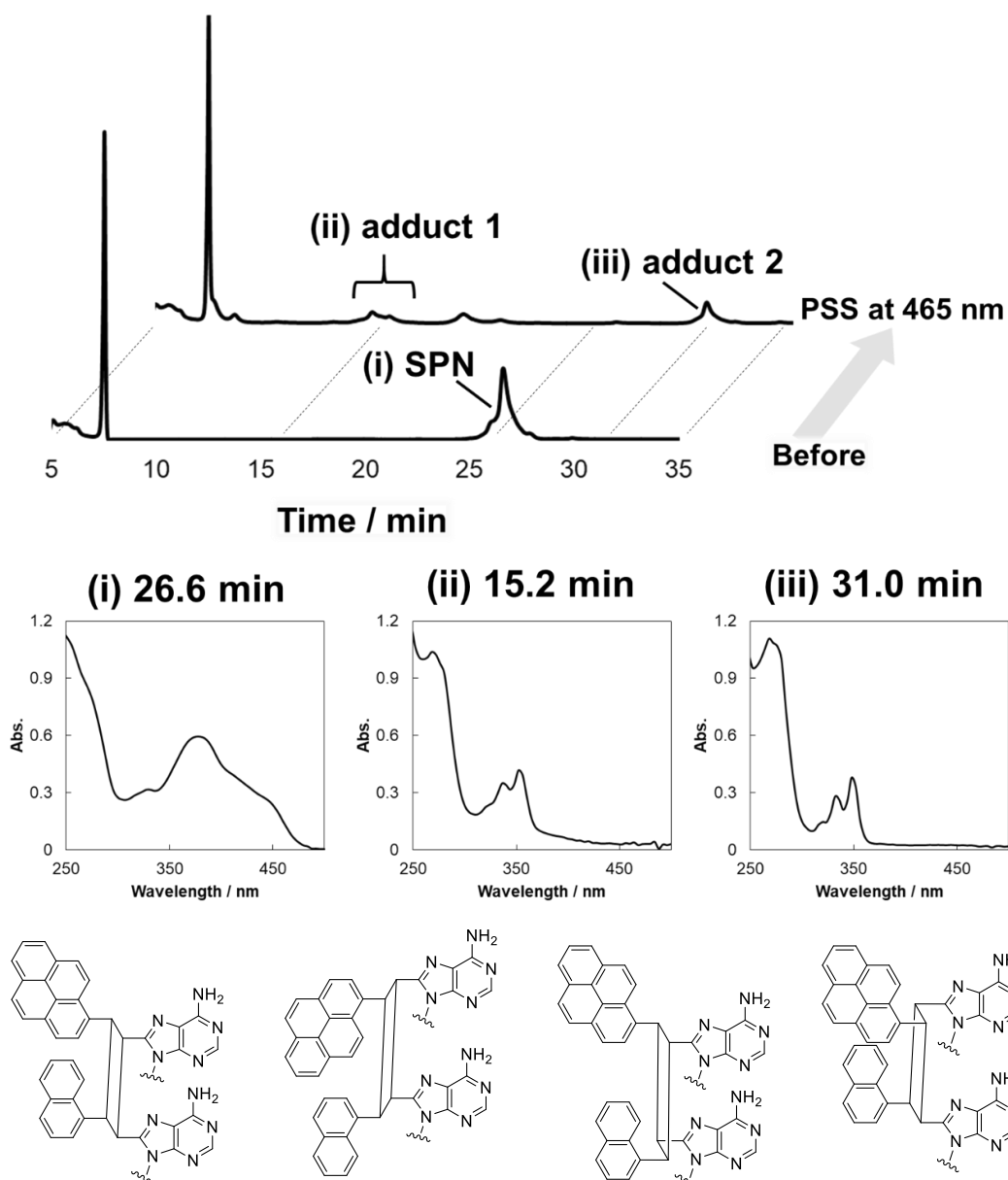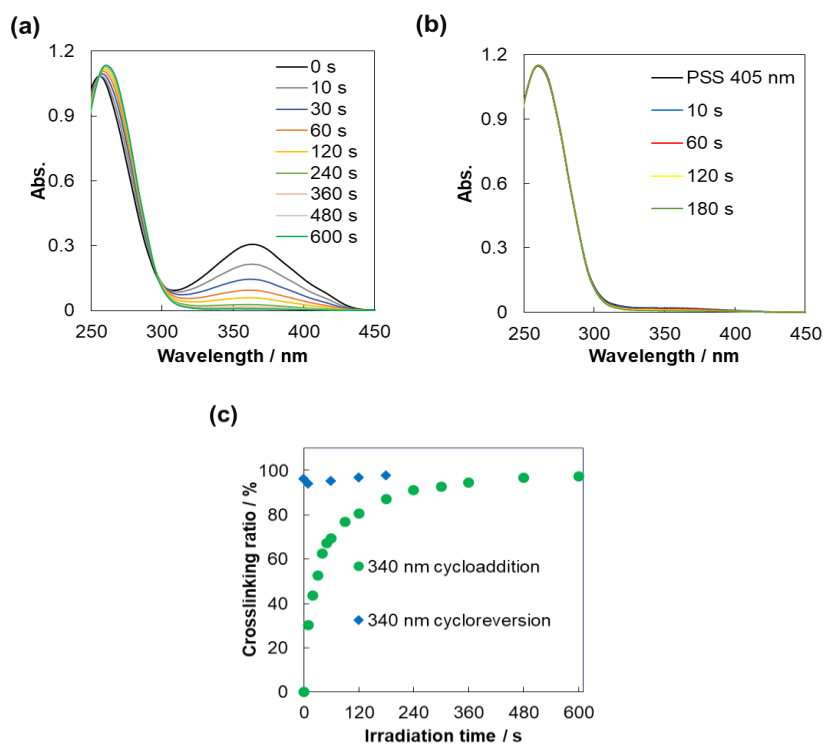

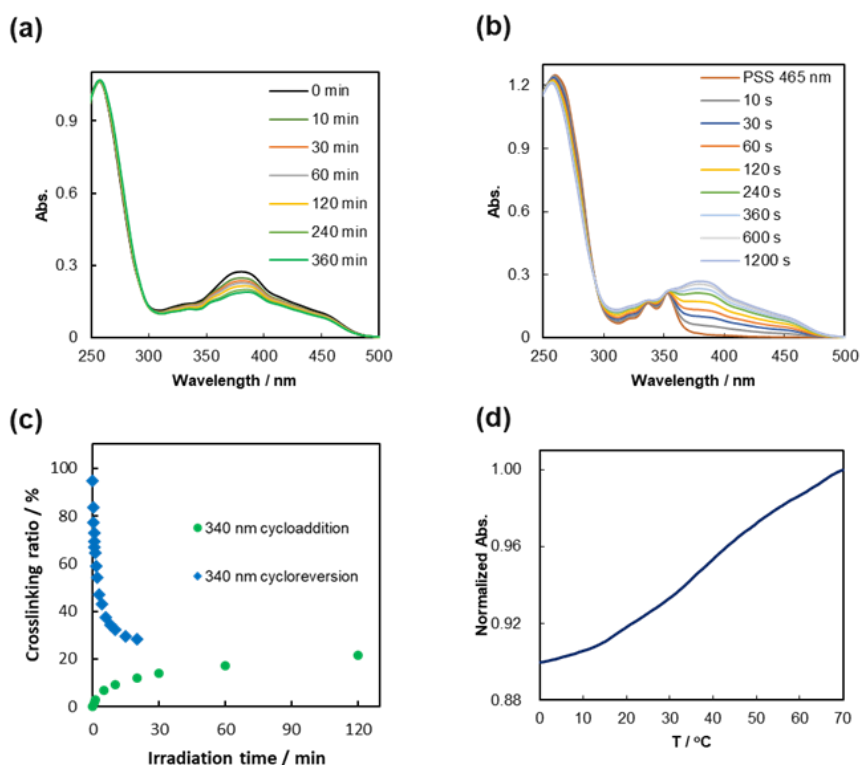**Figure. S3-3** (a) Absorption spectra of SPN/RNA after indicated times of irradiation with 465 nm light. (b) Absorption spectra of SPN/RNA at photo-stationary state (PSS) at 465 nm and after irradiation for indicated times with 300 nm light. Irradiation was performed at 20 °C. Conditions: 100 mM NaCl, 10 mM phosphate buffer (pH 7.0), 20 °C. Concentration of SNA was 5.0 μM.
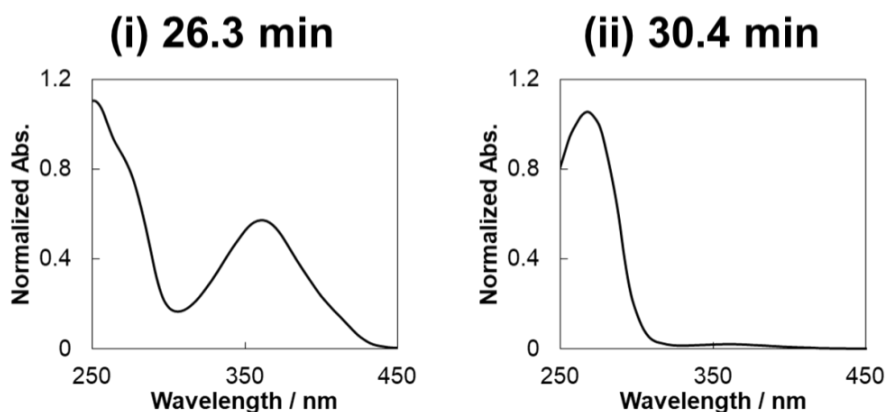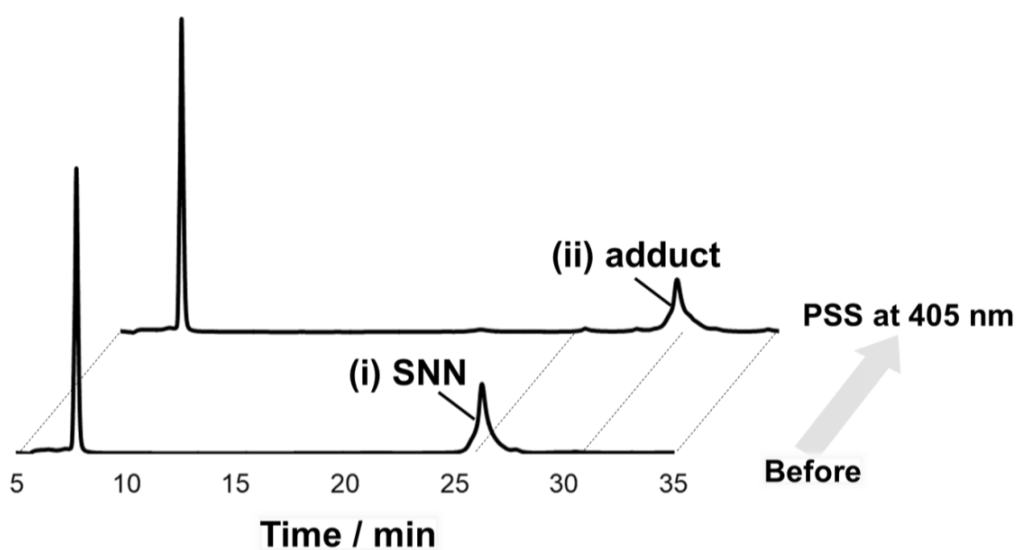
Figure. S3-4 HPLC profiles of SNN/RNA before and after irradiation with 405 nm for 120 s, and absorption spectra corresponding to the peaks at (i) 26.3 min and (ii) 30.4 min. Conditions: 100 mM NaCl, 10 mM phosphate buffer (pH 7.0), 20 °C, Concentration of SNA was 5.0 μM.
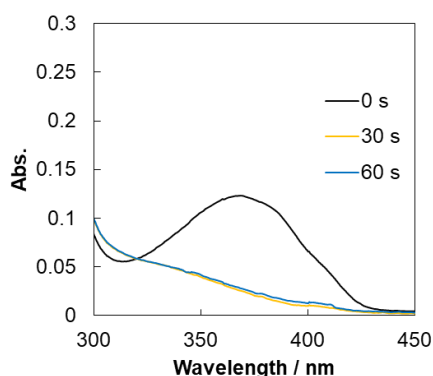
Figure. S3-6 Absorption spectra of SN/RNA after indicated times of irradiation with 405 nm light. Irradiation was performed at 20 °C. Conditions: 100 mM NaCl, 10 mM phosphate buffer (pH 7.0), 20 °C. Concentration of SNA was 5.0 μM.

Figure. S3-7 HPLC profiles of 5.0 μM SPN/RNA before and after irradiation with 465 nm for 60 min, absorption spectra corresponding to each retention time (i: 26.6 min, ii: 15.2 min, and iii: 31 min), and possible diastereomers of crosslinked $^{PV}A/^{NV}A$.

Table. S3-3 Quantum yields of photo-crosslinking reaction of SNN/RNA and SPN/RNA.

	SNN/RNA	SPN/RNA
$\Phi(\times 10^2)$ [a]	2.6	0.021

[a] Quantum yields were determined by using 3,4-dimethoxynitrobenzene actinometry. [17]
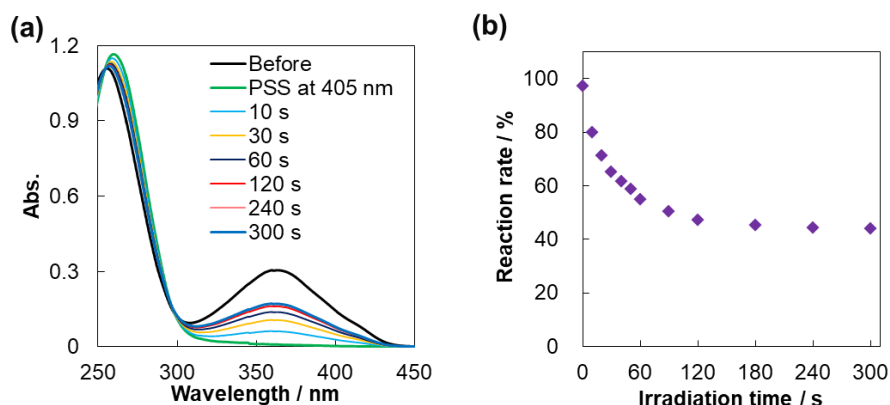
Figure. S3-8 (a) Absorption spectra of SNN/RNA at PSS at 405 nm and after irradiation for indicated times with 254 nm light. Irradiation was performed at 20 °C. (b) Percent crosslinking of $^{NV}A/^{NV}A$ in SNN as a function of irradiation time of SNN/RNA at 254 nm. The percent crosslinking was calculated from absorbance at 363 nm.

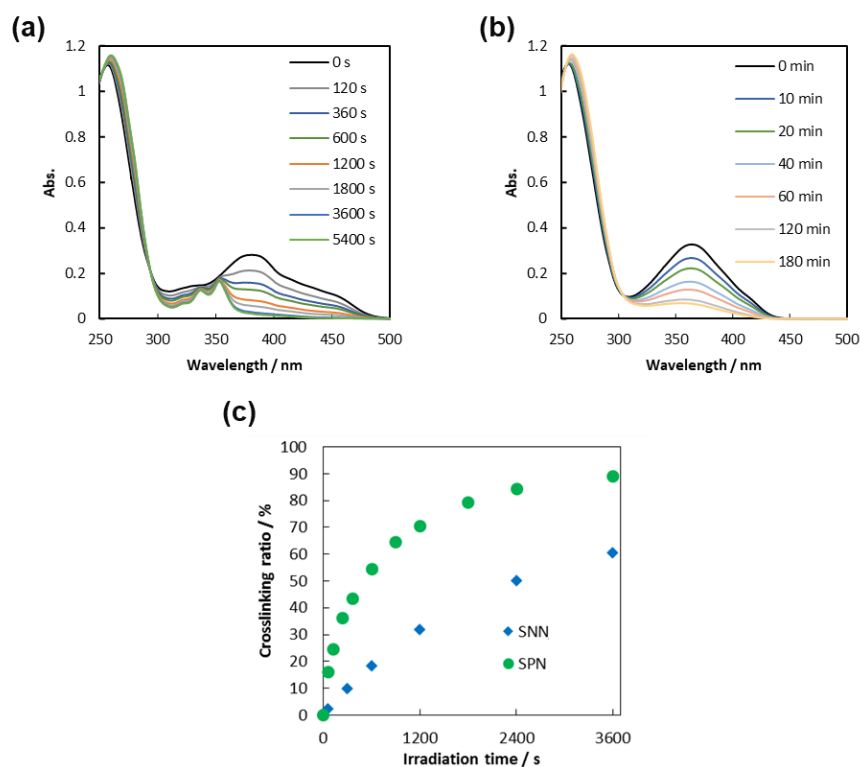**Figure. S3-9** (a) Absorption spectra of SNN/RNA after indicated times of irradiation with 340 nm light. (b) Absorption spectra of SNN/RNA at PSS at 405 nm and after irradiation for indicated times with 340 nm light. Irradiation was performed at 20 °C. (c) Percent crosslinking of $^{NV}A/^{NV}A$ in SNN as a function of irradiation time of the SNN/RNA duplex with 340 nm for cycloaddition (green circles) and 340 nm for cycloreversion (blue square). The percent crosslinking was calculated from the absorbance at 363 nm.
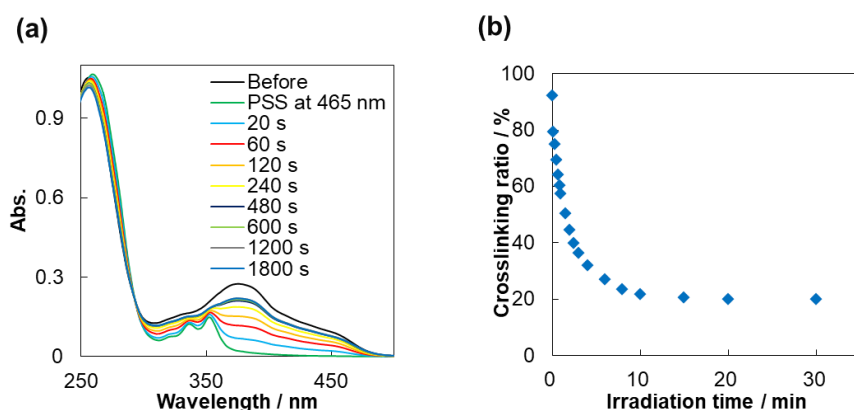
Figure. S3-10 (a) Absorption spectra of SPN/RNA at PSS at 465 nm and after irradiation for indicated times with 254 nm light. Irradiation was performed at 20 °C. (b) Percent crosslinking of $^{NV}A/^{PV}A$ in SPN as a function of irradiation time of the SPN/RNA duplex at 254 nm. The percent crosslinking was calculated from absorbance at 381 nm.
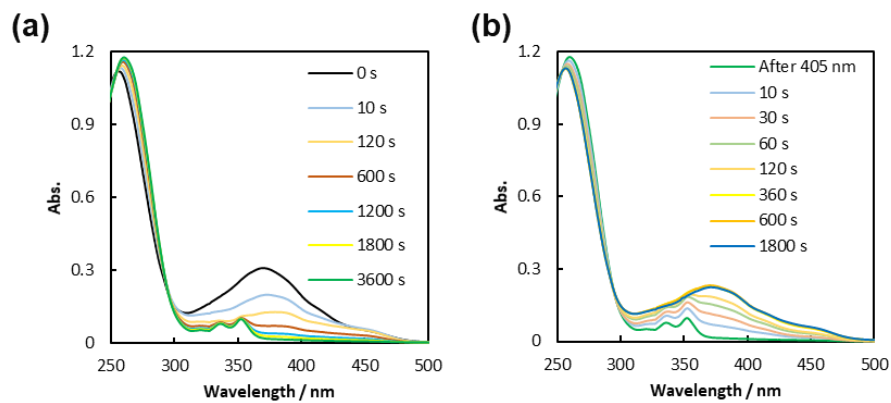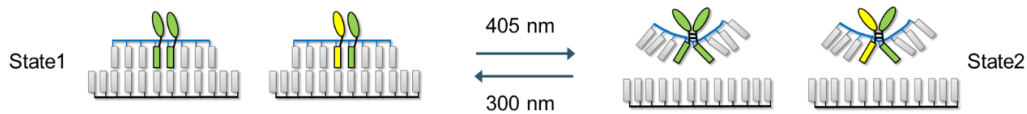

Figure. S3-11 (a) Absorption spectra of SPN/RNA after indicated times of irradiation with 340 nm light. (b) Absorption spectra of SPN/RNA at PSS at 465 nm and after irradiation for indicated times with 340 nm light. Irradiation was performed at 20 °C. (c) Percent crosslinking of $^{NV}A/^{PV}A$ in SPN as a function of irradiation time of the SPN/RNA duplex at 340 nm for cycloaddition (green circles) and 340 nm for cycloreversion (blue square). The percent crosslinking was calculated from absorbance at 381 nm. (d) Melting profile of SPN/RNA after irradiation with 340 nm light.

Figure. S3-12 (a) Absorption spectra of SPN/RNA at indicated times of irradiation with 465 nm light (>450 nm). (b) Absorption spectra of SPN/RNA at indicated times of irradiation with 465 nm light (>450 nm). Irradiation was performed at 20 °C. (c) Percent crosslinking of $^{NV}A/^{PV}A$ in SPN (green circles) and $^{NV}A/^{NV}A$ in SNN (blue square) a function of irradiation time of the both duplexes at 465 nm (>450 nm) for cycloaddition. The percent crosslinking was calculated from absorbance at 381 nm.
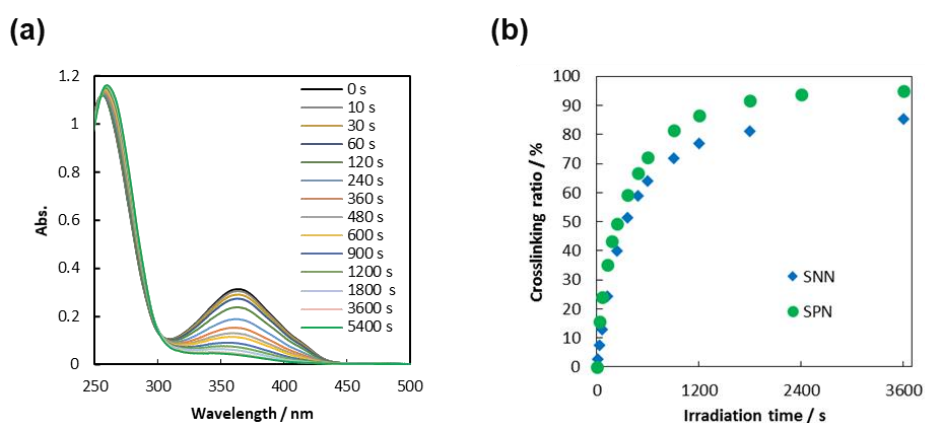
Figure. S3-13 (a) Absorption spectra of SPN/RNA at indicated times of irradiation with 465 nm light. Irradiation was performed at 20 °C. (b) Percent crosslinking of $^{NV}A/^{PV}A$ in SPN (green circles) and $^{NV}A/^{NV}A$ in SNN (blue square) a function of irradiation time of the both duplexes at 465 nm for cycloaddition. The percent crosslinking was calculated from absorbance at 381 nm.

Figure. S3-14 (a) Absorption spectra of State 2 and of State 4 after 340 nm light irradiation. (b) Absorption spectra of State 4 and of State 1 after 300 nm light irradiation. Solution conditions were 2.5 µM SNA, 5.0 µM RNA, 100 mM NaCl, 10 mM phosphate buffer (pH 7.0)
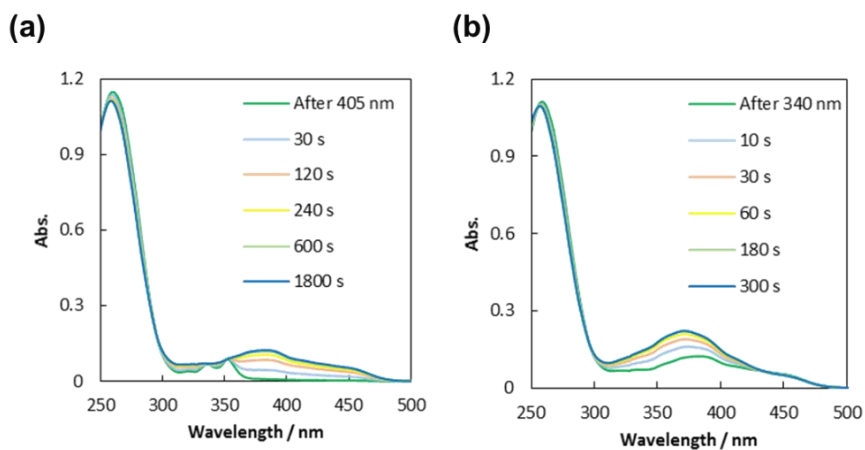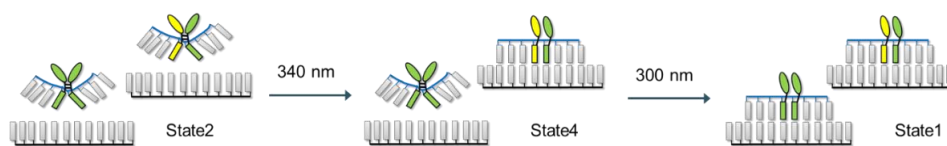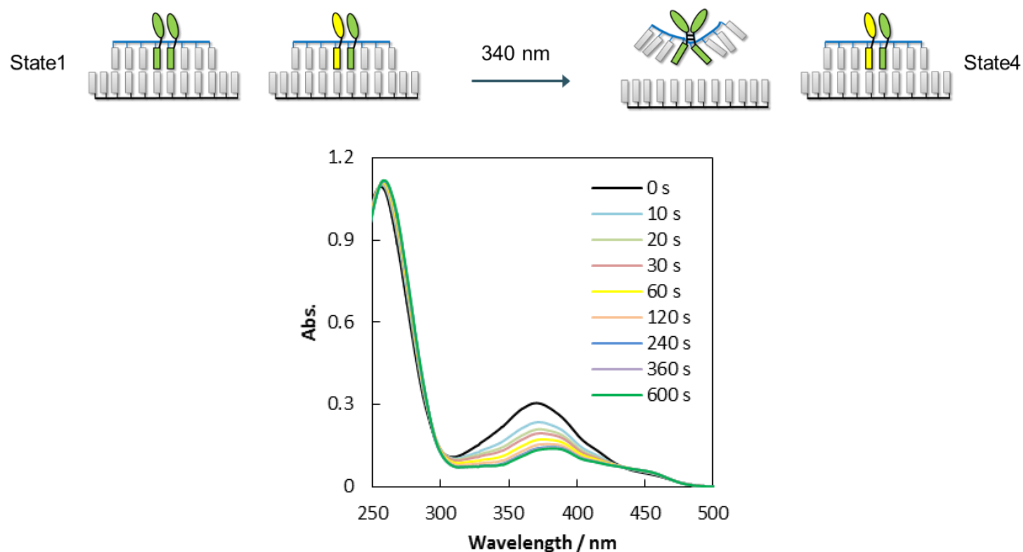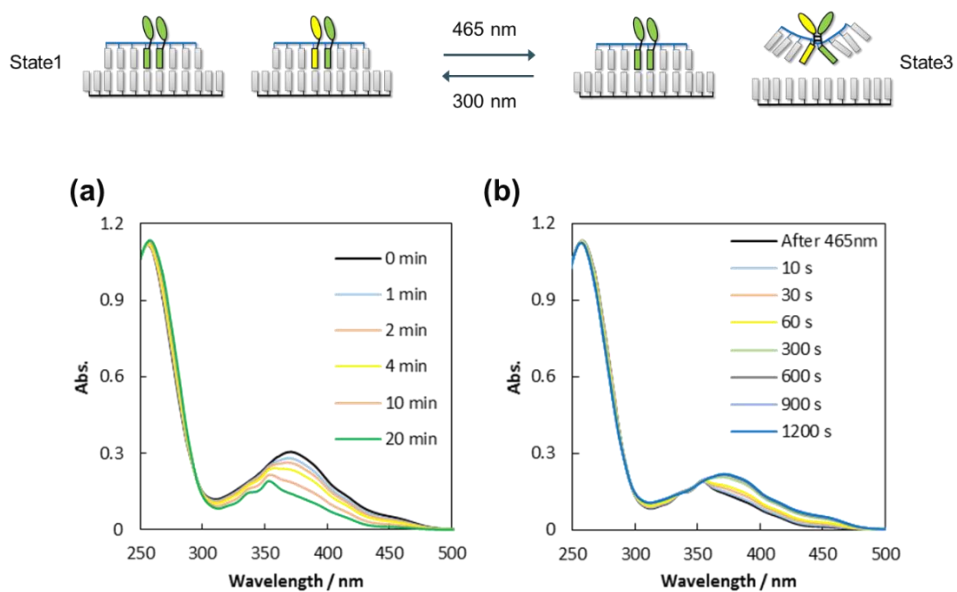

Figure. S3-15 (a) Absorption spectra of State 2 and of State 4 after 340 nm light irradiation. (b) Absorption spectra of State 4 and of State 1 after 300 nm light irradiation. Solution conditions were 2.5 µM SNA, 5.0 µM RNA, 100 mM NaCl, 10 mM phosphate buffer (pH 7.0)

Figure. S3-16 Controlled transition from State 1 to State 4. Absorption spectra of State 1 and of State 4 after 340 nm irradiation. Solution conditions were 2.5 μM SNA, 5.0 μM RNA, 100 mM NaCl, 10 mM phosphate buffer (pH 7.0)

Figure. S3-17 (a) Absorption spectra of State 1 and of State 3 after 465 nm light (>450 nm) irradiation**.** (b) Absorption spectra of State 3 and of State 1 after 300 nm light irradiation**.** Solution conditions were 2.5 μM SNA, 5.0 μM RNA, 100 mM NaCl, 10 mM phosphate buffer (pH 7.0)
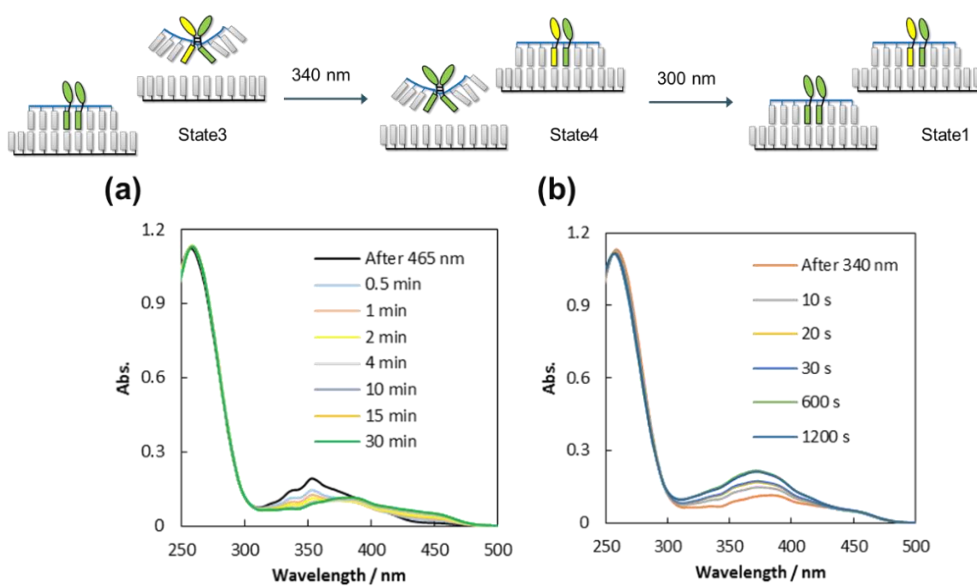
Figure. S3-18 (a) Absorption spectra of State 3 and of State 4 after 340 nm light irradiation. (b) Absorption spectra of State 4 and of State 1 after 300 nm light irradiation. Solution conditions were 2.5 μM SNA, 5.0 μM RNA, 100 mM NaCl, 10 mM phosphate buffer (pH 7.0)
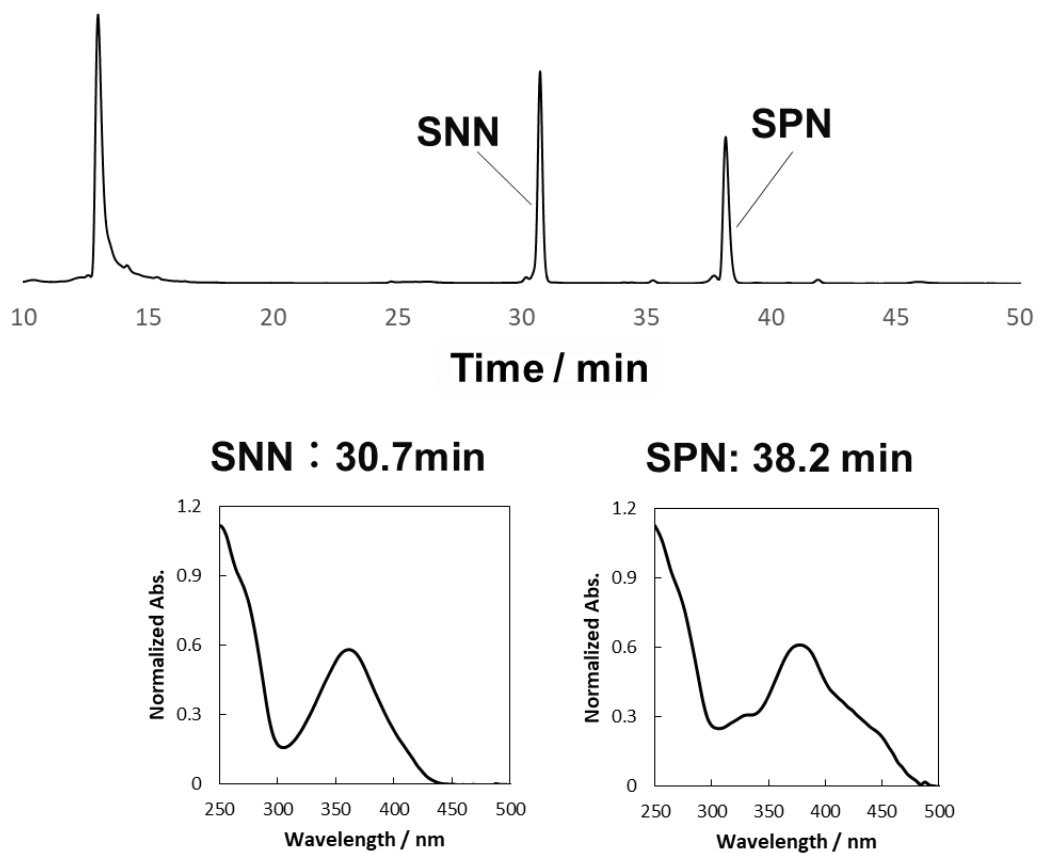

Figure. S3-19 HPLC profile of State 1. Absorption spectra of peak with retention time of 30.7 min (SNN) and of peak with retention time of 38.2 min (SPN).
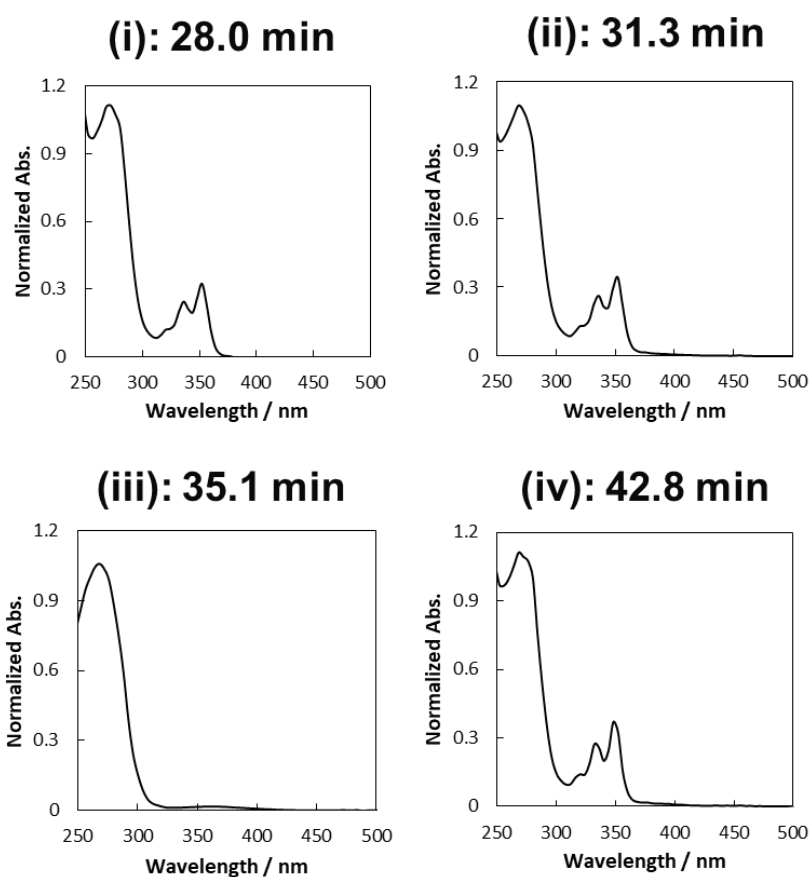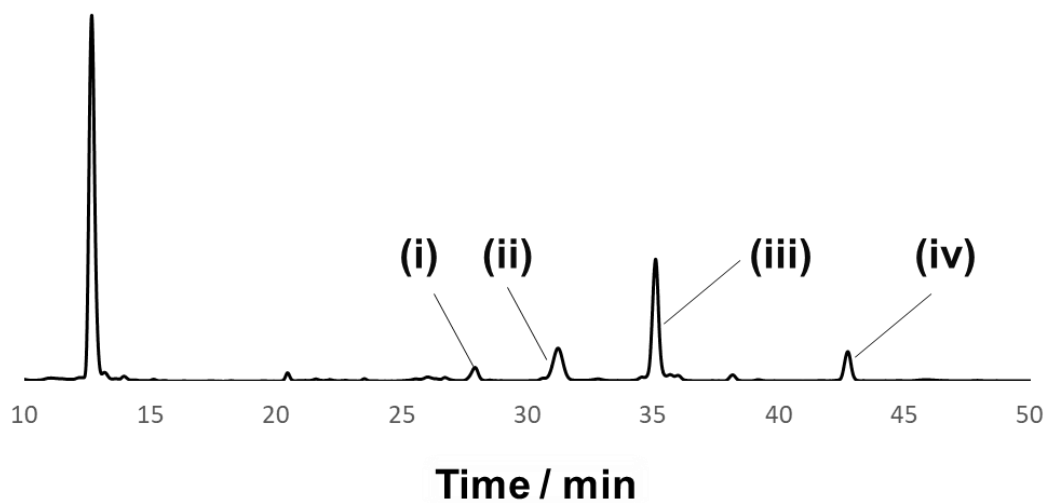
Figure. S3-20 HPLC profile of State 2. Absorption spectra of peaks with retention times of 28.0 min, 31.3 min, 35.1 min, and 42.8 min. The peaks at 28.0 min, 31.3 min, and 42.8 min with characteristics of alkylpyrene and alkylnaphthalene were assigned to SPN adducts. The peak at 35.1 min was assigned to the SNN adduct because it has alkylnaphthalene absorption only.
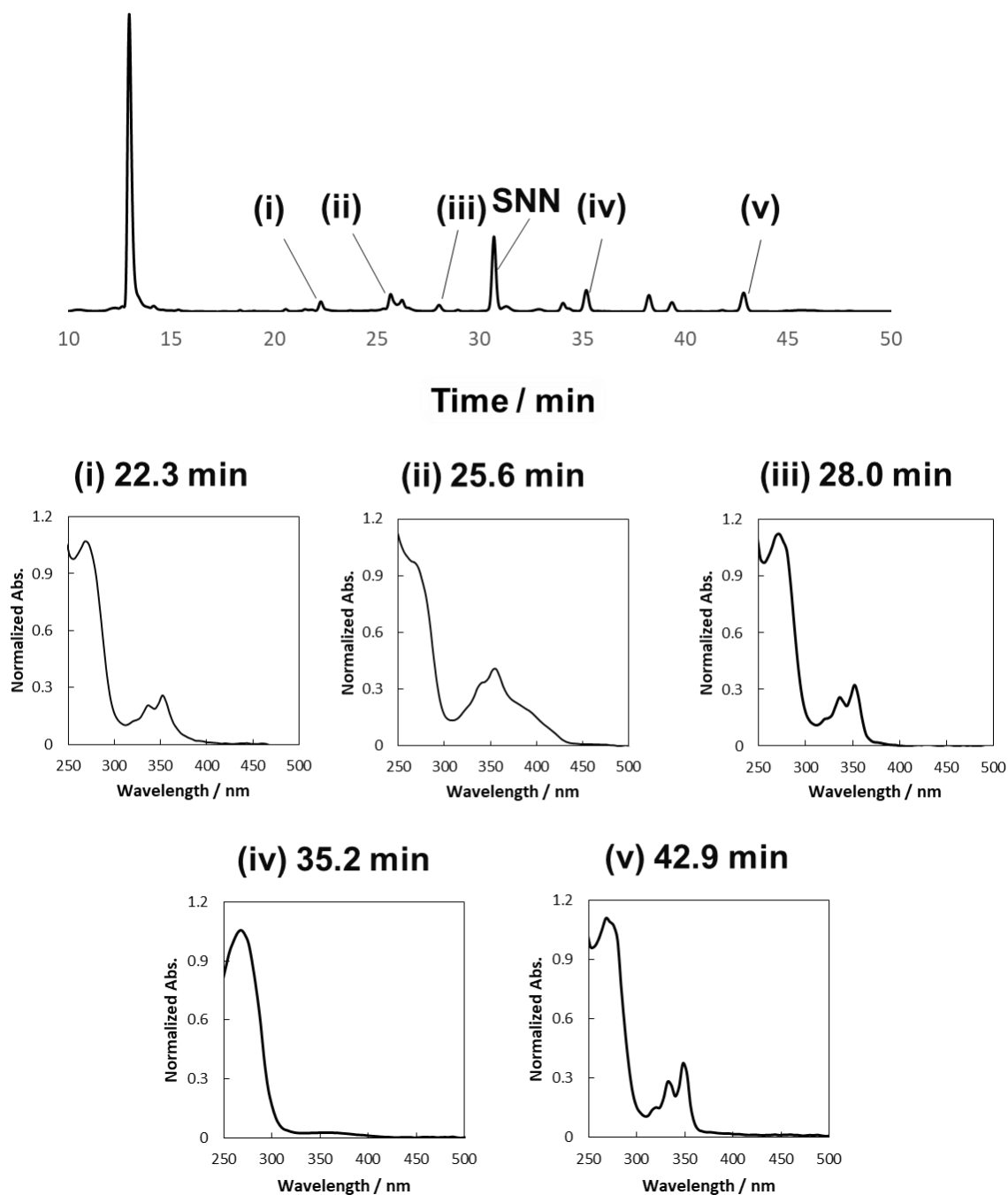
Figure S3-21 HPLC profile of State 3. Absorption spectra of peaks with retention times of 22.3 min, 25.6 min, 28.0 min, 35.2 min, and 42.9 min. The peaks at 22.3 min, 28.0 min, and 42.9 min, with characteristics of alkylpyrene and alkylnaphthalene, were assigned to SPN adducts. Since the peak at 25.6 min has both alkylpyrene and ^{NV}A absorptions, interstrand crosslinking occurred between the ^{PV}A and ^{NV}A in SPN.

108

3-8. References

[1] (a) M. A. C. Stuart, W. T. S. Huck, J. Genzer, M. Müller, C. Ober, M. Stamm, G. B. Sukhorukov, I. Szleifer, V. v. Tsukruk, M. Urban, F. Winnik, S. Zauscher, I. Luzinov, S. Minko, *Nat. Mater.* **2010**, *9*, 101–113; (b) C. de las Heras Alarcón, S. Pennadam, C. Alexander, *Chem. Soc. Rev.* **2005**, *34*, 276–285; (c) Y. Qiu, K. Park, *Adv. Drug Deliv. Rev.* **2001**, *53*, 321-339; (d) E. R. Kay, D. A. Leigh, F. Zerbetto, *Angew. Chem. Int. Ed.* **2007**, *46*, 72–191.

[2] (a) G. Mayer, A. Heckel, *Angew. Chem. Int. Ed.* **2006**, *45*, 4900–4921; (b) C. Brieke, F. Rohrbach, A. Gottschalk, G. Mayer, A. Heckel, *Angew Chem. Int. Ed.* **2012**, *51*, 8446–8476.

[3] (a) C. G. Bochet, *Tetrahedron Lett.* **2000**, *41*, 6341–6346; (b) P. Klán, T. Šolomek, C. G. Bochet, A. Blanc, R. Givens, M. Rubina, V. Popik, A. Kostikov, J. Wirz, *Chem. Rev.* **2013**, *113*, 119–191; (c) M. J. Hansen, W. A. Velema, M. M. Lerch, W. Szymanski, B. L. Feringa, *Chem. Soc. Rev.* **2015**, *44*, 3358–3377; (d) V. San Miguel, C. G. Bochet, A. del Campo, *J. Am. Chem. Soc.* **2011**, *133*, 5380–5388; (e) L. Fournier, I. Aujard, T. le Saux, S. Maurin, S. Beaupierre, J. B. Baudin, L. Jullien, *Chem. Eur.J.* **2013**, *19*, 17494–17507; (f) J. M. Amatrudo, J. P. Olson, G. Lur, C. Q. Chiu, M. J. Higley, G. C. R. Ellis-Davies, *ACS Chem. Neurosci.* **2014**, *5*, 64–70.

[4] (a) M. A. Priestman, L. Sun, D. S. Lawrence, *ACS Chem. Biol.* **2011**, *6*, 377–384; (b) W. A. Velema, J. P. van der Berg, W. Szymanski, A. J. M. Driessen, B. L. Feringa, *ACS Chem. Biol.* **2014**, *9*, 1969–1974.

[5] (a) X. Zhang, W. Xi, S. Huang, K. Long, C. N. Bowman, *Macromolecules* **2017**, *50*, 5652–5660; (b) L. García-Fernández, C. Herbivo, V. S. M. Arranz, D. Warther, L. Donato, A. Specht, A. del Campo, *Adv. Mater.* **2014**, *26*, 5012–5017; (c) H. Frisch, F. R. Bloesser, C. Barner-Kowollik, *Angew. Chem. Int. Ed.* **2019**, *58*, 3604-3609; (d) H. Frisch, D. Kodura, F. R. Bloesser, L. Michalek, C. Barner-Kowollik, *Macromol. Rapid Commun.* **2020**, *41*,1900414.

[6] (a) M. A. Azagarsamy, K. S. Anseth, *Angew. Chem. Int. Ed.* **2013**, *52*, 13803–13807; (b) D. B. Pacardo, B. Neupane, S. M. Rikard, Y. Lu, R. Mo, S. R. Mishra, J. B. Tracy, G. Wang, F. S. Ligler, Z. Gu, *Nanoscale* **2015**, *7*, 12096–12103.

[7] (a) A. Rodrigues-Correia, X. M. M. Weyel, A. Heckel, *Org. Lett.* **2013**, *15*, 5500–5503; (b) A. Rodrigues-Correia, D. Knapp-Bühle, J. W. Engels, A. Heckel, *Org. Lett.* **2014**, *16*, 5128–5131.

[8] K. Fujimoto, S. Sasago, J. Mihara, S. Nakamura, *Org. Lett.* **2018**, *20*, 2802–2805.

[9] H. Nishioka, X. Liang, T. Kato, H. Asanuma, *Angew. Chem. Int. Ed.* **2012**, *51*, 1165–1168.

[10] M. W. Haydell, M. Centola, V. Adam, J. Valero, M. Famulok, *J. Am. Chem. Soc.* **2018**, *140*, 16868–16872.

[11] M. Škugor, J. Valero, K. Murayama, M. Centola, H. Asanuma, M. Famulok, *Angew. Chem. Int. Ed.* **2019**, *58*, 6948-6951.

[12] H. Kashida, K. Murayama, T. Toda, H. Asanuma, *Angew. Chem. Int. Ed.* **2011**, *50*, 1285–1288.

[13] K. Murayama, Y. Yamano, H. Asanuma, *J. Am. Chem. Soc.* **2019**, *141*, 9485–9489.

[14] K. Murayama, H. Asanuma, *ChemBioChem* **2020**, *21*, 120 – 128.

[15] Theoretically, photo-reaction of SNN should not proceed upon irradiation with 465 nm light because [NV]A has almost no absorption band around 465 nm. However, study of the quantum yield of the crosslinking reaction revealed that crosslinking between [NV]A residues was over 100 times faster than crosslinking of [PV]A and to [PV]A or [NV]A (Table. S3-3). This high yield might facilitate photo-crosslinking in SNN by excitation with 465 nm light regardless of very slight absorbance at around 465 nm (Figure. S3-13). Despite the unintended reaction of SNN by 465 nm light, clear difference in percent crosslinking of chromophores in SNN and SPN was observed after 20 min of irradiation with 465 nm with a longpass optical filter which remove the light below 450 nm (Figure. S3-12)

[16] The HPLC peaks of the SPN crosslinked adduct after irradiation at 465 nm and the those in State 3 did not completely match (Figure.3-11 and Figure. 3-18). Irradiation at 465 nm should allow the formation of inter-strand crosslinked adduct with both [PV]A/[PV]A and [NV]A/[NV]A cycloaddition. On the other hand, when the light at <450 nm was cut (State 3), the reaction between [NV]As should be suppressed: it is expected that an inter-strand crosslinked adduct with only [PV]A/[PV]A cycloaddition was obtained instead. These interchain cross-linking reactions should also induce double-strand dissociation.

[17] J.-Y.Zhang, H. Esrom, I. W. Boyd, *Appl. Surf. Sci.* **1999**, *138–139*, 315–319.

List of Publications

1. K. Murayama, Y. Yamano, H. Asanuma, " 8-Pyrenylvinyl Adenine Controls Reversible Duplex Formation between Serinol Nucleic Acid and RNA by [2 + 2] Photocycloaddition", *J. Am. Chem. Soc.* **2019**, *141*, 9485–9489.

2. Y. Yamano, K. Murayama, H. Asanuma, "Dual crosslinking photo-switches for orthogonal photo-control of hybridization between serinol nucleic acid and RNA " *Chem. Eur. J.* **2021**, *27*, accepted

List of Presentations

International Conference

Oral

1. Yuuhei Yamano, Keiji Murayama, Hiroyuki Asanuma, "Photo-regulation of SNA duplex formation and dissociation by introducing crosslink type artificial nucleobases" 1st G'L'owing Polymer Symposium in KANTO (GPS-K 2018), 2018 年 12 月 15 日, 早稲田大学, 高分子学会 関東支部

2. "Functional control of serinol nucleic acid (SNA) by reversible photocycloaddition of 8-pyrenylvinyl adenine", ○Yuuhei Yamano, The Fourth A3 Roundtable Meeting on

Asia Chemical Probe Research Hub, 2019 年 11 月 18-21 日, 仙台, Asia Chemical Probe Research Hub

Poster

3. "Development of photo-responsive SNA by introduction of modified nucleobases", ○Yuuhei Yamano, Keiji Murayama, Hiroyuki Asanuma, Nagoya Univ.-Tsinghua Univ.-Toyota Motor Corp.-Hokkaido Univ. Joint Symposium (NTTH2017), 2017 年 7 月 12-14 日, 高山, NTTH

4. "Photo-regulation of SNA duplex stability by introducing modified nucleobases", ○Yuuhei Yamano, Keiji Murayama, Hiroyuki Asanuma, The Second International Symposium on Biofunctional Chemistry (ISBC2017), 2017 年 12 月 14-16 日, 京都 大学, 日本化学会 生体機能関連化学部会

Internal Conference

20 presentations. Omitted.

List of Awards

---

1) 東海高分子研究会学生研究奨励賞，「光架橋型修飾塩基の導入による機能性 SNA の設計」, 2017 年 9 月 2 日, 高分子学会 東海支部

2) 第 67 回高分子学会年次大会優秀ポスター賞，「可逆的[2+2]環化付加反応を利用した SNA 二重鎖の光制御」, 2018 年 5 月 25 日, 高分子学会

3) IGER Annual Meeting 2018 Poster Award, "Photo-regulation of SNA duplex formation and dissociation by using reversible [2+2] cycloaddition reaction", 2019 年 1 月 9 日, IGER

4) 優秀学生発表賞（口頭）, "Functional control of serinol nucleic acid (SNA) using photo-crosslink type nucleobase: 8-pyrenylvinyl adenine", 2019 年月 9 日 12 日, 光化学協会

5) 東海高分子学生優秀発表賞，「光架橋型修飾 Adenine を用いた人工核酸 SNA の光制御」, 2019 年月 11 日 10 日, 中部化学関係学協会支部連合協議会

Acknowledgements